MAY, 1972

INVESTIGATION OF AURORAL IONOSPHERIC
AND PROPAGATION PHENOMENA RELATED TO THE
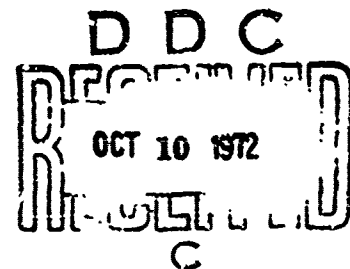POLAR FOX II EXPERIMENT

BY

JOHN R. HERMAN AND RICHARD VARGAS-VILA

PREPARED BY

ANALYTICAL SYSTEMS CORPORATION
11 RAY AVENUE
BURLINGTON, MASSACHUSETTS   01803

PREPARED FOR

MASSACHUSETTS INSTITUTE OF TECHNOLOGY
LINCOLN LABORATORY

D D C

OCT 10 1972

C

DOCUMENT CONTROL DATA - R&D

(Security classification of title, body of abstract and indexing annotation must be entered when the overall report is classified)

1. ORIGINATING ACTIVITY *(Corporate author)*	2a. REPORT SECURITY CLASSIFICATION
Analytical Systems Corporation under Purchase Order No. CC-731 to M.I.T. Lincoln Laboratory	Unclassified
	2b. GROUP None

3. REPORT TITLE

Investigation of Auroral Ionospheric And Propagation Phenomena Related To The Polar Fox II Experiment

4. DESCRIPTIVE NOTES *(Type of report and inclusive dates)*

Technical Report covering the period 15 August 1971 to 31 March 1972

5. AUTHOR(S) *(Last name, first name, initial)*

Herman, John, R. and Vargas-Vila, Richard

6. REPORT DATE	7a. TOTAL NO. OF PAGES	7b. NO. OF REFS
May 1972	110	34

9a. CONTRACT OR GRANT NO. F19628-70-C-0230	9a. ORIGINATOR'S REPORT NUMBER(S)
b. PROJECT NO. ARPA Order 600	ASCR 72-02
c. Purchase Order No. CC-731	9b. OTHER REPORT NO(S) *(Any other numbers that may be assigned this report)*
d.	ESD-TR-72-213

10. AVAILABILITY/LIMITATION NOTICES

Approved for public release; distribution unlimited.

11. SUPPLEMENTARY NOTES	12. SPONSORING MILITARY ACTIVITY
None	Advanced Research Projects Agency Department of Defense

13. ABSTRACT

Auroral phenomena can have pronounced effects upon HF radiowave propagation traversing polar regions. To further understand the implications and predict the resulting effects, a continuation of the investigation of auroral phenomena and their impact upon Polar Fox II measurements is presented. In this report, special emphasis has been placed on a study of the fine structure and motions of spread F as related to spectral spreading; the main ionospheric trough and magnetic activity; analysis of radar auroral absorption and Auroral sporadic E as they relate to propagation coverage predictions.

14. KEY WORDS

polar ionosphere
auroral absorption
sporadic E
ionospheric troughs
radio propagation
magnetic activity
Polar Fox II

ASCR 72-62
May 1972

Investigation Of Auroral Ionospheric And Propagation Phenomena Related To The Polar Fox II Experiment

BY

John R. Herman and Richard Vargas-Vila

Prepared By

Analytical Systems Corporation
11 Ray Avenue
Burlington, Massachusetts   01803

For

Massachusetts Institute Of Technology
Lincoln Laboratory

Under

Purchase Order No.   CC-731

Prime Contract No.   F19628-70-0230

ARPA Order No.   600

This Report Covers The Period
15 August 1971 to 31 March 1972

Analytical Systems CORPORATION _ASC_ (617) 272-7910

11 RAY AVENUE
BURLINGTON, MASSACHUSETTS 01803

ABSTRACT

Auroral phenomena can have pronounced effects upon HF radio-
wave propagation traversing polar regions. To further understand
the implications and predict the resulting effects, a continua-
tion of the investigation of auroral phenomena and their impact
upon Polar Fox II measurements is presented. In this report,
special emphasis has been placed on a study of the fine structure
and motions of spread F as related to spectral spreading; the
main ionospheric trough and magnetic activity, analysis
of radar auroral absorption and auroral sporadic E as they
relate to propagation coverage predictions.

iii

Analytical Systems CORPORATION *ASC*   (617) 272-7910

11 RAY AVENUE
BURLINGTON, MASSACHUSETTS 01803

ACKNOWLEDGEMENTS

iv

SYSTEMS ANALYSIS ■ PLANNING ■ DEVELOPMENT

Analytical Systems CORPORATION

Contents

Analytical Systems CORPORATION ◢▰◣▱

FIGURES

Analytical Systems CORPORATION ᐊᒥᐧ

Analytical Systems CORPORATION ◢◢◢

Analytical Systems CORPORATION ▲⌐

1.0 INTRODUCTION

High frequency (HF) radar experiments in polar and auroral regions are expected to be profoundly affected by ionospheric phenomena peculiar to high latitudes. These effects include signal scattering, spreading, attenuation and anomalous propagation processes imposed by the medium.

For the purposes of devising appropriate experimental observations and schedules, predicting expected effects and analyzing and interpreting the experimental results; it is necessary to have the ionospheric characteristics and their propagation effects expressed in terms directly relatable to the radar experiment.

The purpose of this report is to summarize the results of investigations carried out during the period of August 15, 1971 to March 31, 1972, of certain polar ionospheric characteristics in terms of how they may be expected to impact on Polar Fox II measurements. Attention has been directed to: the fine structure and motions of spread F as related to spectral spreading (Section 2); the relationship between spread F regions, the main ionospheric trough and magnetic activity (Section 3); auroral absorption (Section 4); and auroral sporadic E (Section 5). Expanded versions of Sections 3 and 4 will be published in the proceedings of the Monterey, California, OHD Annual Review Meeting (May 3-4, 1972).

2.0 Spread F Fine Structure And Motions

2.1 IRREGULARITY SIZE AND INTENSITY

A small-scale irregularity in the F region can be considered to have an electron density of $N + \Delta N$ where N is the density of the ambient ionosphere. The strength (or intensity) of the irregularity is, then, $\varepsilon = \Delta N/N$. For a magnetic field-aligned enhancement the excess density ΔN may be imagined to be distributed in a gaussian shape transverse to **and** centered on a guiding field line. In such a case the transverse "size" of the irregularity will depend upon the frequency of the probing radiowave; the higher the frequency the smaller the apparent size. Furthermore, it is apparent that at a given frequency the size will depend upon the intensity of the irregularity; with large ε the transverse size will appear larger than with small ε.

With this background in mind, it is not surprising to see reports (reviewed by Herman, 1966) of 10-meter (m) irregularities observed on 50 MHz, 200-300 m sizes deduced from 20 MHz satellite scintillation measurements, and 1400-4000 m sizes from topside sounder results in the 1-15 MHz frequency range. The sizes of small-scale, field-aligned irregularities of importance to Polar Fox II measurements lie in the range of a few hundred meters to a few kilometers.

Deductions of irregularity intensity from past ground-based and topside radio measurements indicate that ε magnitudes of a few

percent ($\tilde{<}$ 10%) are adequate to produce spread echoes (Herman, 1966).
In situ measurements in polar regions by Alouette 2 (Dyson, 1969)
have shown magnitudes of $\Delta N/N$ ranging up to 70% in irregularities
with widths less than 2 km. Explorer 20 observations combined
with simultaneous auroral backscatter measurements at College,
Alaska (Lund, et al, 1967) indicate that 200 to 500% enhancements
in electron density with scale sizes of 1 to 10 km may occur in
the vicinity of the auroral oval.

With these ranges of irregularity sizes and intensities as
observed in the polar ionosphere, one may anticipate backscatter
echoes on the Polar Fox II radar having a range of amplitudes
over a period of time.

2.2 SPREAD-F HEIGHT DISTRIBUTION

Ionospheric irregularities leading to spread F and spectral
spread are principally an F-region phenomenon. Strong backscatter
echoes may be observed from E region heights as well as the F
region, and radiowave scintillations on radio star signals may
be produced by irregularities in the height range 100 to 1000 km
(c.f., Herman, 1966). This section is concerned with F-region
irregularities.

Past observations utilizing 20 MHz satellite scintillations
suggest irregularity height distributions maximizing at about 300 km
(at or just below the F-region peak height) over Australia. The
irregularities appear to be distributed over the height range

3

270-320 km over England, 300-325 km over the United States, 280-360 km over Russia, 300-500 km over Norway in high latitudes, and 250-640 km over College, Alaska. The Alaskan results indicate an equal probability of occurrence at all altitudes in the 250-640 km range. The high latitude observations (Norway and Alaska), showing greater altitudes of occurrence compared to the lower · latitude results imply that the field-aligned irregularities are more strongly developed and extend to greater heights in auroral regions.

Backscatter HF sounding techniques used at College, Alaska, have revealed a height range from about 250 km to 400 km. The bottom of the height distribution thus appears to be at about 250 km on the basis of radar backscatter and scintillation observations in the night sector of the auroral oval.

If we consider that precipitating energetic electrons are responsible for the production of spread-F irregularities by direct ionization, it is clear (from Figure 1) that electrons of initial energies less than about 1 keV will deposit their energy in F-region heights, from 150 km upwards depending on initial pitch angle. The lack of observed irregularities below 250 km implies that a simple model involving only the direct production of ion pairs by precipitating particles is insufficient; the effect of secondary electrons and the loss processes due to recombination and attachment in the ionosphere must also be accounted for as a function of height. Relying upon observational evidence only, we

tentatively conclude that F-region irregularities of importance
to Polar Fox II exist in heights of 250 km up to the peak of the
F layer.

Since the reflection height of an incident signal decreases
as a function of frequency, it should be possible to select
observing frequencies to minimize the effect of F region irregu-
larities. That is, frequencies selected to reflect below an
altitude of about 250 km should at times have less spectral
spread than higher frequencies reflecting from greater heights.
This rather heuristic argument is supported by vertical incidence
ionosonde observations. For example, the ionogram trace illus-
trated in Figure 2, taken at Godhavn during spread F conditions,
exhibits spread echoes only near the peak of the layer (i.e.,
within about 2 MHz of the penetration frequency). At the lower
frequencies no spread is evident, so an oblique signal having an
equivalent vertical frequency less than about 4 MHz in this parti-
cular example should suffer relatively little spectral spread.

It is not always possible to utilize this downward frequency
shift to avoid spreading, however, because spread F ionograms
taken at polar stations frequently are spread over the whole
range of observable frequencies from fmin to foF2. The occurrence
statistics of completely spread ionograms are presently unavailable,
so a determination of the fraction of time that spectral spread
may be avoided even under otherwise "spread F conditions" cannot
be made here. Thus, a portion of the analysis effort in Polar Fox II

should be devoted to determining the extent to which spread F
effects can be avoided by judicious frequency selection. .

2.3 Velocities And Motions Of Ionospheric Irregularities

The production of spectral spread on signals passing through
or backscattered from an irregular F region can be considered to
depend upon real or apparent motions of reflection points and
scattering surfaces in the ionosphere. Physical mechanisms under-
lying these movements include wavelike disturbances (possibly
acoustic-gravity waves) propagating through the medium, bulk
motion of ionization irregularities, and shifting reflection-
point location through the appearance and disappearance of short-
lived ionization enhancements.

Since a frequency spectrum is derived mathematically by
transformation of the signal from the time domain to the frequency
domain, a spread spectrum is produced by rapid signal amplitude
and phase fluctuations within the sampling period. Such fluctu-
ations in the signal are produced by short-period variations in
the propagation medium.

Wavelike disturbances propagating horizontally through the
ionosphere travel typically at acoustic velocities; about 300 m/sec.
The wave front can be considered as large compared to a probing
HF radar signal, so that a coherent echo having a doppler shift
proportional to the wave velocity would be expected. Recent observa-
tions by Davis and daRosa(1969) at Stanford Research Institute
indicate that acoustic waves may be generated within the auroral oval
and then propagate equatorward. The wavefronts extend along geomagnetic
parallels, with a long dimension up to 1000 km. The location of

6

the Polar Fox II radar, being south of the auroral oval, provides

favorable geometry to investigate the passage of these waves.

Because the doppler shift (Δf_1) imposed on a signal is proportional

to the ionospheric wave velocity component in the direction of

signal propagation, spectrums obtained at different azimuths would

exhibit different Δf's according to the orientation of the wavefront

with respect to the Polar Fox II radar site.

Bulk motion of ionization irregularities, i.e., an actual

transport of electron density inhomogeneities, seems to be an

unlikely candidate for producing spectral spread, or indeed, large

doppler shifts in received echoes, since the associated velocity

appears to be of the order 20 to 100 m/sec (See Section 3.2). Further-

more, it is not clear whether or not bulk motion of ionization "blobs"

over significant distances, in fact, takes place; past observations

may be indicative, rather, of a movement of the ionizing source

whose origin is in the magnetosphere.

The third physical process hypothesized above, that is,

appearance and disappearance (scintillation) of short-lived

reflection regions within a range gate and azimuth sector, would

lead to a whole spectrum of phase path lengths fluctuating with

time. The doppler shift imposed by this mechanism is

$$\Delta f = - (f/c) \left(\frac{dP}{dt} \right) \tag{2.1}$$

and since the change in path length ($\frac{dP}{dt}$) of the signal at

frequency f can be large, large Δf's can be expected. Additionally,

the scintillation (as used here) of scattering centers at arbitrary locations within the radar field of view would lead to a range of values of dP/dt and, therefore, a spectrum of Δf's. With such scattering centers appearing and disappearing with approximately equal intensities ($\Delta N/N$) one could expect a relatively flat, broadly spread spectrum, if the effective mean lifetime(as defined below) of each center were less than the integration time utilized in deriving the spectrum.

Effective mean lifetime of scattering centers is established in two ways: (1) geometrically, by the length of time that a center is favorably oriented for scattering of the observed signal or is in the field of view; (2) by the time span that the inhomogeniety actually exists. DeBarber and Ross (1966) have deduced lifetimes of about one second for equatorial spread-F irregularities from amplitude fading measurements, and the apparent velocity associated with the spectrum was about 1000 m/sec.

Assuming a random distribution of scattering centers having a mean lifetime T within a radar gate width W, it can be hypothesized that as the scatterers appear and disappear the maximum excursion in phase path length will be:

$$\left(\frac{dP}{dt}\right)_{max} \approx \frac{W}{T}$$

(2.2)

Also, since the scatterers scintillate throughout the range gate width, dP/dt can take on all proportional values from 0 to W.

What this means is that the frequency spectrum will extend out to
a maximum given by

$$\Delta f = (f/c)\ (W/T) \tag{2.3}$$

For example, with f = 20 MHz, W = 15 km, and assuming T = 1 sec,
in a situation where the whole field of view of the radar is filled
with spread F irregularities leading to slant F echoes, the maximum
spectral width would be 1000 Hz.

Based on consideration of field-aligned-electron diffusion,
Lund et al (1967) predict lifetimes for the coherent structure of
auroral F-region irregularities of up to about 30 sec. If this be
the case, the spectral width of the above-cited example would be
33 Hz. Polar Fox II measurements have revealed flat spectrums con-
siderably in excess of 30Hz at times, so the lifetime of the
causative irregularities in those cases must be less than 30 sec
according to the above argument.

Direct F echoes may stem from strong ($\Delta N/N$ = 200 to 500%),
field-aligned irregularities imbedded in a region of less-intense
spread F as described by Lund et al (1967). Because the strong
irregularities would have a longer lifetime, one could expect to
see in the corresponding spectrum a large amplitude peak (at a Δf
associated with any actual motion of the strong irregularity) super-
posed on a flat background generated by the weaker slant-F irregu-
larities within the range bin of measurement.

It would be interesting to see the effect of narrowing the
Polar Fox II range gate on the spectral shape and width at times
when spread F is present.

9

3.0 Ionospheric Troughs

3.1 Background

Examination of ionospheric trough characteristics has demonstrated that this basic high-latitude ionospheric feature can have marked effects on HF radio propagation in polar regions (Herman and Vargas-Vila, 1971). The main trough is a region of very low electron density compared to the ambient density; it is only a few degrees wide in latitude but may extend several thousand kilometers in the magnetic east-west direction on the evening and night side of the earth. Other general features of the trough and its historical development have been discussed in the report by Herman and Vargas-Vila (1971).

The present investigation has revealed a close association between the trough, spread F occurrence and magnetic activity. This interrelationship and its relevance to Polar Fox II are discussed in this section.

3.2 Motions and Variation with Magnetic Activity

Rycroft and Burnell (1970) have recently demonstrated that the best measure of magnetic activity for use in correlations with ionospheric troughs is the K_p index. Although the AE (Auroral Electroject) index is nearly as good, it is less readily available than K_p data. The good correlations with K_p found by Liszka (1967), Rycroft and Burnell (1970) and Muldrew (1965) are indicative of a close association between

trough movement and solar wind velocity.

Muldrew (1965) has shown that the main trough position moves southward (in the northern hemisphere) with increasing magnetic activity, at a rate of approximately 3.5° latitudinal shift per unit increase in K_p (Fig. 3). The appropriate trough center positions in G/T space for $K_p = 0$ through 4 adapted from Jelly and Petrie (1969) and Muldrew (1965), are sketched here in Fig. 4. At a fixed station (-62.6° geomagnetic latitude in the Antarctic), Bowman (1969) has observed that the "onset time" for appearance of the trough overhead is earlier on magnetically active than quiet days. This observation is consistent with the picture in Fig. 4, wherein it is seen that the trough reaches a latitude of 62.6° at about 2000 LT when $K_p = 2$ and 1700 LT when $K_p = 4$.

As a fixed point on a latitude equatorward of the trough rotates beneath the sun-oriented pattern in Fig. 4, it is obvious that there will be a relative motion of the trough toward the observing point. Apparent horizontal velocities of this motion have been derived from vertical incidence ionograms by measuring the change in range of oblique echoes as a function of time. The oblique echoes are assumed to be reflected by the edge of the approaching trough, as suggested by Stanley (1966). Ansari's (1963) results

11

indicate apparent horizontal velocities of 20 to 170 m/sec over College, Alaska; Herman's (1966) give 30 to 105 m/sec over Churchill; and Mirkotan's (1962) range from 80 to 180 m/sec over Russia. For strict comparison these velocities would have to be converted to the velocity component perpendicular to the trough alignment relative to the observing point. Bowman (1969) has done this, and he finds speeds of 60 to 160 m/sec, with an average of 111 m/sec.

Apart from the apparent motion observed at a fixed station, the mean position of the whole trough travels equatorward with increasing magnetic activity. The addition of this latitudinal movement in G/T space to the apparent motion would yield a higher total horizontal speed during magnetic disturbances than during quiet periods. Bowman (1969) has found that this is in fact the case.

HF echoes from the edge of the trough and signals passing through the trough region will be doppler shifted in frequency due to the above-described bulk motions; the shift will be somewhat larger with high K_p, but at worst will probably be only a few Hertz in the HF band. The main impact of trough dependence on magnetic activity centers on the possible discrepancies in range and azimuth introduced by refractive effects as a function of relative orientation of the trough with respect to the experimental site. This impact can be assessed by appropriate ray tracing calculations.

3.3 CORRELATIONS WITH OTHER PHENOMENA

It is obvious that ionospheric troughs are not the only circumpolar phenomena. There are, in addition, the auroral oval, particle precipitation zones, sporadic E, and riometer absorption patterns, as well as spread F occurrence patterns, (Herman and Vargas-Vila, 1971). All these various phenomena are related to magnetospheric processes and magnetic activity, and the trough is apparently no exception. The main trough, is, however, the most equatorward of all (Akasofu, 1968), so perhaps it should be regarded as the absolute boundary of all polar and auroral ionospheric phenomena.

Muldrew (1965) suggested a close association between the main trough and "Carpenter's Knee" (Carpenter, 1963) and Rycroft and Burnell (1970) have shown statistically that the centers of the two observed phenomena lie precisely on the same L shell. The Knee, first discovered through whistler studies (Carpenter, 1963; 1966), is now recognized as the "plasmapause" dividing the inner plasmasphere, where the electron density is in approximate diffusive equilibrium, from the outer magnetosphere, where small scale irregularities in the density distribution are found and energetic particle precipitation in the loss cone takes place. Projected along field lines to ionospheric heights in G/T space, the plasma-pause coincides with the main trough position, and according to Rycroft and associates, it maintains that coincidence at all levels of magnetic activity.

It appears that poleward of the trough, ionospheric effects due to interactions between outer magnetospheric processes and the ionosphere take place. Thus, spread F , the auroral oval, sporadic E and auroral absorption are all above the main trough. Since the trough moves equatorward with increasing magnetic activity, so in concert should the lower boundaries of the various auroral phenomena also move.

To compare the average auroral oval position with that of the main trough as a function of magnetic activity, it can be assumed that equal values of K_p and Q represent a similar degree of magnetic activity. Although the latter is a measure of local activity and K_p is worldwide, the assumption is valid for the statistically averaged trough and oval positions considered here.

Now, at 0200 magnetic local time the equatorward boundary of the auroral oval as depicted by Whalen (1970) is at 70.5°, 65.5° and 63° corrected geomagnetic latitude for Q = 0, 2 and 4 respectively. From Fig. 4 it is evident that the trough is equatorward of these oval positions by 3.5°, 6.5° and 12° latitute for K_p = 0,2 and 4, respectively. This comparison indicates that as the planetary magnitudes k_p index increases from 0 to 4, the plasmapause moves inward from $L\sim7$ to ~2.6 in the night side and the hard electron precipitation boundary mapped by the auroral oval position correspondingly moves from $L\sim9$ to ~4.8. Thus the magnetospheric processes

remain separated by about 2 earth radii (Re) in L space
even though the latitudinal separation of their
consequences at ionospheric heights increases from about
3.5° to 12° for an increase in K_p from 0 to 4.

The importance of this finding to the Polar Fox   II
experiment is that consideration of the auroral oval alone
is insufficient to predict the time and space variations
of all ionospheric effects on the HF radar signals,
especially during disturbed periods. It is shown in the
next section, for example, that spread F irregularities
occur in a region well to the south of the auroral oval
boundary.

3.4 SPREAD F AND IONOSPHERIC TROUGHS

For many years evidence suggesting a close association
between the main trough and spread F occurrence has been
accumulating, but it has not heretofore been interpreted as
such. Here we re-examine that evidence to show a very
close link between the two phenomena.

A study by Stanley (1966) based on ionograms taken at
College from 1964 to 1966 established that a certain type
of oblique echo is caused by reflections from the edge of
the main trough located at some slant range from the
observing stations. This type echo has been referred to
variously as a "replacement layer" (Bellchambers, et al,
1962), "extra traces" (Vaughn Agy, 1950, unpublished),
"moving ionospheric disturbance" (Ansari, 1963), "travelling

15

reflection" (Herman, 1966) and "oblique echo" (Stanley, 1966).

Typically, the travelling reflection first appears on
an otherwise quiet ionogram at a greater apparent range than
the echo trace made by reflection from the overhead quiet
ionosphere. In succeeding ionograms the oblique echo moves
closer in apparent range until, over a period of an hour or so it
reaches a virtual height consistent with the overhead ionosphere
(Herman, 1966). Stanley (1966) interpreted the echo as
coming from the poleward side of the main trough, and showed
that when it passed over the observing station the critical
frequency decreased dramatically as would be expected
with the trough directly overhead. Bowman (1969) observed that
in addition to the decrease in foF2 the virtual height (h'F)
of the F layer is much higher in the trough than outside.
Unpublished work by Agy in 1950 had already shown the
correlation of extra trace appearance with decreased foF2 and
increased h'F, but the association with the main trough was
not made at that time.

That spread F irregularities appear within or just
poleward of the trough was demonstrated indirectly by
Herman's (1964, 1966) analysis of one year of Churchill
ionograms which showed that spread F invariably developed
when the travelling reflection (signifying the arrival of
the trough overhead) reaches the observing station. A smaller
sampling of Anchorage ionograms gave the same result . Two
examples of trough approach toward Ellsworth, Antarctica

16

given by Bowman (1969) are both followed by spread F development
on subsequent ionograms. Aircraft ionosonde measurement of
F-layer reflections on flights transverse to the main trough
invariably detected pronounced spread F on the poleward side
of the trough (Gassmann, 1971).

Less direct evidence which nevertheless qualitatively
implies an association between the main trough and spread F
is the pronounced inverse correlation between spread F
occurrence and the magnitude of foF2 over a fixed high
latitude station (Singleton, 1962a, b); that is, the
occurrence probability increases with a decrease in foF2, and
moreover, Singleton found that h'F increased at the same time.
The similarity of this behavior of foF2 and h'F with the
arrival of the trough suggests that Singleton's result can
be interpreted as a direct correlation between spread F
occurrence and the main trough appearance.

From the foregoing evidence it appears certain that
the arrival of the main trough over an observing station signals
the onset of spread F.

Since the mean position of the main trough shifts equatorward
with increasing magnetic activity (Section 3.2), it can now
be argued that the region of F-region irregularities spreads
equatorward in concert. To examine this argument in detail,
it is of interest to compare the trough positions depicted in
Fig. 4 with the spread F contour maps presented by Herman and
Vargas-Vila (1971). For the moment let us restrict ourselves to the
"auroral oval component" of spread F occurrence as reproduced in Figs 5,

17

and 7 for autumn (Sept), winter (Jan) and summer (July) respectively.

As discussed earlier (Herman and Vargas-Vila,1971), these occurrence-percentage maps were generated without regard to the degree of magnetic activity; rather they represent the percentage of time during the month in each hour that spread F was observed. For comparison with the main trough mean position at different K_p levels, then, it is necessary to determine the spread F boundary positions(% contour lines) as a function of K_p, also.

Previous single -station analyses (c.f. Herman, 1966 Shimazaki, 1962) have established a strong positive correlation between high-latitude spread F occurrence and magnetic activity. This result implies that the probability of spread F occurrence should match that of magnetic activity and it leads to the following analysis.

Mean daily magnetic activity levels ($\bar{K}_p$) were derived from reported values of $\Sigma K_p/8$ for all days in 1968 and 1969 for the months of September, October and November (180 data points) for Autumn; December, January, February (Winter); and June, July, August (Summer). For each season a cumulative probability distribution showing the percentage of time each $\bar{K}_p$ level was exceeded was computed (Fig8.)

From these distributions the $\bar{K}_p$ value corresponding to each spread F contour level(20, 40, 60 and 80%) was extracted. Then, straight line interpolations were made in Fig. 4 to determine the main trough mean position corresponding to those $\bar{K}_p$ values.

The results of this procedure tell us two things: (1)
it gives the mean level of magnetic activity associated with
the spread F region encompassed by a given % contour level, and
(2) it implies the fraction of time that the main trough can
be found in a given position.

The salient results for September are depicted in Figures
9, 10, 11 and 12, for spread-F occurrence contours of 80, 60,
40 and 20% respectively. The corresponding trough position
(Figure 4) for the $\overline{K}p$ associated with each contour level (Figure
8) is mapped in Figures 9-12 by broken lines. For comparison the
Feldstein oval of visual aurora occurrence at each magnetic
activity level (assuming $\overline{K}p \propto Q$) is also given.

It is vividly evident in these maps that as magnetic activity
increases the spread-F southern boundary migrates equatorward
in concert with the migration of the trough.

The auroral oval also expands with increasing magnetic index,
but its southern boundary is poleward of the spread-F and trough
lines by 3° to 8° geomagnetic latitude; maximum separation occurs
at the largest magnetic index.

The latitudinal position of the spread-F boundary is prac-
tically coincident with the main trough position for all levels
of magnetic activity and all times depicted in Figures 9-12
except for a portion of the time in Figure 9. It is possible that
the trough develops much later in the local evening and disappears

19

earlier in the morning in periods of extreme magnetic quiet compared to more active periods (Muldrew, 1965; Rycroft and Burnell, 1970). Thus, the lack of correspondence between the trough and spread-F positions before 00 LT and after 02 LT in Figure 9 may not be real; on the contrary, the trough may not exist outside the 00-02 LT period on very quiet days.

A similar comparison (not shown) using the Winter and Summer spread-F contours (Figures 6 and 7) shows equally good correspondence with the main trough positions except for quietest times (80% contour) in Summer. Again, there are little Summer trough data available (Muldrew, 1965), so the Summer exception is not considered to be serious.

The exceptionally good agreement between the trough position and spread-F boundaries found in this study is somewhat surprising in view of the large number of assumptions, interpolative smoothing processes (in the spread-F maps), statistical averaging and lack of time coincidence (not months but years) that underlie the basic data utilized. However, because such good agreement emerged despite the drastic limitations, it is safe to conclude that spread F is almost invariably found immediately poleward of the main trough at all levels of geomagnetic activity in mid-solar cycle years.

These results indicate that it should be possible to define the position of the spread F boundary at any time on the basis of

the level of magnetic activity, and specific Polar Fox II observations can thereby be integrated quickly without necessarily awaiting statistical results of long-term measurements. This concept is applied in the next section to a particular period in April, 1971.

3.5 CASE STUDY OF APRIL 6, 1971

The particular period 0100-0400UT, April 6, 1971, was selected for illustration partly because it coincides with SRI radar observations exhibiting unusual features (John Ames, private communications). The Kp 3-hour range indices were 3+ and 4- for 00-03UT and 03-06UT, respectively (Lincoln, 1971), and $\overline{Kp}$ for the day was approximately 2+ or 3-.

Assuming the September spread-F maps to be applicable to April, we see (Figure 12) that the 20% contour would represent the spread F boundary on April 6. The spatial distributions of spread F for 00UT and 03UT are shown in Figures 13 and 14, along with the locations of the following vertical incidence ionosonde stations in operation that night:

MH - Millstone Hill

OT - Ottawa

SJ - St. Johns

NS - Narssarssuaq

GD - Godhavn

At 00UT, both Ottawa and Millstone Hill are south of the 20% contour boundary, while SJ, NS, and GD are all within the region of expected spread F. At 03UT (Figure 14), the Earth has rotated beneath the spread F pattern so that now all of the stations except MH are in the spread F region. Thus, throughout the 01-04UT period of interest, no spread F is expected at Millstone Hill, and it should be present at SJ, NS and GD. Ottawa, on the other hand, should see spread F develop sometime between 00UT and 03UT.

22

Inspection of all ionograms taken at 15 minute intervals at these five stations between 01UT and 04UT completely bear out the prediction. (Millstone Hill ionograms are courtesy of Dr. J. V. Evans; the others were obtained from World Data Center A.) That is, Millstone Hill recorded no spread F but St. Johns, Narssarssuaq and Godhavn had spread conditions throughout the period. Ottawa was free of spread F until about 0230UT, at which time an oblique echo from the edge of the trough was observed, and light spreading of the main traces developed (Figure 15a). Following this time, spread F intensified over Ottawa until at 0330UT (Figure 15b) the spread was complete. Note also the decrease in critical frequency (fxF) from about 7.4 MHz to 6.3 MHz in this time interval, signifying the arrival of the trough overhead Ottawa. Oblique UHF observations at Millstone Hill at 0121 and 0321UT detected scintillations beginning at ranges within $\pm 2°$ latitude of the predicted spread F boundary.

The excellent agreement between prediction and observation found in this case study lends strong credence to the prediction method, although the possibility of fortuitous agreement cannot be completely ruled out. It does appear, however, that Polar Fox II data may be fruitfully analyzed and interpreted in this light.

23

4.0 Auroral Absorption

4.1 Introduction

Radio Waves propagating through the polar ionosphere
may experience some four distinct kinds of abnormal absorption
in addition to the normal nondeviative absorption. These four
characteristic types of absorption are related to certain major
solar flares, specifically those occurring in the vicinity of
magnetically complex sunspots. The first absorption effect of a
solar flare would be Sudden Cosmic Noise Absorption (SCNA), which
occurs as a result of solar x-rays generated when the flare
erupts. Next Polar Cap Absorption (PCA) may occur from very
energetic solar cosmic ray particles, which are ejected with the
erruption of the flare and take about one to two hours to reach
the earth. Then Sudden Commencement Absorption (SCA) may be
observed as a result of the interaction of the earth's magneto-
sphere with the shock-front that preceeds the flare ejected solar
plasma cloud. Finally, the occurrence of Auroral Absorption (AA)
takes place when the solar flare ejected plasma cloud impinges
upon the earth some 20 to 40 hours after the onset of the flare.

Although the occurrence of AA has been related to solar
flare phenomena, it is also observed at other times. In fact,
AA is the dominant type of absorption observed at auroral
latitudes. AA has been observed to exhibit a definite recurrence
pattern with a period of 27 days, suggesting that it is also
related to solar "M" regions. M-regions are associated with

24

solar corpuscular radiation but are not necessarily the source
of these particle streams which travel through interplanetary
space and bombard the earth, and are responsible for the
particle precipitation which generates AA. This report is solely
concerned with AA and a means for estimating its effect upon
high latitude radio circuits. Agy (1970), has presented a method
for computing the median level of absorption, while this report
presents a technique for calculating the absorption for any per-
centage of time up to the median.

Riometer observations form the basis for present day
continuous AA measurements. AA occurs in addition to normal
nondeviative D-region absorption, however, it is so much stronger
(AA can be as much as 10 db at 30 MHz) than normal absorption
that the observed absorption is essentially entirely auroral in
nature. AA is associated with local magnetic disturbances,
visible aurora, particle precipitation and magnetospheric substorms.
It reaches a distinct maximum in the auroral zone and decreases
poleward both in amplitude and probability of occurrence.
Generally, the magnitude of the attenuation is twice as much in
Winter months as it is in Summer, and it decreases by a factor of
two from sunspot maximum to minimum. AA events may last from a
few minutes to several hours with the median duration on the
order of 30 to 40 minutes. When AA is plotted as contours of
probability of occurrence in corrected geomagnetic coordinates

a diurnal variation is apparent with a pronounced maximum showing

about four hours before local geomagnetic noon and a small secon-

dary maximum occurring just before midnight. Absorption events

occurring before midnight are discrete events of short duration

compared to diffuse absorption events occurring during the morning

and lasting several hours. The discrete events coincide with

the splash type precipitating electrons of 10 keV while the diffuse

events agree in time with the drizzle type precipitating electrons

of 40 keV. Figure 16 (from Hartz and Brice, 1967) shows in

corrected geomagnetic coordinates the zones of these two types

of particle precipitation. The 10 keV electron precipitation

peaks between 2000 and 2400 local geomagnetic time while the 40

keV electron precipitation reaches a maximum between 0600 and

1000 local geomagnetic time. Although AA occurs in discrete

events these events may overlap in both space and time and are

characterized by the rapid and irregular variation of the cosmic

noise level as observed by riometers. This lends it to interpre-

tation by statistical analysis.

4.2 DATA BASE

The data used in this study were gathered over a period
of eight years and consist of maps giving the probability of
occurrence of auroral absorption events. Plotting of the maps
is done in corrected geomagnetic latitude and corrected geomagnetic
time. These maps were generated from observations of chains of
riometer stations located along three different longitudes.
Specifically the Alaskan data (Hook, 1967) shows the percentage
time occurrence of auroral absorption of 3 dB or greater, while
the Canadian and Norwegian data (Hartz, 1963) were used to
generate time percentage of occurrence maps of 1 dB or more and
0.425 dB or more auroral absorption respectively. These maps
are for vertical absorption at 30 MHz and are shown in Figures
17,18 and 19 (the Norwegian data was collected at 27.6 MHz and
corrected to 30 MHz by $1/f^2$).

Digitization of these maps was made to enable computer usage.
This was accomplished in the following manner; referring to
Fig. 17 for example, radials are chosen at intervals of spacing
determined by whether a given probability contour is constant
for a given geomagnetic latitude. Therefore, the spacing of
radials is not equal but is further apart if the probability
contour changes slowly for a given latitude. For example, many
more radials are needed in the interval between 1800 corrected

27

geomagnetic time (CGT) and 2000 CGT than in the interval from 0500 CGT to 0700 CGT. Enough radials, along which digitization is made, are chosen to preserve the fine detail of the maps. Points between radials are determined by linear interpolation. The maps were extended poleward on a linear scale from the contour of lowest probability to a value of zero at the pole. The data maps were not extended to lower latitudes.

All riometers used in the collection of the 1 dB data maps were pointing towards the celestial pole. This was done so that the riometers would be observing the same source all day long, and hence avoid any diurnal variation in the measurements. For this reason, it was necessary to multiply these data points by the sine of the geographic latitude in order to transform the data maps into equivalent vertical incidence absorption maps.

In addition to these absorption maps, median values of absorption were computed according to a method described by Hargreaves (1966). He reported on an analysis of two years of auroral radio absorption data. Since auroral absorption is essentially a random occurring phenomena which can change significantly over periods of a minute or so to periods of an hour or more, the data were reduced to extract statistical properties of auroral absorption. Statistical distribution of absorption values were determined for four different time sectors of the day, for three different riometer stations. Of these stations, one

was located near the maximum of the auroral oval, a second at a higher latitude and the third at a lower latitude. All the probability distributions show that each distribution is well represented by a power law above some minimum level of absorption. The results of this analysis over the ranges studies show that the probability of absorption can be represented by the following expression:

$$Q = K A_m^n$$

where Q = probability of absorption $\geq$ 1 dB

A_m = median level of absorption

and for the best fit of the observed probability distributions:

K = 22

n = 3.5

Hence the median auroral absorption can be expressed as:

$$A_m = [\frac{Q}{22}]^{\frac{1}{3.5}}$$

4.3 METHOD

A "fan" graph such as is shown in Figure 20 is first drawn, the apex of which is located at the transmitter site. Transmission to a given point in that fan graph defines a range and azimuth for the terminal point of the ray path. Propagation over a curved earth is assumed to take place by either a single hop F layer mode with a reflection height of 300 km or a one hop E layer mode with the reflection point

29

at a height of 110 km. Accordingly, two points, A and B are defined, see Figure 21. These points correspond to the areas where the ray passes through the auroral absorption region which in this case is assumed to occur at a height of 85 km. Points A and B then each define a range and azimuth for which the computer first calculates the geographic coordinates then the corrected geomagnetic latitudes. Then some time of interest is chosen from which the local corrected geomagnetic time is approximately given by:

$$LGT = UT + [\Lambda_c - 70°]/15$$

where LGT = Local Corrected-Geomagnetic Time

UT = Universal Time

Λ_c = Corrected Geomagnetic Longitude

Once having chosen the time, range and azimuth and making the appropriate coordinate transformation, then as will be described, cumulative probability distributions are calculated at each of the corrected geomagnetic coordinates corresponding to these two absorbing regions A and B. For a specified percentage of time the equivalent vertical incidence absorption is determined for both points.

In all cases it is assumed that the absorption at A takes place at the same time as it does at B. While the spatial correlation of AA is not precisely known, some

attempts have been made to describe it. Examination of
onset times of AA events indicates that these disturb-
ances originate from an apparent source at geomagnetic
midnight. They then travel at different velocities (on
the order of 1 to 3 km/sec) in different directions
around the auroral oval. Figure 22 gives an indication
of the progression of the median onset times in tens of minutes.
These curves were obtained by projecting along the mag-
netic field lines, measurements made near the South Pole
which were reported on by Hargreaves (1968). Other invest-
igations (Toman, et al, 1971) indicate spatial correlation
coefficients of 0.7 out to distances of 1000 km and more.
The assumption, therefore, that the absorption at A and B
occur in the same time domain, although not exactly true,
is generally valid, especially if A and B are close
together, in that auroral absorption is a relatively long-
lived phenomena lasting from maybe ten minutes to a few
hours, with a median duration of 30 to 40 minutes.

From the data maps and the calculated median
absorption previously described a set of cumulative
probability distributions are generated showing the
percentage of time that the occurrence of auroral absorp-
tion exceeded a given level of vertical incidence absorption
at 30 MHz. A probability distribution is made for each
coordinate of corrected geomagnetic latitude and time of

interest, of which Figure 23 is an example. Generation of these cumulative distribution curves is performed in the following manner. For each specified corrected geomagnetic latitude and time, the computer selects one value of probability from each of the three probability maps and calculates the median level of absorption. Interpolation between the time percentage of occurrence values is made on a logarithmic scale. Interpolation between levels of absorption is made on a linear scale. The result is a cumulative probability distribution where the end points are defined by the median value and points extracted from the 3 dB maps. No seasonal nor solar cycle variation was assumed as the data were smoothed over a period of several years.

Having specified a probability, the total path loss is determined from the cumulative probability distribution curves by the following expression:

$$L = [L_{v_{30A}} + L_{v_{30B}}] \sec\alpha \left(\frac{30}{f}\right) 1.8$$

where

L = Total path loss in dB

$L_{v_{30A+B}}$ = equivalent vertical incidence absorption at 30 MHz in dB for points A and B

f = The operating frequency in MHz

α = angle of incidence at 85 km height

32

A secant relationship is assumed between vertical and oblique passage through the D Region. To extend the computed absorption values to frequencies below 30 MHz a frequency dependence of absorption proportional to $(\frac{1}{f})^{1 \cdot 6}$ was assumed. This value was taken from Lerfald, et al (1964) who found a range for frequency dependence of auroral absorption from $(1/f)^{1 \cdot 4}$ to $(1/f)^{2 \cdot 2}$ Their distribution showed a maximum at $(1/f)^{1 \cdot 6}$.

This process is repeated as a function of range and azimuth after which contours of constant absorption are plotted on the "fan" graph. Separate absorption plots are generated as a function of frequency, time of day, E or F layer propagation and percent probability.

4.4 DISCUSSION

Sample range azimuth plots of radar auroral absorption are shows in Figures 24 through 47. By "radar" absorption it is meant that the calculated path loss has been doubled since it is assumed that the ground backscatter signal traces the same path (for forward propagation) back to the transmitter. Range coverage extends from 1000 km to 4000 km from the transmitter in the case of F layer propagation, and 500 km to 2200 km for E layer propagation. It should be remembered that the attenuation indicated is that component due only to AA. Normal D-region absorption as well as $1/R^2$ losses have been omitted.

33

Some of the gross features of the data are as follows:
For any given frequency the absorption is greatest at about
12 UT (07LT at transmitter site). This corresponds to the
time when the morning maximum is in the middle of the fan.
Similarly the absorption reaches a minimum for all
frequencies at around 2000 UT.For any frequency and time
the absorption is greatest in the northeast and northwest
sectors of the range azimuth fan. This is so because the
energy propagates along the AA zone in these directions.
For propagation paths transverse to the AA zones, the
attenuation increases going poleward away from the trans-
mitter. Generally speaking, the losses are relatively
small for frequencies above 20 MHz propagating via either
a one hop E layer or F-layer mode.

As was stated earlier, no seasonal variation was
assumed, therefore to obtain an estimate of the absorption
during Winter months, the plotted absorption values should
be multiplied by 1.33. For Summer months the plotted
values should be multiplied by 0.67. The 50% contours
would give the system designer a feeling for the "normal"
behavior of an HF communications system, while 10% contours
would give an indication of the required system sensitivity

in order to achieve effective communications for a specified
percentage of time, or to obtain a desired probability of
detection.

4.5 SUMMARY

A method has been described to compute the amount of
auroral absorption that would be observed by a high latitude
HF radio circuit. It incorporates data from three different
riometer networks, which is possible since the observed
distribution of absorption events is similar. The results
are presented as contours of constant absorption for a
specified percentage of time. These are useful aids for the
design of HF radar and communications circuits in high
latitude regions, in addition to being a valuable tool for
the analysis of high latitude propagation data and the inter-
pretation of excess losses. Absorption contours can be plotted
for any percentage of time up to the median.

5.0 Auroral Sporadic E

5.1 INTRODUCTION

Conversion of maps giving the probability of occurrence
of the top frequency of sporadic E (fF_s) for various frequencies
and conditions of magnetic activity as reported by Herman and
Vargas-Vila (1971) into plots showing the percent time that HF
radiowave propagation is supported by the occurrence of auroral
sporadic E (Es) in the Polar Fox II fan is the major effort dis-
cussed in this section. Generation of the fan plots is described
below and plots are shown at two hour intervals indicating as
a function of range and azimuth the percent time that E_s will
support the forward propagation of frequencies up to 30 MHz.
Basically these maps show that during the nightime hours the
occurrence of E_s is sufficient to support propagation of HF
radiowaves up to 50 per cent of the time at certain ranges and
azimuths. This can be quite significant especially during those
times when the maximum usable frequency provided by normal F
layer propagation might decrease, or if the sporadic E should
become blanketing.

5.2 METHOD AND RESULTS

To construct the range azimuth fan graphs showing contours of
per cent time that propagation at 30 MHz or less would be supported
by E_s, the following procedure was employed. The assumption that a

secant law relationship exists between vertical and oblique incidence reflections implies that sporadic E with a top frequency of 3 MHz or more denoted by $fE_s \geq 3$ MHz will support forward scatter propagation at frequencies up to 30 MHz at a distance of 2000 km when the E_s occurs at the path midpoint at a height of about 100 km. Assuming a flat earth geometry as depicted in Figure 48, the probability of occurrence of $fE_s \geq 3$ MHz is determined (as will be explained momentarily) at a range of 1000 km from the transmitter and plotted at the path end point (2000 km) for that particular azimuth. This process is repeated as a function of azimuth for some specific time of day.

Azimuthal distribution was determined by superimposing the range azimuth fan graph on the data base maps and recording, at a range of 1000 km, the percent time of expected E_s at a specified time, which is the time at the transmitter site. In order to determine the probability of occurrence of E_s at a particular location, the data points recorded from the superposition of the range azimuth fan graphs on the three data base maps for $fE_s \geq 3$ MHz were weighted and averaged. Weighting was made according to the cumulative probability distribution for magnetic activity shown in Figure 49. The value of percent occurrence of $fE_s \geq 3$ MHz for magnetically quiet days accounts for 33% of the average occurrence of E_s, for moderate magnetic conditions the values contribute 50% towards the average while the occurrence values for disturbed magnetic conditions are weighted to account for 17% of the average occurrence of E_s.

Next, the azimuthal distribution of the probability of occurrence of $fE_s \geq 6$ MHz is determined at a range of 500 km for the same time of day and plotted at the path and point. As can be seen in Figure 48, it is 1000 km from the transmitter in this case since the occurrence of E_s at a range of 500 km and a height of about 100 km with a top frequency of 6 MHz or more would support HF propagation up to 30 MHz at a range of 1000 km. The same procedure was followed as before including the determination of the average incidence of occurrence of $fE_s \geq 6$ MHz. Again using the same probability distribution of magnetic activity, maps of $fE_s \geq$ 9 MHz were weighted to give the average incidence of E_s at a range of 325 km which would support propagation of 30 MHz to a range of 650 km.

Finally, contours of equal probability were drawn showing the percent time that propagation of frequencies up to 30 MHz is supported by E_s as a function of range and azimuth for a specified time of day. Similar maps were made at two hour intervals for an entire day and are shown in Figures 50 through 58.

It should be noted that all types of E_s events were lumped together in the collection of data upon which this study is based. Specifically, night E is considered to be the same as sporadic E which is a good assumption in that they both have the same influence in supporting oblique incidence HF propagation. Also of importance is the fact that these E_s supported HF propagation predictions are based upon the top frequency of E_s (fE_s) which can be significantly different from the blanketing frequency of E_s ($f_b E_s$). The immediate implication of this is that it is possible for both E and F layer propagation to occur simultaneously.

38

A closer examination of Figures 50 through 58 reveals no E_s supported propagation at 30MHz from the hours of 1600UT through 2000UT. From 1200UT through 1400UT and from 2200UT through 00UT, the incidence of E_s supported 30MHz propagation is minimal,(10% of the time at ranges of 1500km and beyond). From 0200UT through 1000UT, HF propagation via the E layer is maximum, with the greatest amount occurring looking northward and slightly northwest, at the farther ranges, and the least amount occurring looking eastward at the shorter ranges. The physical explanation for this diurnal pattern rests on the temporal and spatial distribution of polar E_s which is auroral in nature and therefore, rotates through the radar fan throughout the course of a 24 day.

5.3 Summary

Auroral Sporadic E has a high enough frequency of occurrence for it to exert a significant influence upon the normal F layer propagation of HF radiowaves at high latitudes. This effect is greatest during the evening hours from about 0200UT to 1000 UT or approximately 2100LMT to 0500LMT when the critical frequency of the F layer decreases with the subsequent decrease in maximum usable frequency afforded by the F layer. While patches of sporadic E may completely disrupt F layer propagation they will also create new paths that will support HF radio transmissions.

Figures 50 through 58 show that HF propagation up to 30 MHz will be supported by E_s up to 50 percent of the time during the evening hours at the ranges and azimuths shown. Frequencies less than 30 MHz will propagate by the E_s mode for the amount of time shown or more. Daytime occurrence of E_s is not sufficient to support HF radiowave propagation for an appreciable amount of time in the range azimuth sector of the radar.

6.0 References

Agy, V., "HF Radar and Auroral Absorption," Radio Science Vol 5, No. 11, pp. 1317-24, Nov. 1970.

Akasofu, S.I., 1968, Polar and Magnetospheric Substorms, SpringerVerlag, New York, Inc.

Ansari, Z.A., 1963, J. Atmos. Terr. Phys., 25, p.210.

Bellchambers, W.H., Et al, 1962, Roy. Soc. IGY Expedition Halley Bay, D. Brunt, Ed., p. 179.

Bowman, G.G., 1969, Planet. Space Sci. 17, p. 777.

Carpenter, D.L., 1963, J. Geophys., Res., 68. p. 1675.

Carpenter, D.L., 1966, J. Geophys. Res. 71, P. 693.

Davis, M.J. and A.V. daRosa, "Traveling Ionospheric Disturbances Originating In The Auroral Oval During Polar Substorms" Journal of Geophysical Research, Vol. 74, No. 24, November, 1969.

DeBarber, J.P. and W.J. Ross, 1966, Chap. 2-7 in Spread F and its Effects Upon Radiowave Propagation and Communications, (P. Newman, Ed.) W and J. Mackay and Co., London, P. 357.

Dyson, P.L., 1969, J. Geophys. Res., 74, P. 6291.

Gassmann, G.J., 1971, Paper presented at ARPA/Air Force Review Meeting, Washington, D.C., March.

Hargreaves, J.K., "On the Variation of Auroral Radio Absorption with Geomagnetic Activity," Planetary Space Science, Vol. 14, pp 991-1006, 1966.

Hargreaves, J.K., "Auroral Motions Observed With Riometers: Latitudinal Movements and a Median Global Pattern," JATP, Vol. 30, pp. 1461-1470, 1968.

Hartz, T.R., "Multi-station Riometer Observations," Radio Astronomical and Satellite Studies of the Atmosphere, pp. 220-37, 1963.

Hartz, T.R., and Brice, N.M., "The General Pattern of Auroral Particle Precipitation," Planetary Space Science Vol. 15, p. 301, 1967.

Herman, J.R., 1964, Research on Spread F st : es AVCO Corp., Report No. RAD-TR-64-9.

Herman, J.R., 1966, Rev. Geophys., 4, p. .255.

Herman, J.R. and R. Vargas-Vila, 1971, Polar Fox II Study Phase, Final Tech. Rpt., RADC-TR-71-276.

Hook, J.L., "Morphology of Auroral Zone Radiowave Absorption In the Alaska Sector, " JATP, Vol 30, pp 1341-51, 1968.

Jelly. D.H., and L. E. Petrie, 1969, Proc. IEEE, 57. p. 1005.

Kamiyama, H., 1966, Rpt. Ionosphere and Space Res. Japan, 20, p. 374.

Lerfald, G.M., Little, C.G. and Parthasarathy, R., "D-Region Electron Density Profiles During Auroras," JGR, Vol 69, No. 13. July, 1964

Lincoln, J.V., 1971, J. Geophys. Res., 76, p. 5377

Liszka, L., 1967, J. Atmos. Terr. Phys., 29, p. 1243.

Lund, D.S., R.D. Hunsucker, H.F. Bates, and W. B. Murcray, 1967, J. Geophys. Res., 72, p . 1053.

Mirkotan, S.F., 1962, Geomag. Aeronomy English Transl. 2, p. 578.

Muldrew, D.B., 1965, J. Geophys. Res. 70, p. 2635.

Rycroft, M.J. and S.J. Burnell, 1970, J. Geophys. Res., 75, ρ. 5600.

Shimazaki, T., 1962, J. Geophys. Res., 67, p. 4617.

Singleton, D.G., 1962a, J. Atmos. Terr. Phys., 24, p. 871.

Singleton, D.G. 1962b, J. Atmos. Terr. Phys., 24, p. 885.

Stanley, G.M., 1966, J. Geophys. Res 71, p. 5067.

Toman, K., Cormier, R. and Corbett, J., "Spatial Correlation of Auroral Radio Absorption," AFCRL Environmental Research Paper, No. 372, Sept. 1971.

Whalen, J.A., 1970, AFCRL, Rpt. AFCRL-70-0422.
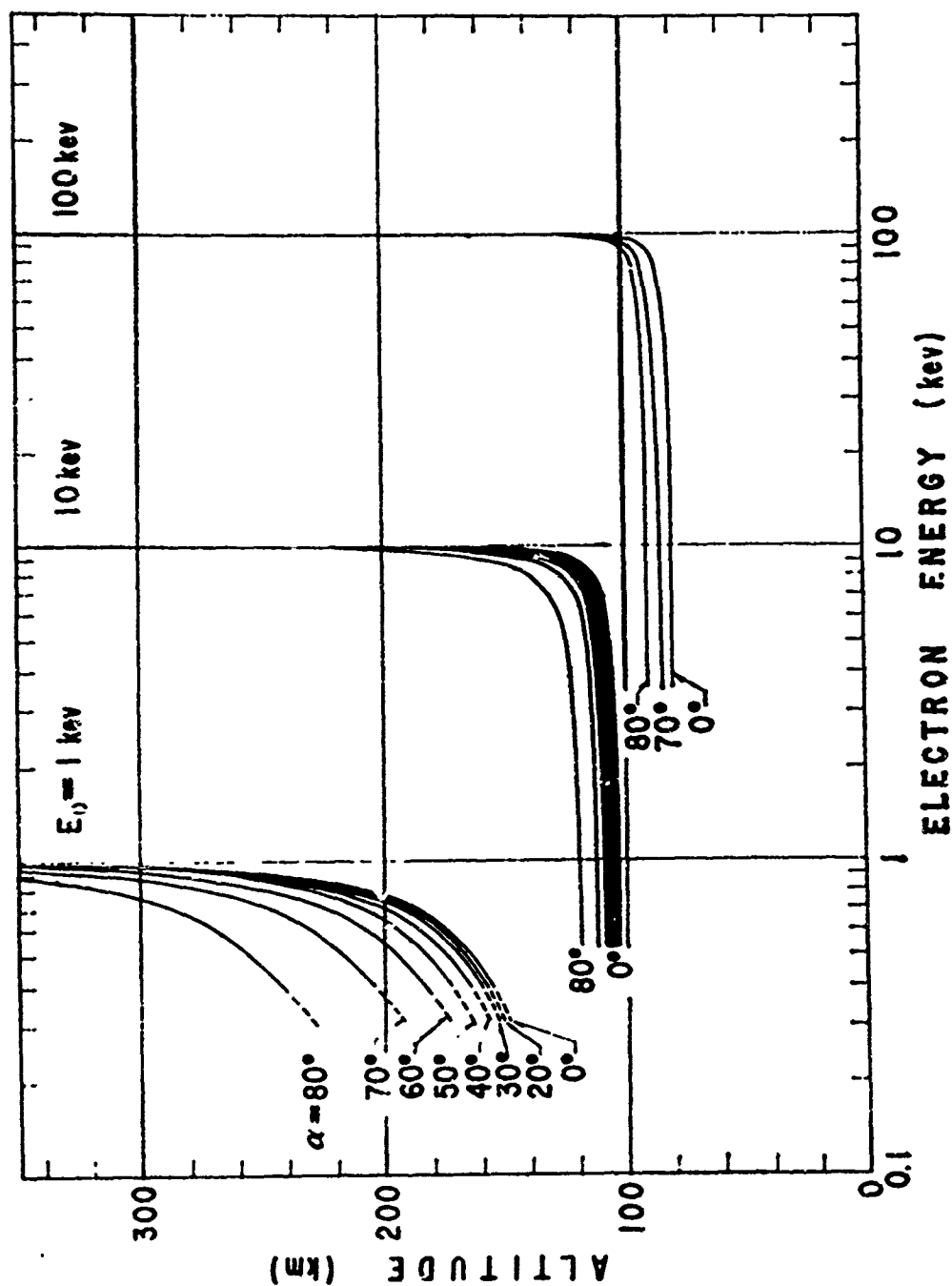
Energy of precipitating electrons shown as function of altitude for particular initial energies and pitch angles.

Figure 1 - Energy of precipitating electrons shown as a function of altitude for particular initial energies and pitch angles.
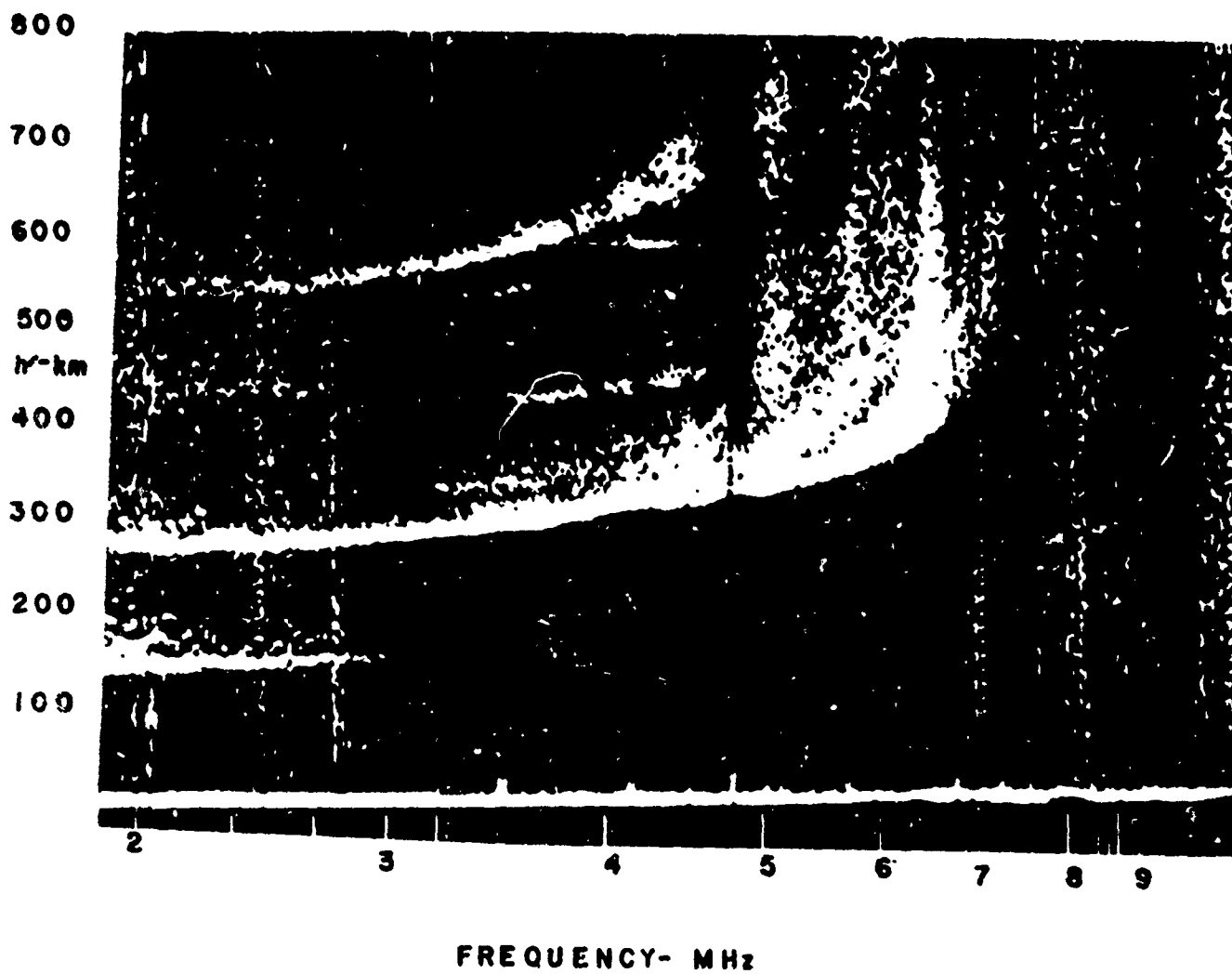
Figure 2.- Ionogram taken at Godhavn at 0100 U T, April 6, 1971 illustrating typical spread F occurrence
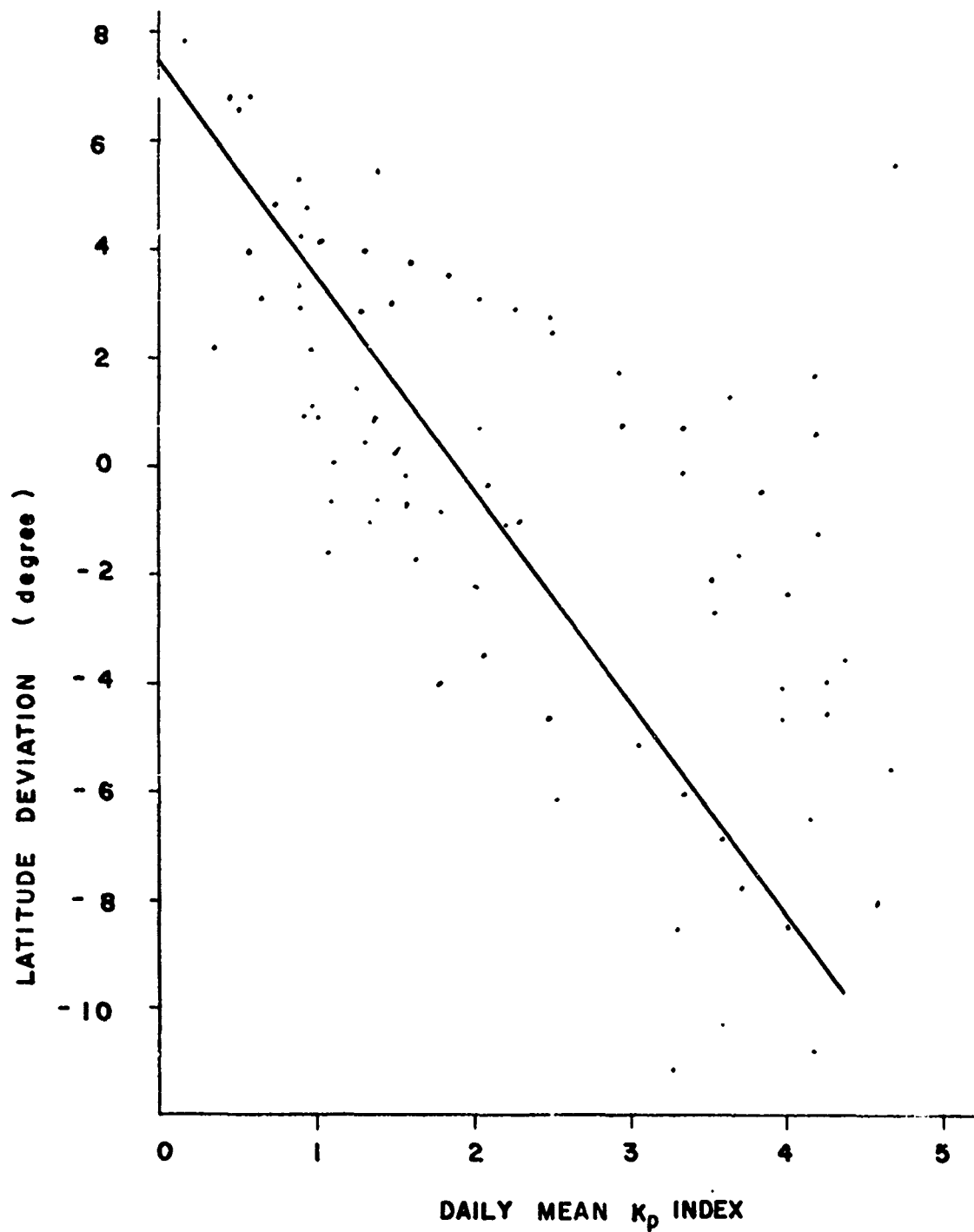
Fig. 3 Position of main trough center as a function of magnetic activity (K_p) after Muldrew (1965)

44
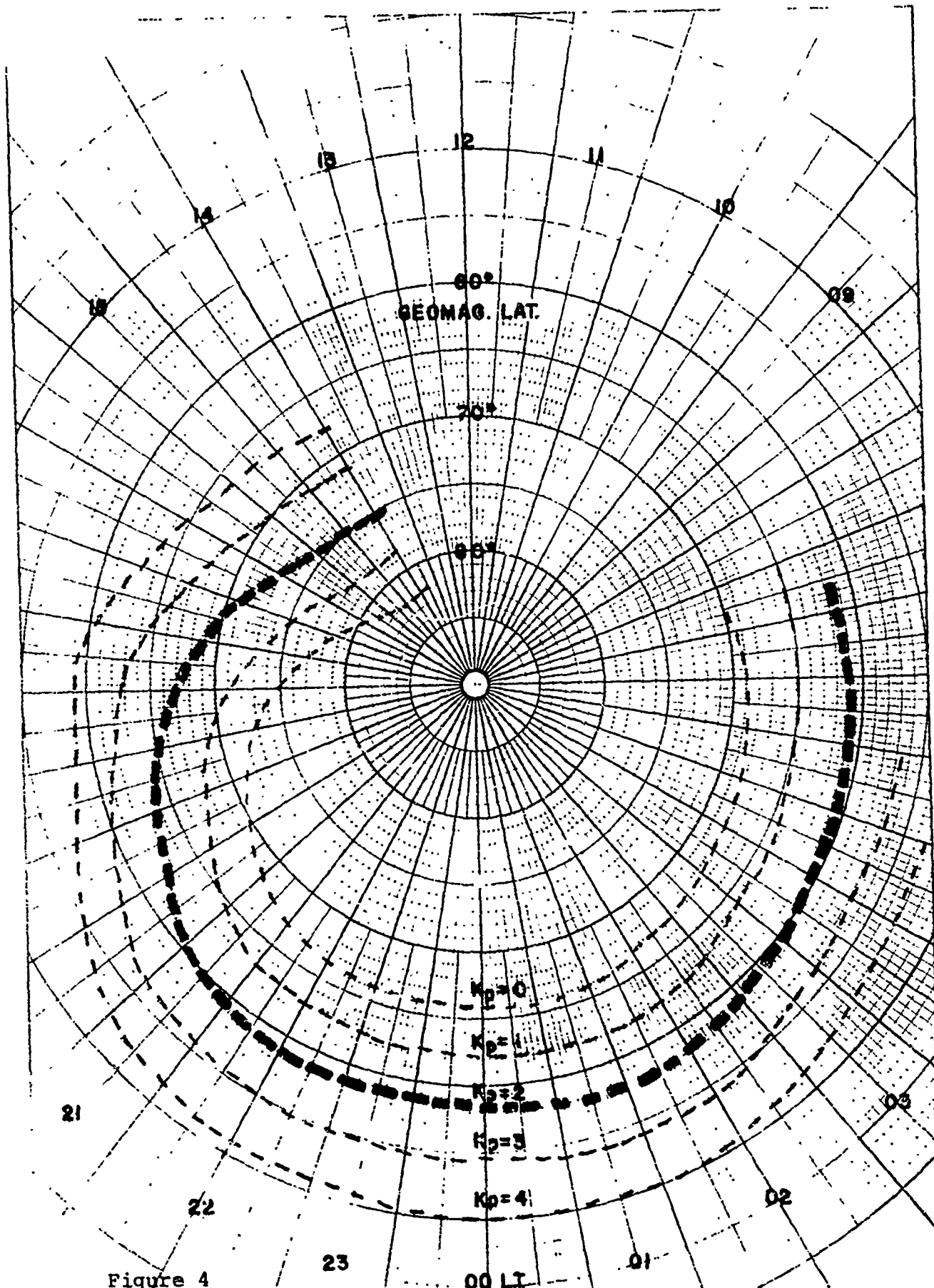
Figure 4
Mean Position of main ionospheric trough center as a function of magnetic K_p index.

45
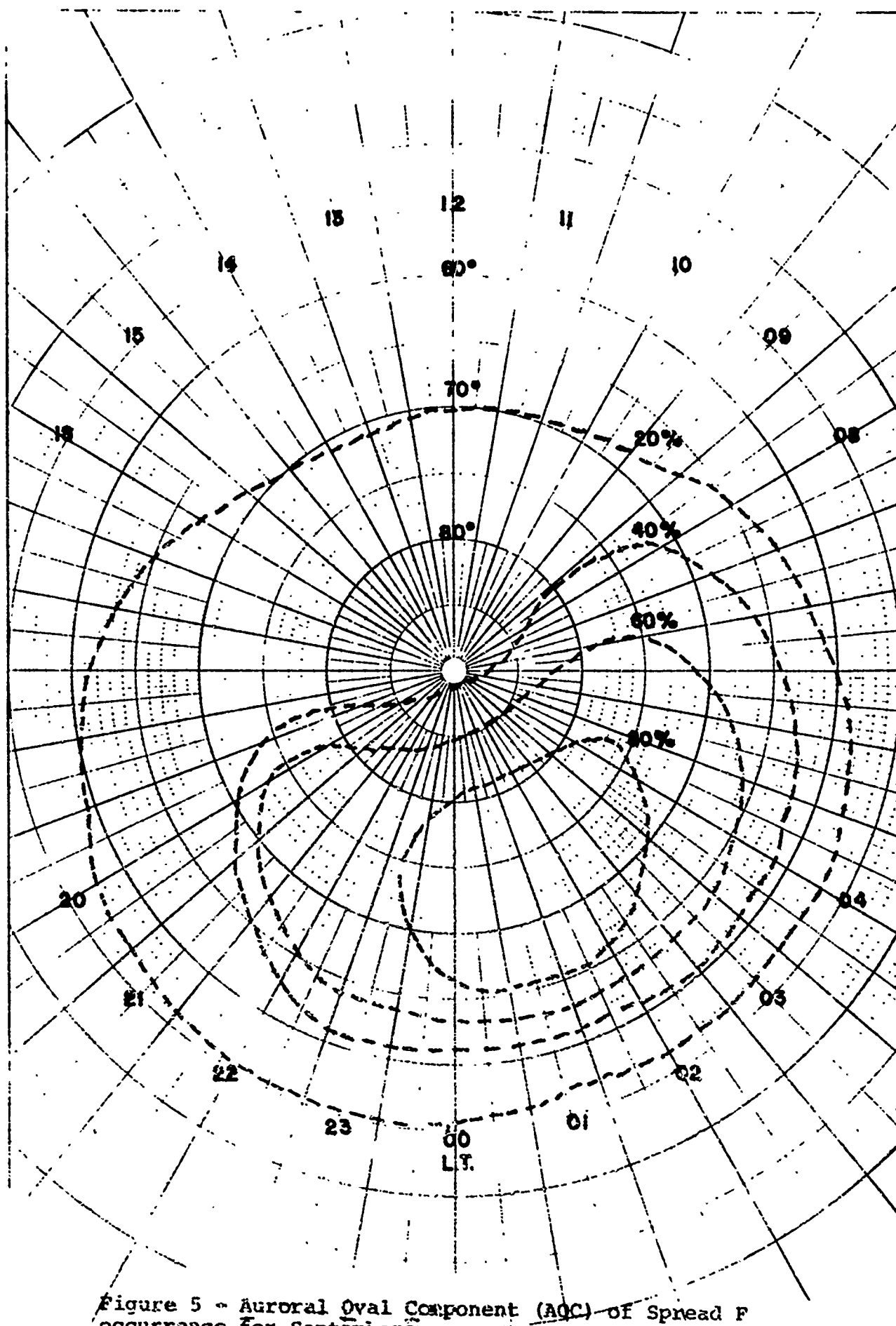
Figure 5 – Auroral Oval Component (AOC) of Spread F
occurrence for September
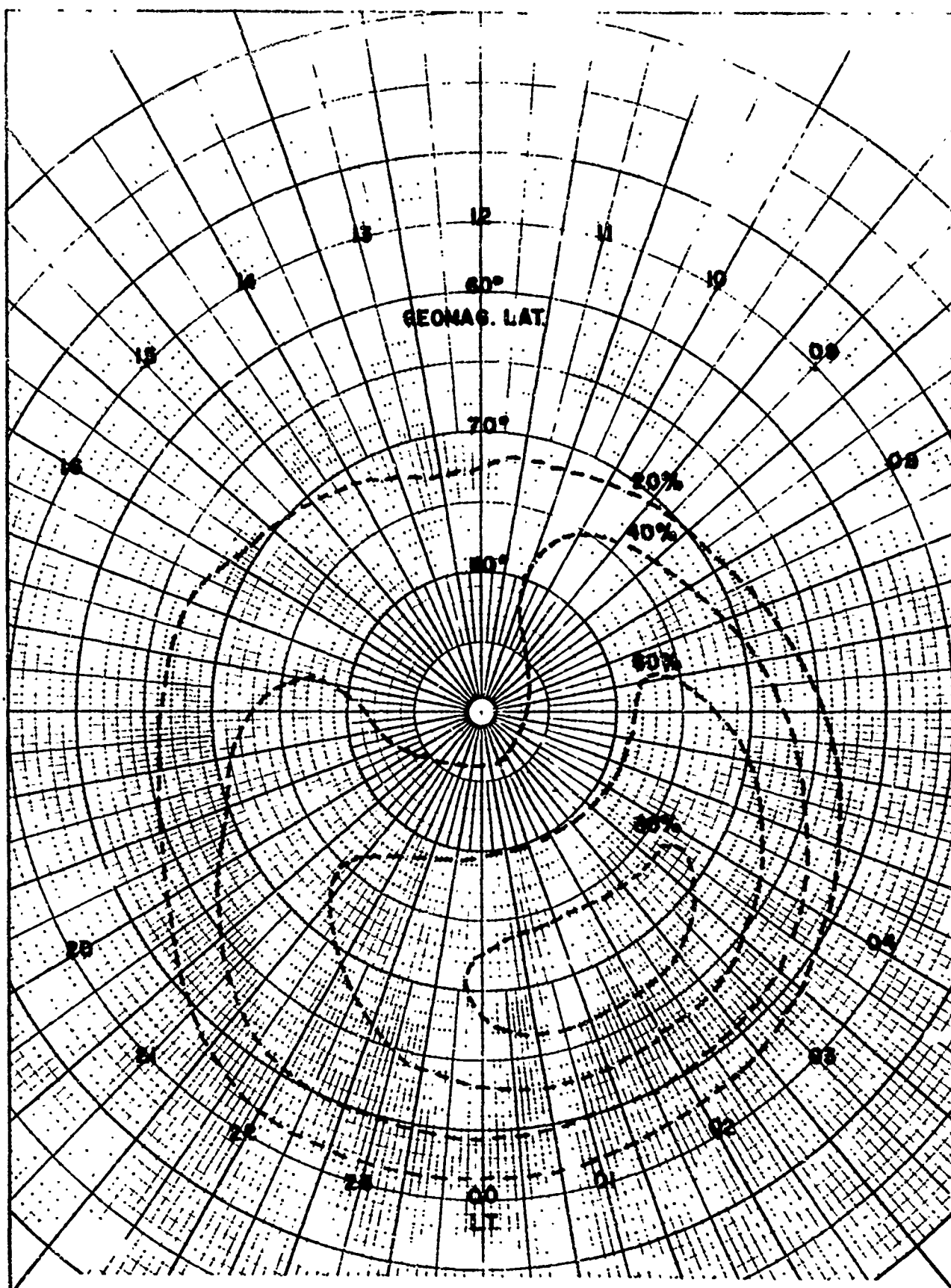
Figure 6 -Auroral Oval Component (AOC) of Spread F occurrence for January
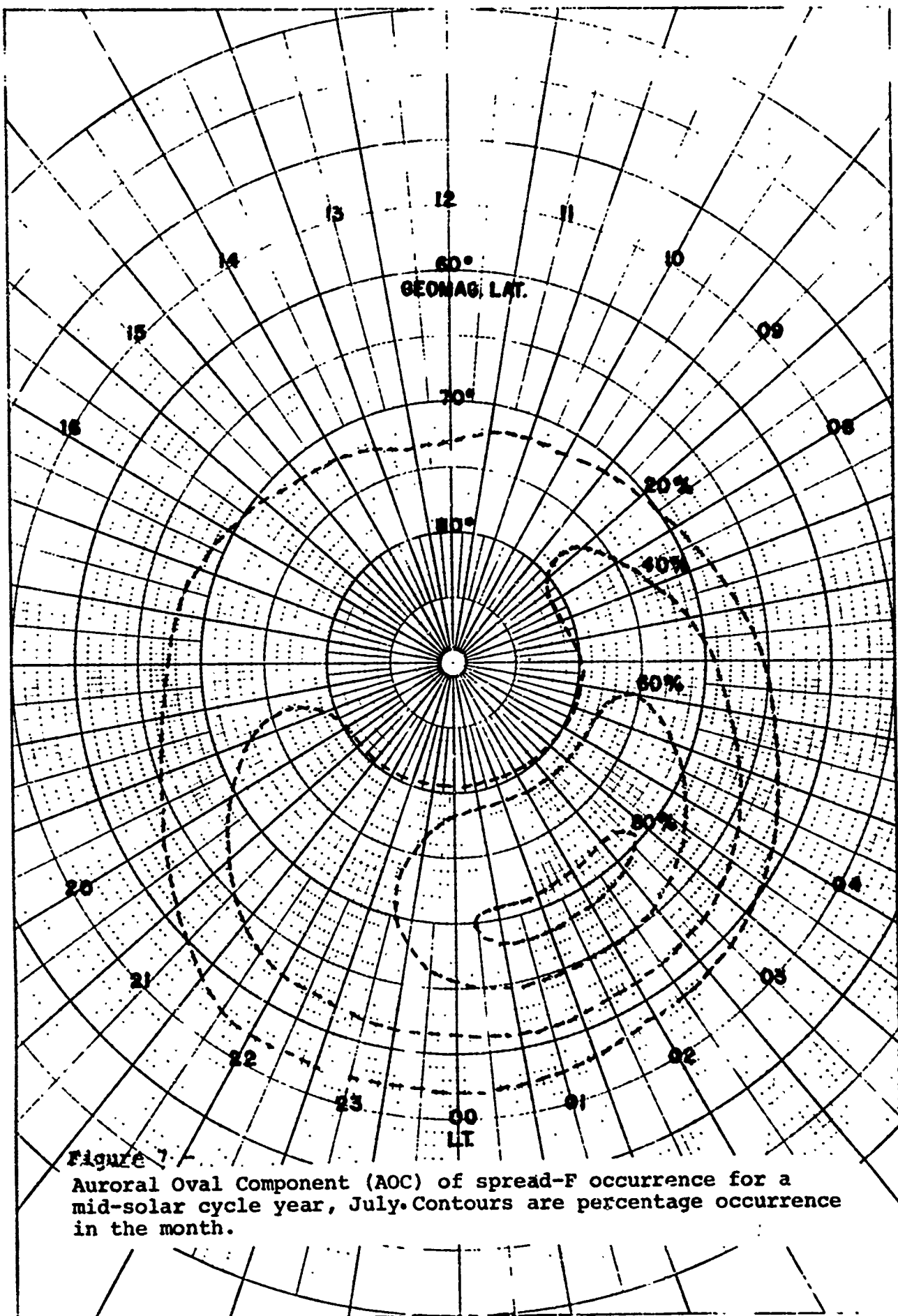
Figure 7 -
Auroral Oval Component (AOC) of spread-F occurrence for a
mid-solar cycle year, July. Contours are percentage occurrence
in the month.
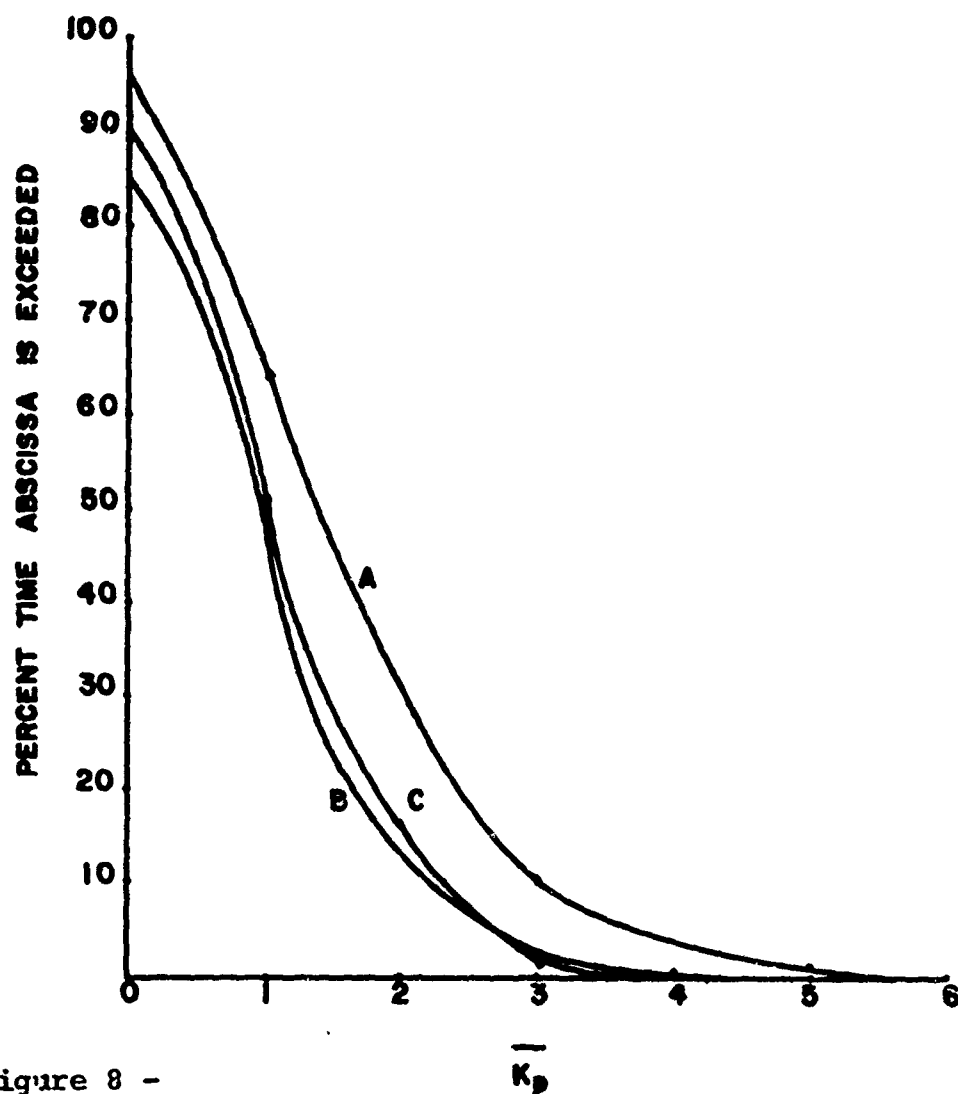
Figure 8 –

Cumulative Probability distributions of mean daily K_p index $(\overline{K_p})$.

A. Sept. Oct. Nov, 1968/69 (180 points)
B. Dec. Jan, Feb, 1968/69 (180 points)
C. June, July, Aug. 1968/69 (180 points).

49
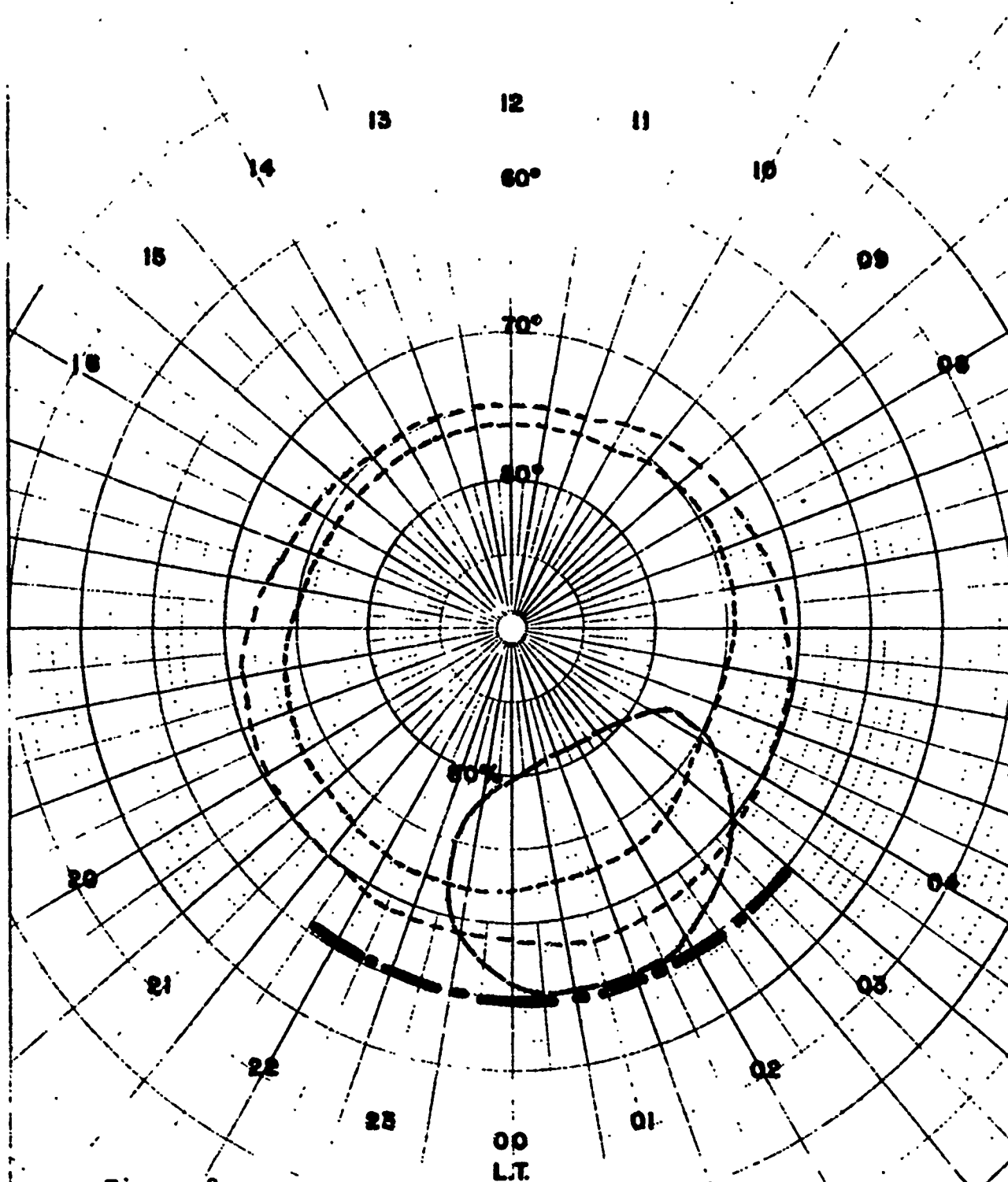
Figure 9 –

G/T Pattern of 80% spread contour, main trough and auroral oval for September with $\bar{K}_p \approx 1-$.

Figure 10.

G/T Pattern of 60% spread-F contour main trough and auroral
oval for September with $R_p \approx 1°$ to 1+.
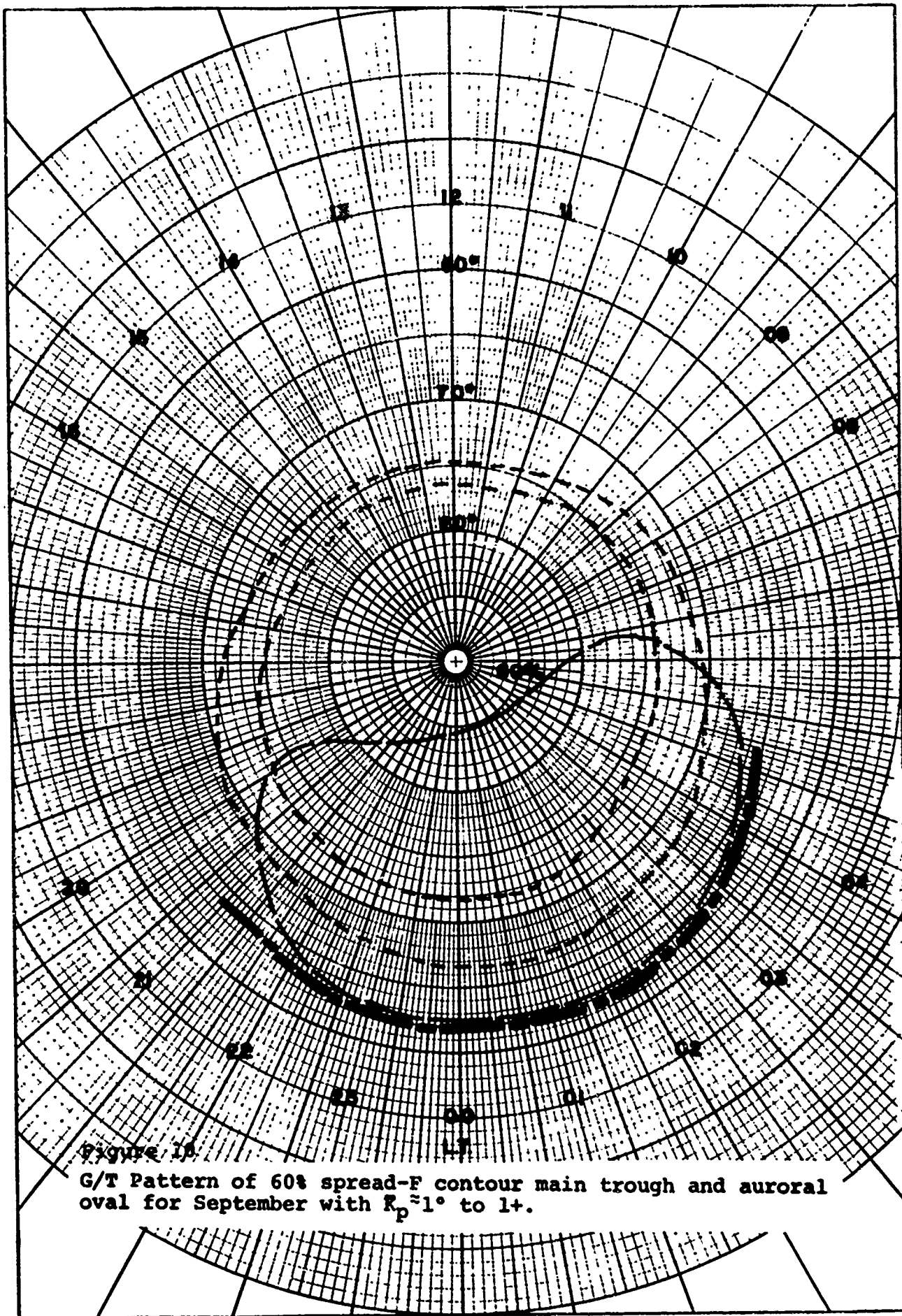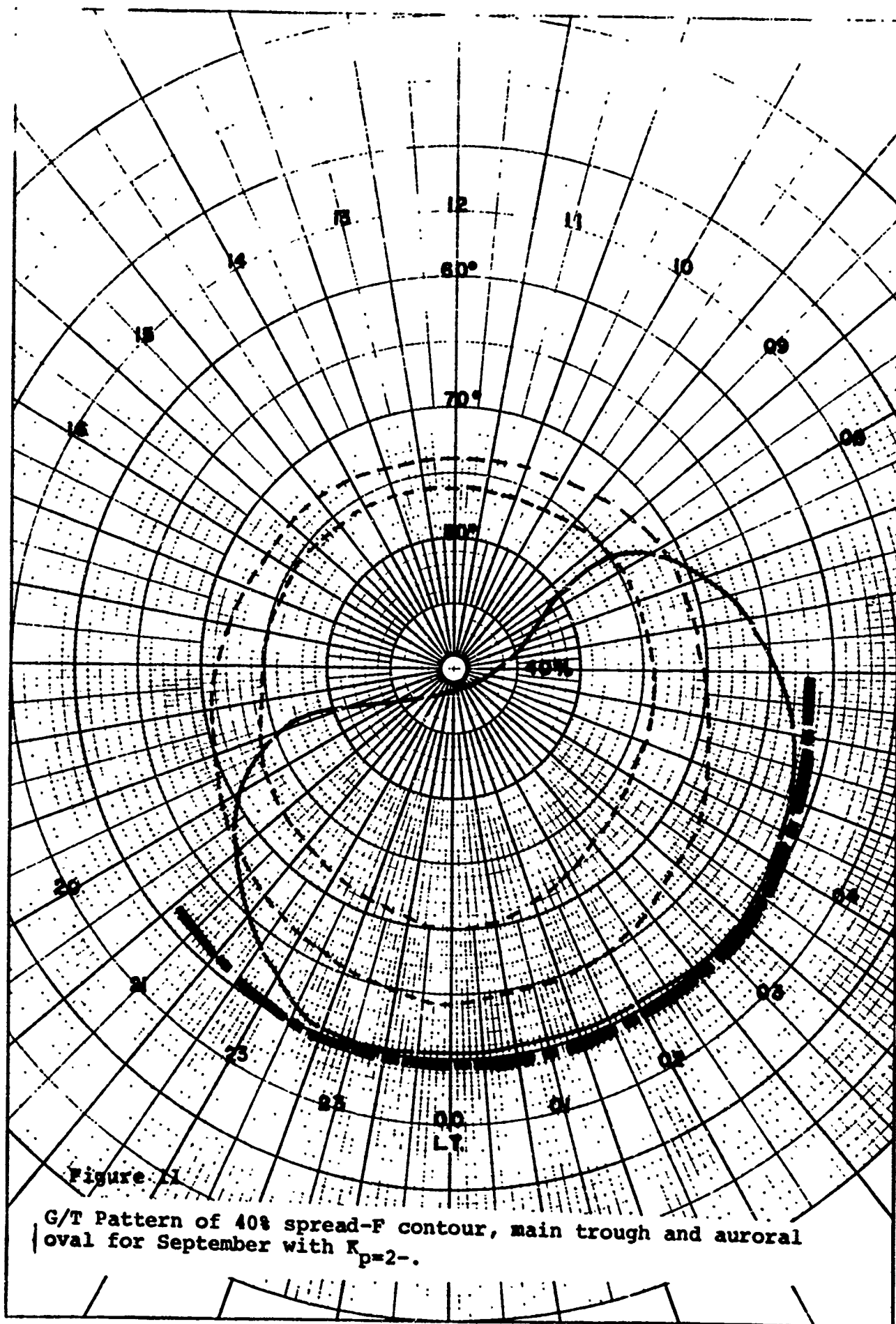
Figure 11

G/T Pattern of 40% spread-F contour, main trough and auroral oval for September with $K_{p=2-}$.
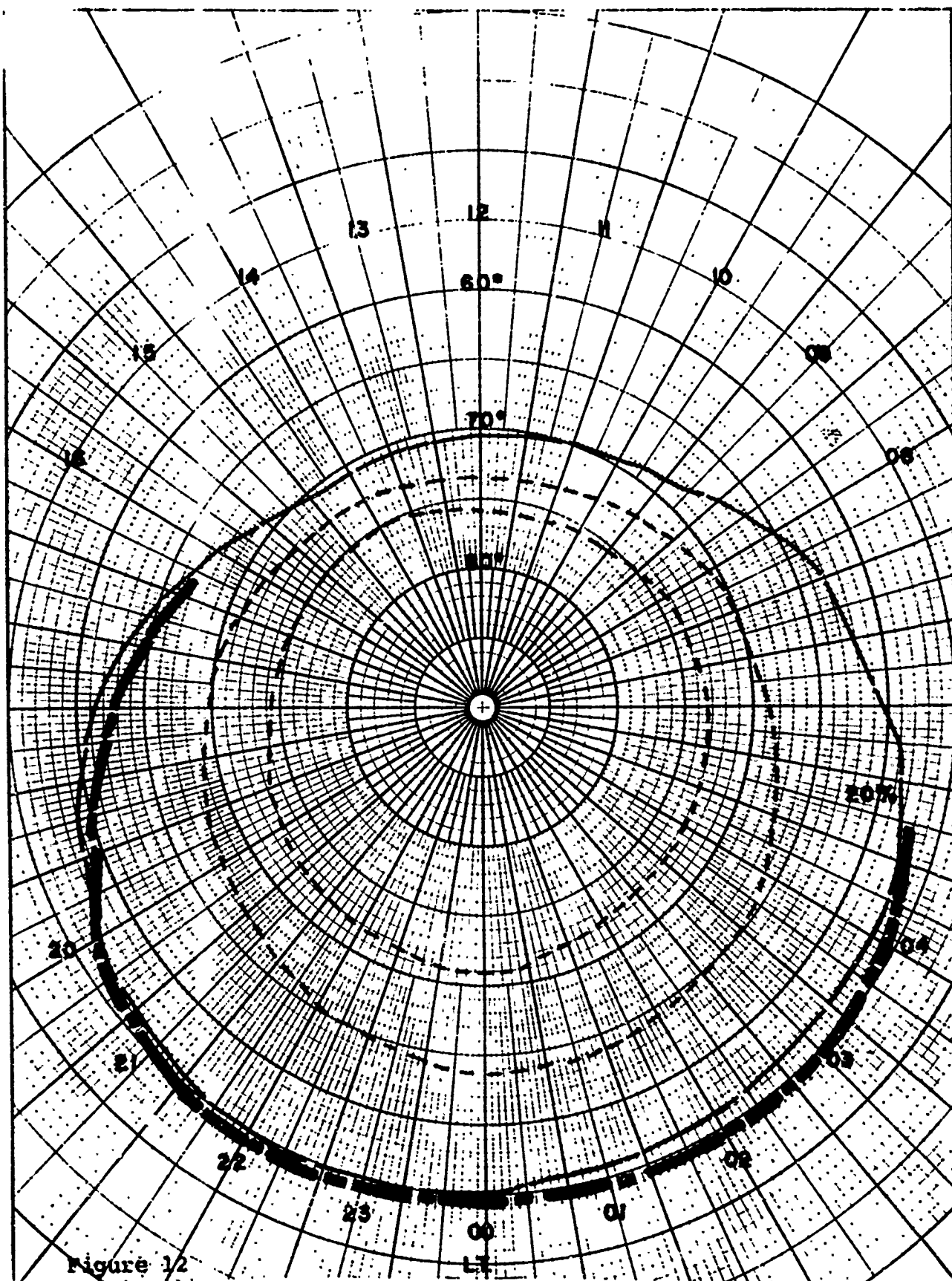
Figure 12

Geomagnetic latitude/local time pattern of 20% spread-F contour (broken line), Main trough position (Heavy Line), and Feldstein auroral oval (Dashed line) for September with K_p= 2+.

Fig 13 Probability of overhead spread F occurrence projected to September 1971 (geomagnetic latitude and longitude) 0000 UT

Figure 14   September 1971, 0300 UT

Vertical Spread F Occurrence

55
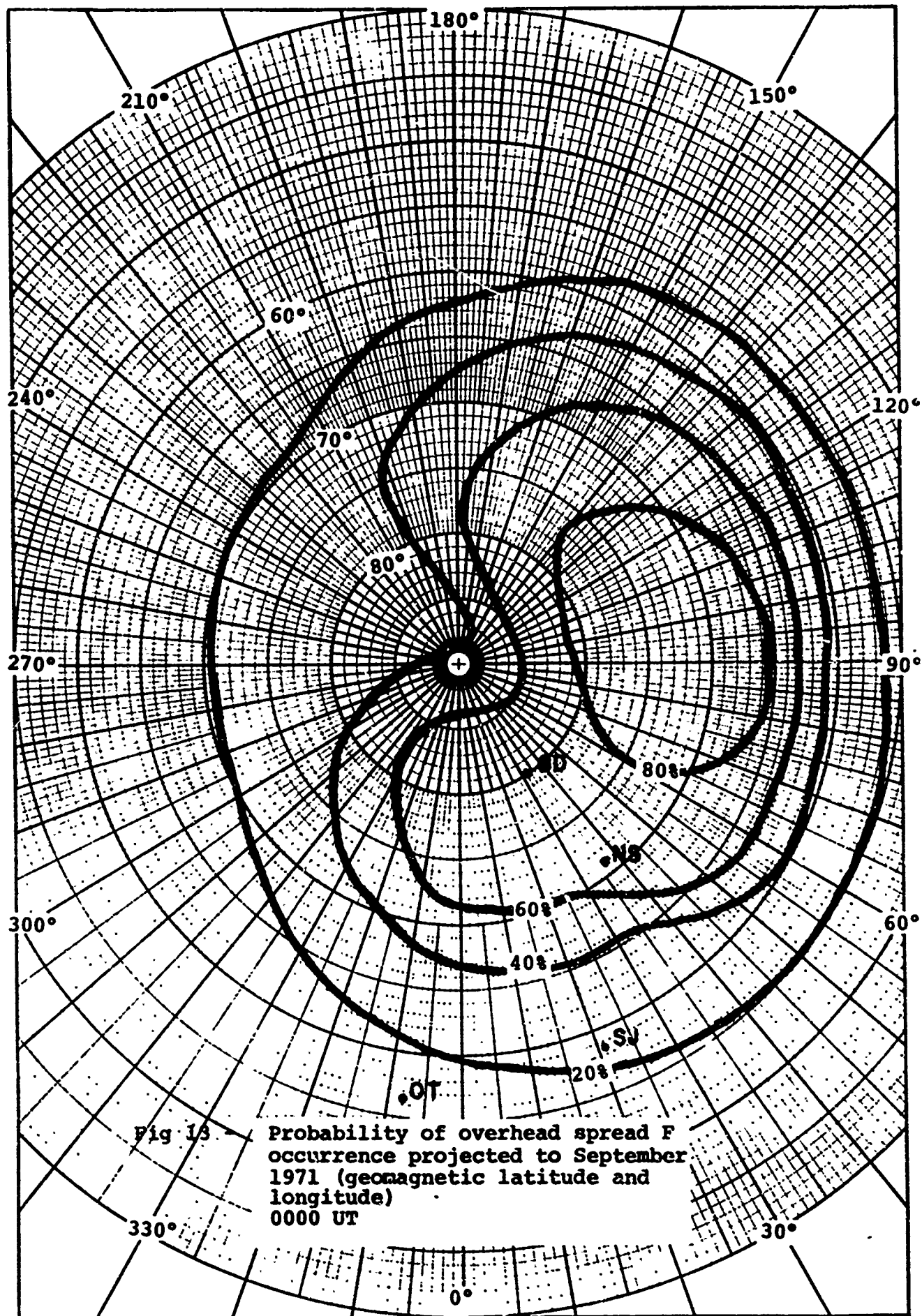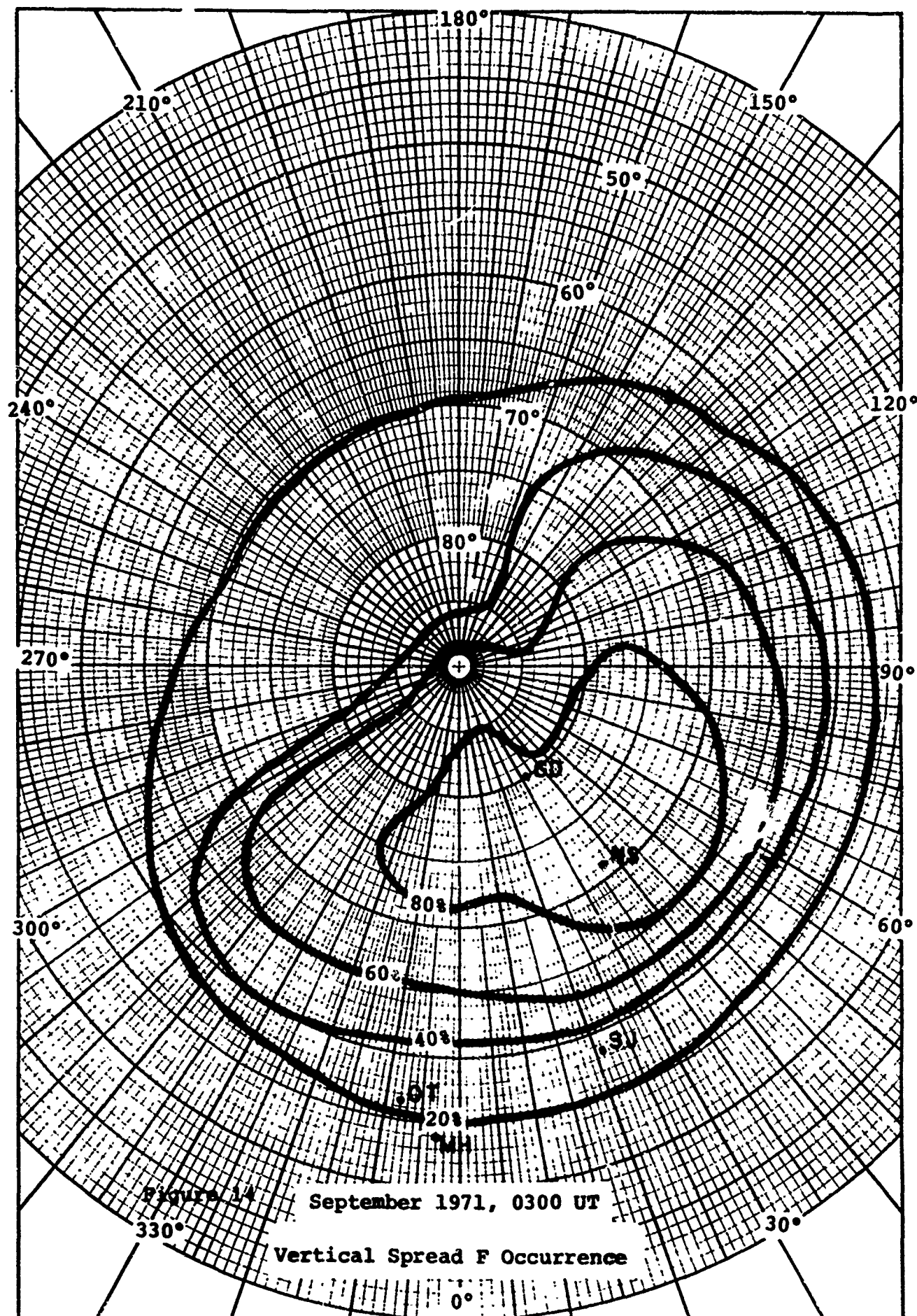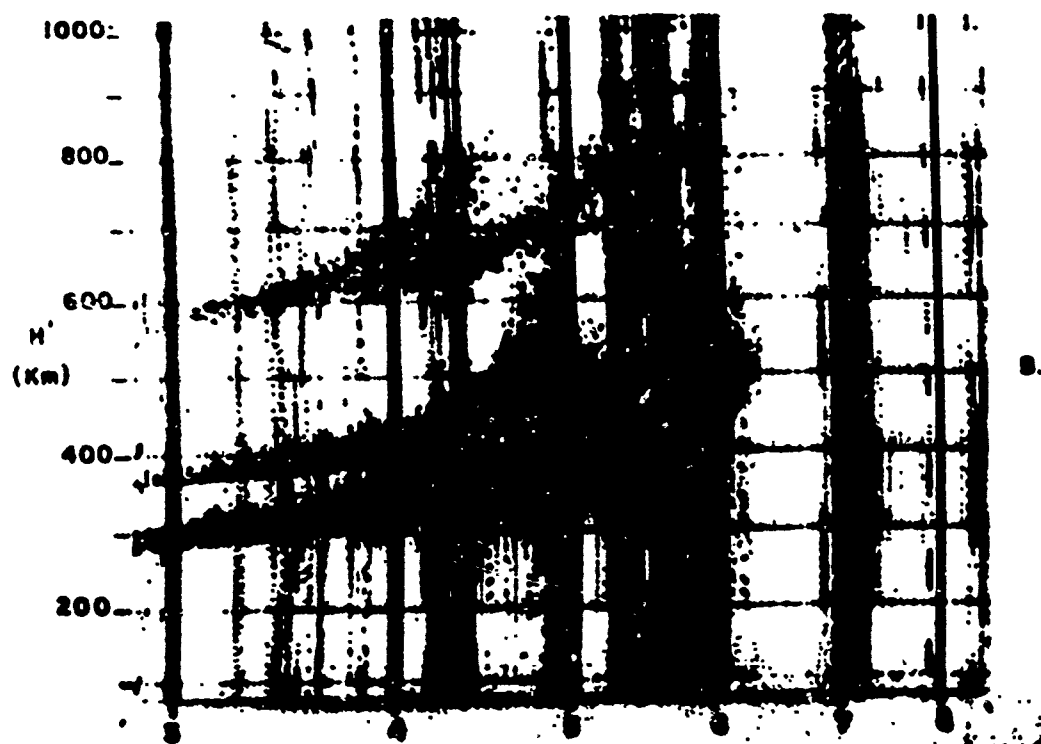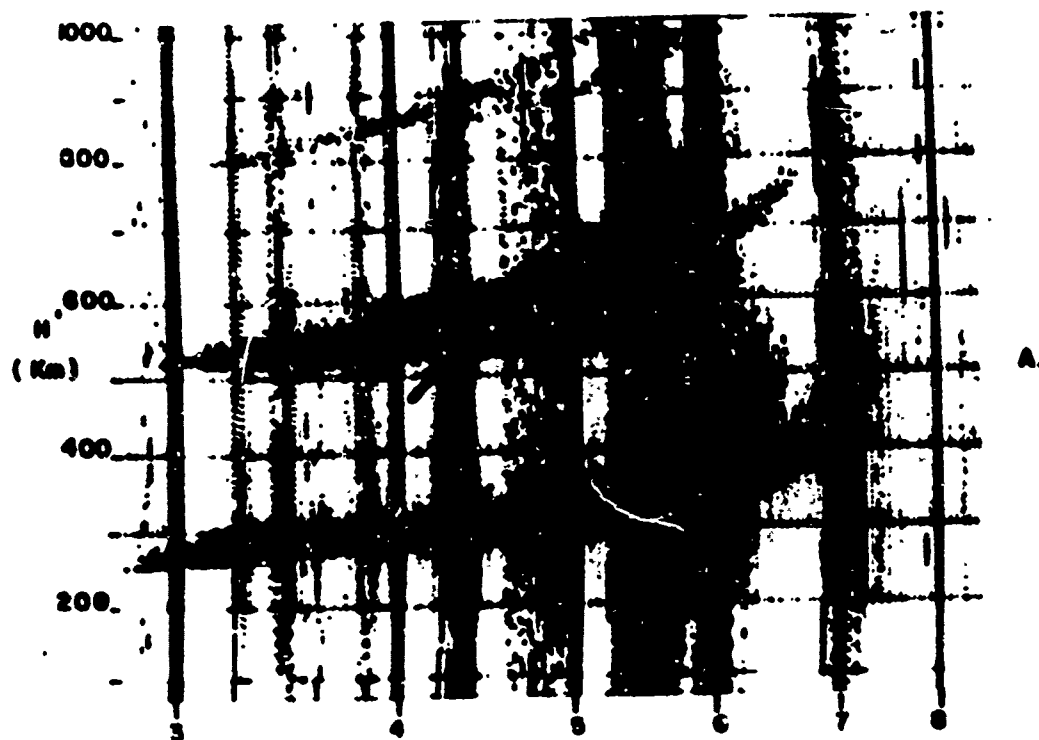
FREQUENCY (MHz)

Figure 15 Vertical incidence ionograms for Ottawa,
April 6, 1971 at 0230(A) and 0300UT (B) showing
approaching trough echo (arrow) and culmination in
Spread F (Courtesy World Data Center A, Boulder, Colorado)

56
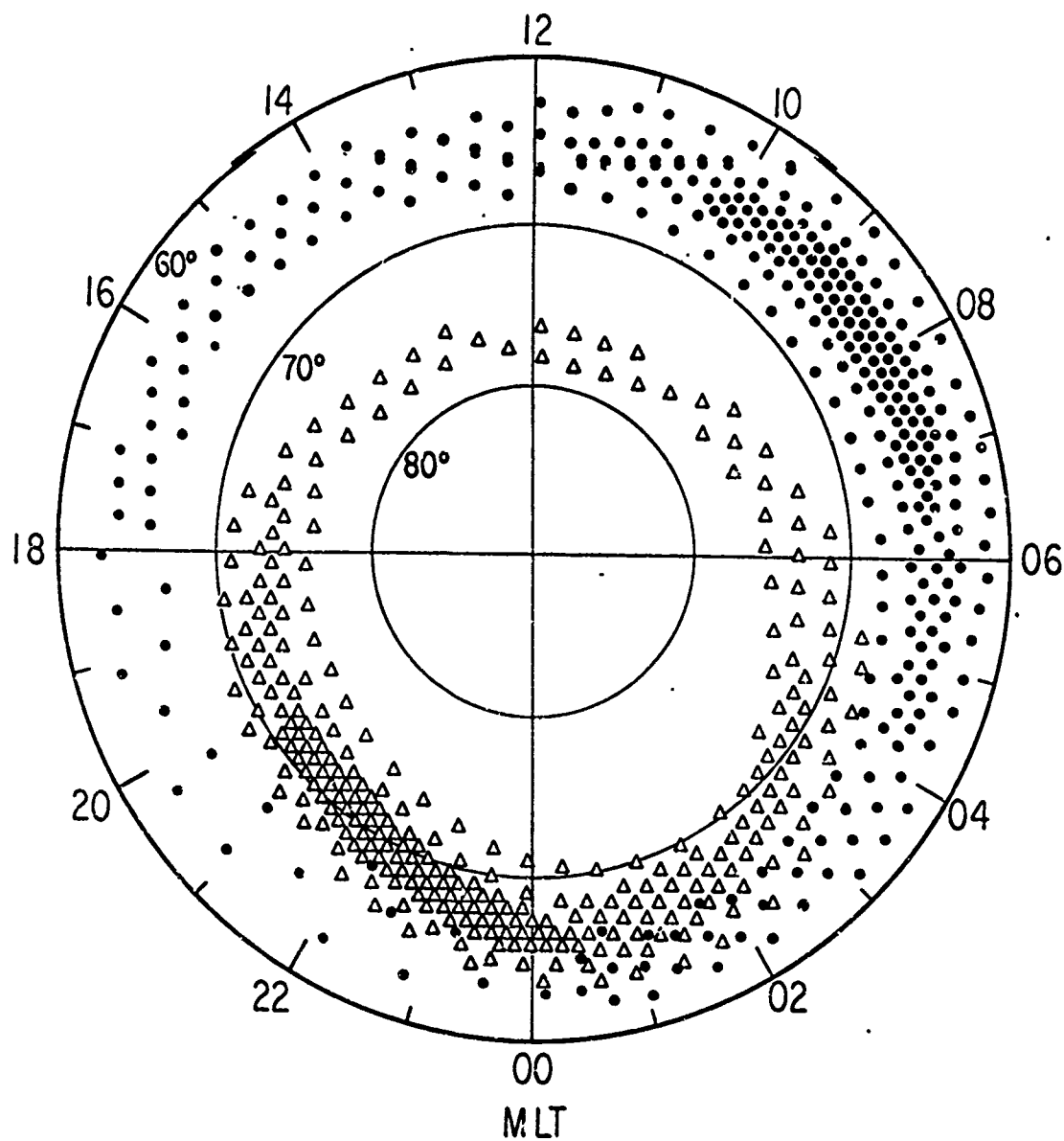
Figure 16

Zones of auroral particle precipitation in geomagnetic
coordinates as derived by Hartz and Brice (1967). Dots
represent diffuse (drizzle) precipitation and triangles
indicate discrete (splash) precipitation. Particle
flux density is roughly shown by symbol density.

57

Figure 17

Probability of occurrence of auroral absorption ≥ 0.43 dB in corrected geomagnetic latitude and time.

58
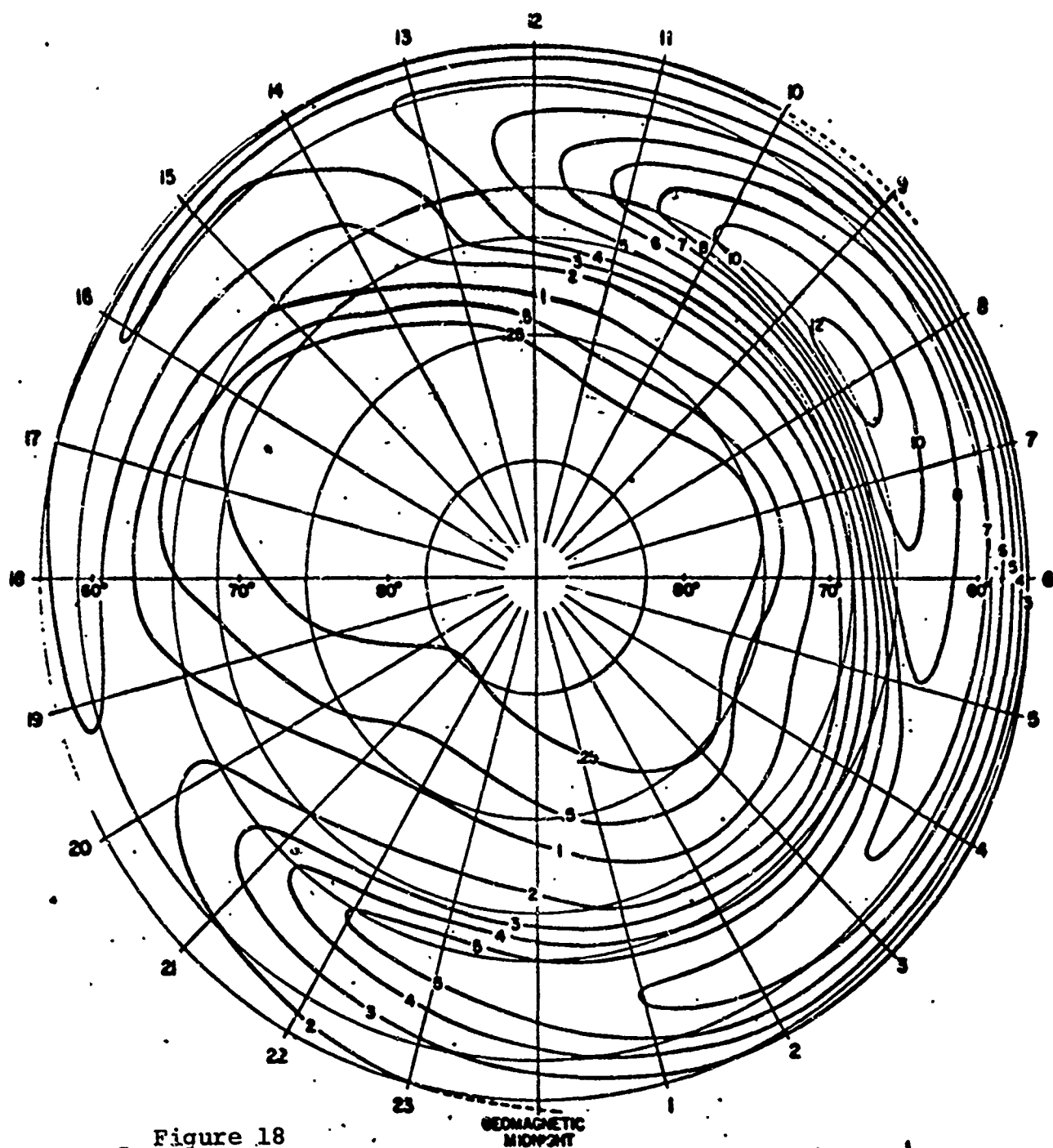
Figure 18

Probability of occurrence of auroral absorption ≥1.0 dB
in corrected geomagnetic latitude and time.
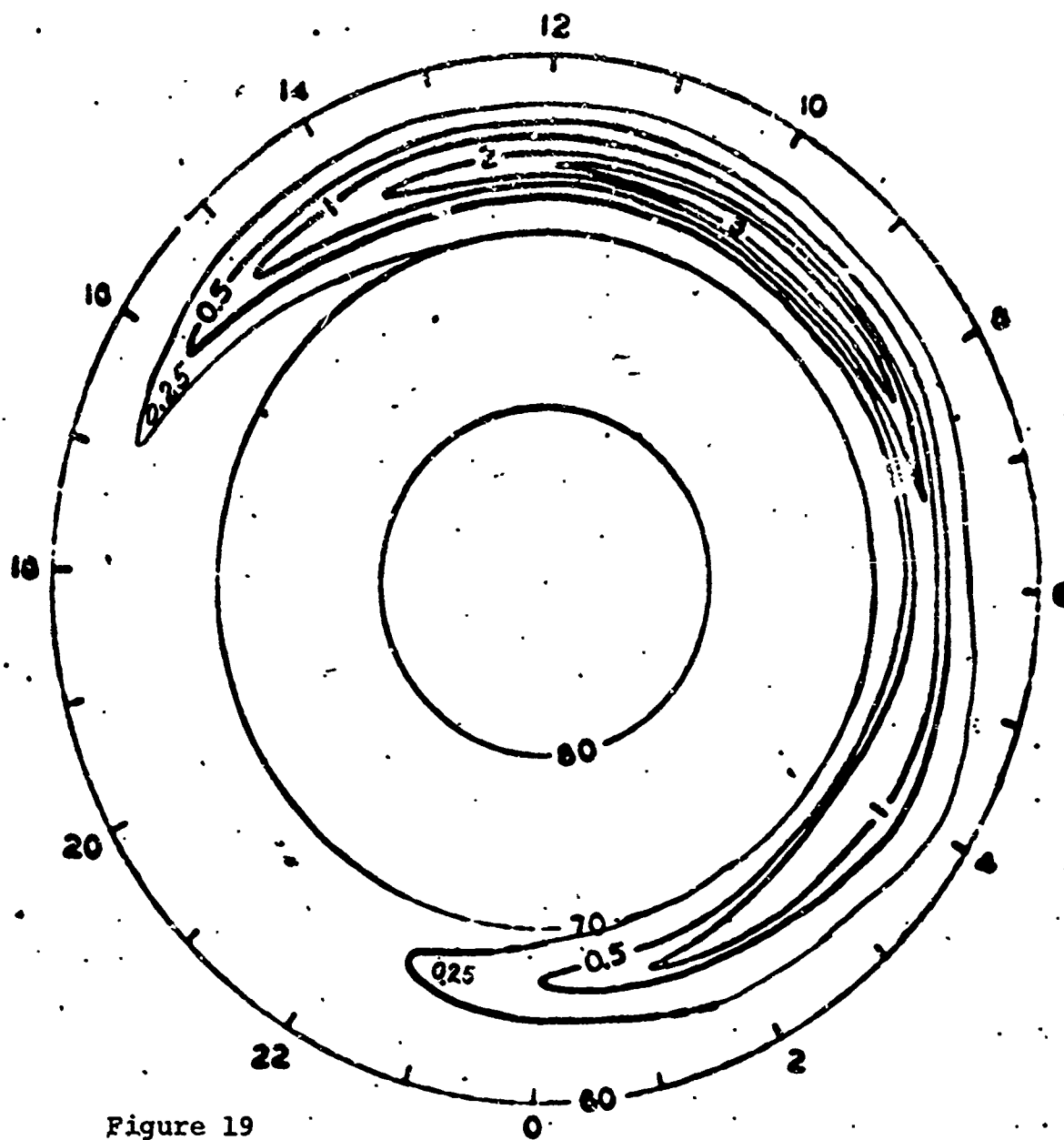
Figure 19

Probability of occurrence of auroral absorption ≥ 3.0 dB in corrected geomagnetic latitude and time.

60
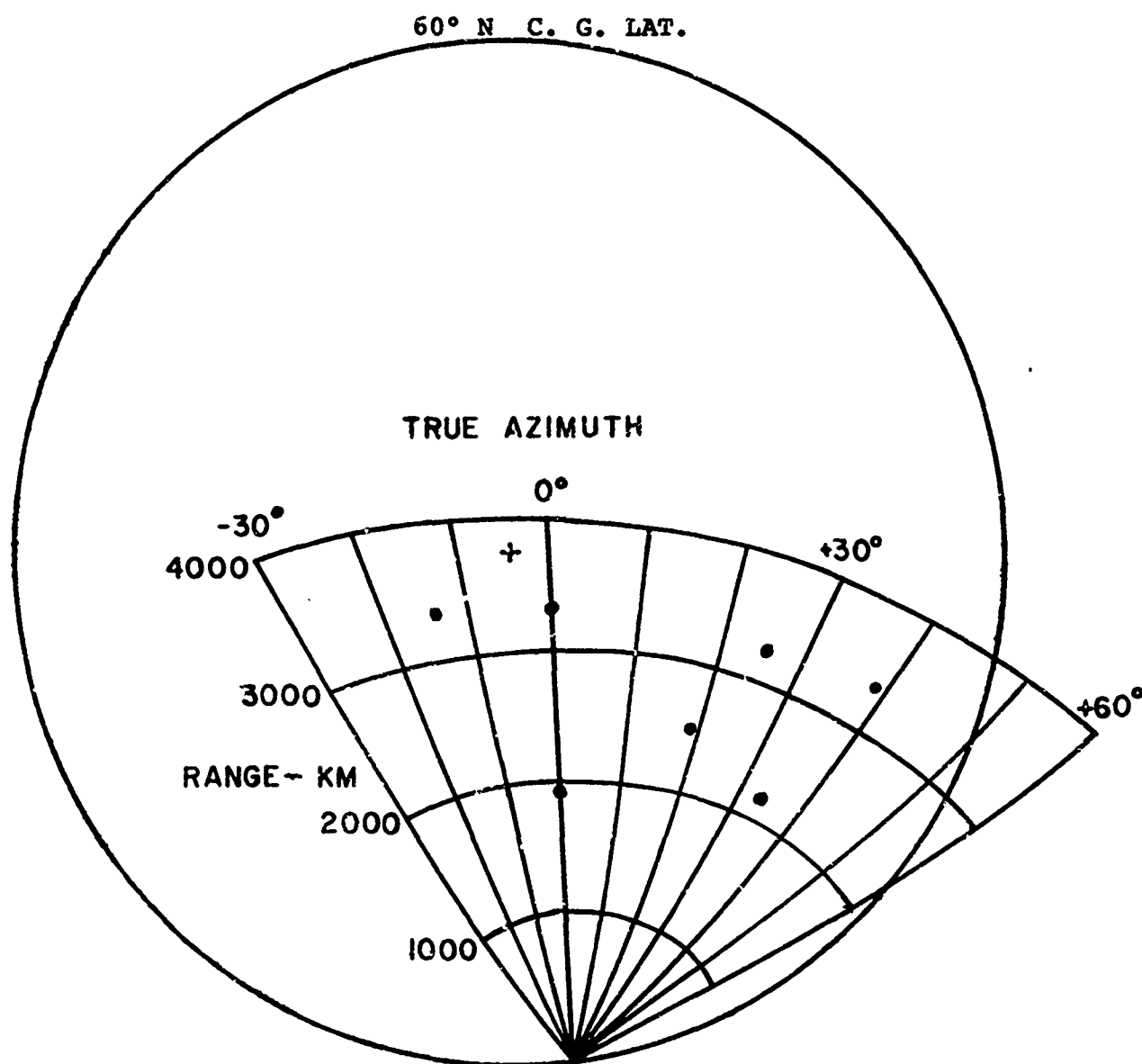
FIGURE 20   RANGE AZIMUTH FAN GRAPH IN CORRECTED
GEOMAGNETIC COORDINATES

H = 110 OR 300Km
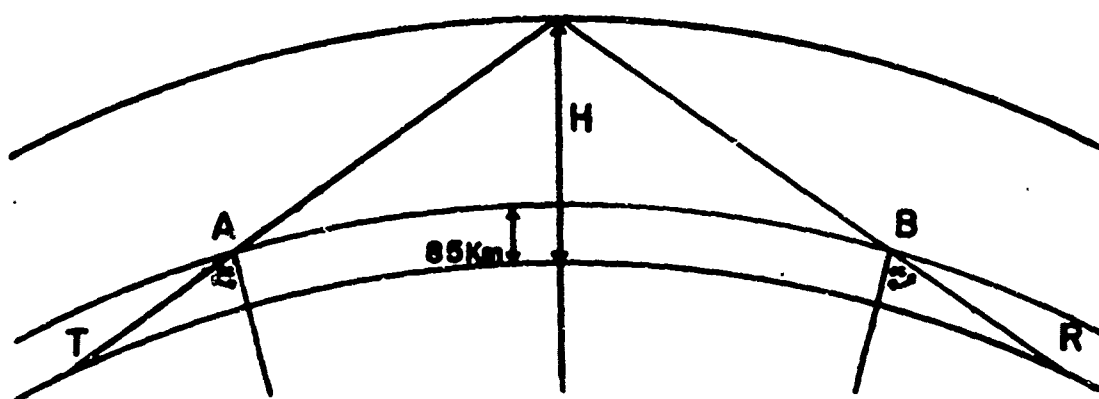
Figure 21

Curved earth geometry with absorption regions at A and B.
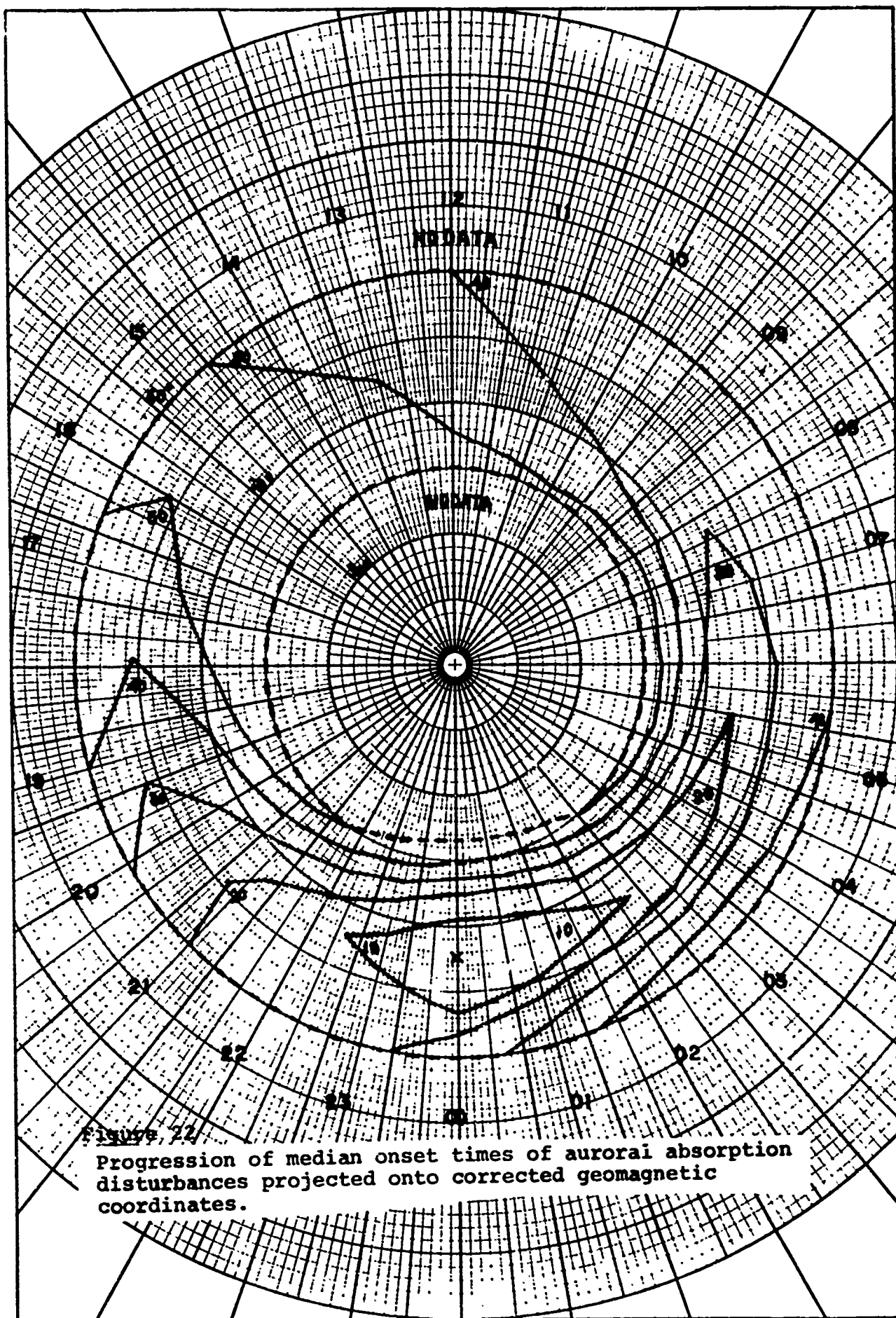
Figure 22. Progression of median onset times of auroral absorption disturbances projected onto corrected geomagnetic coordinates.
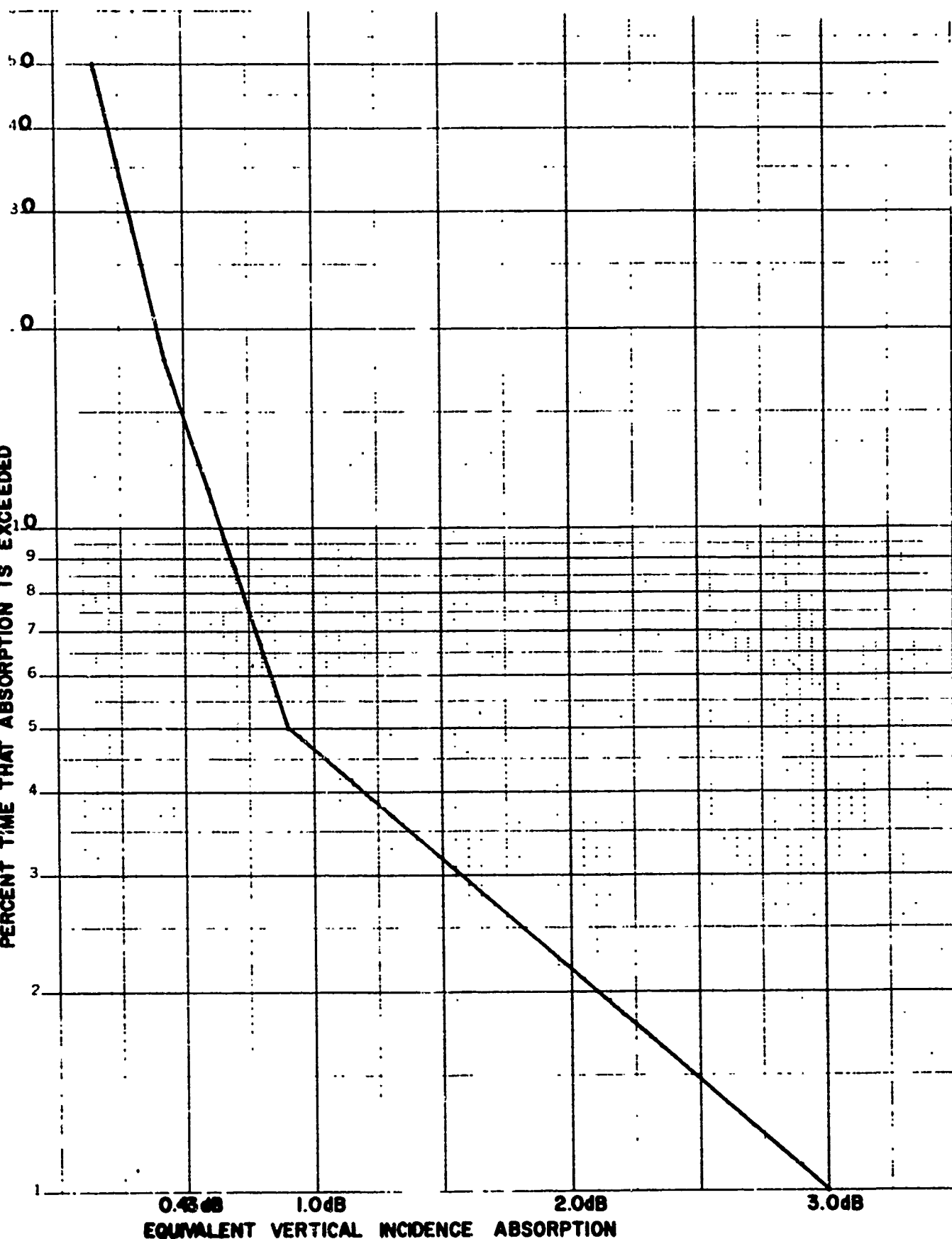
Fig. 23 Cumulative probability distribution showing percentage of time that a given level of absorption is equaled or exceeded.

RADAR AURORAL ABSORPTION
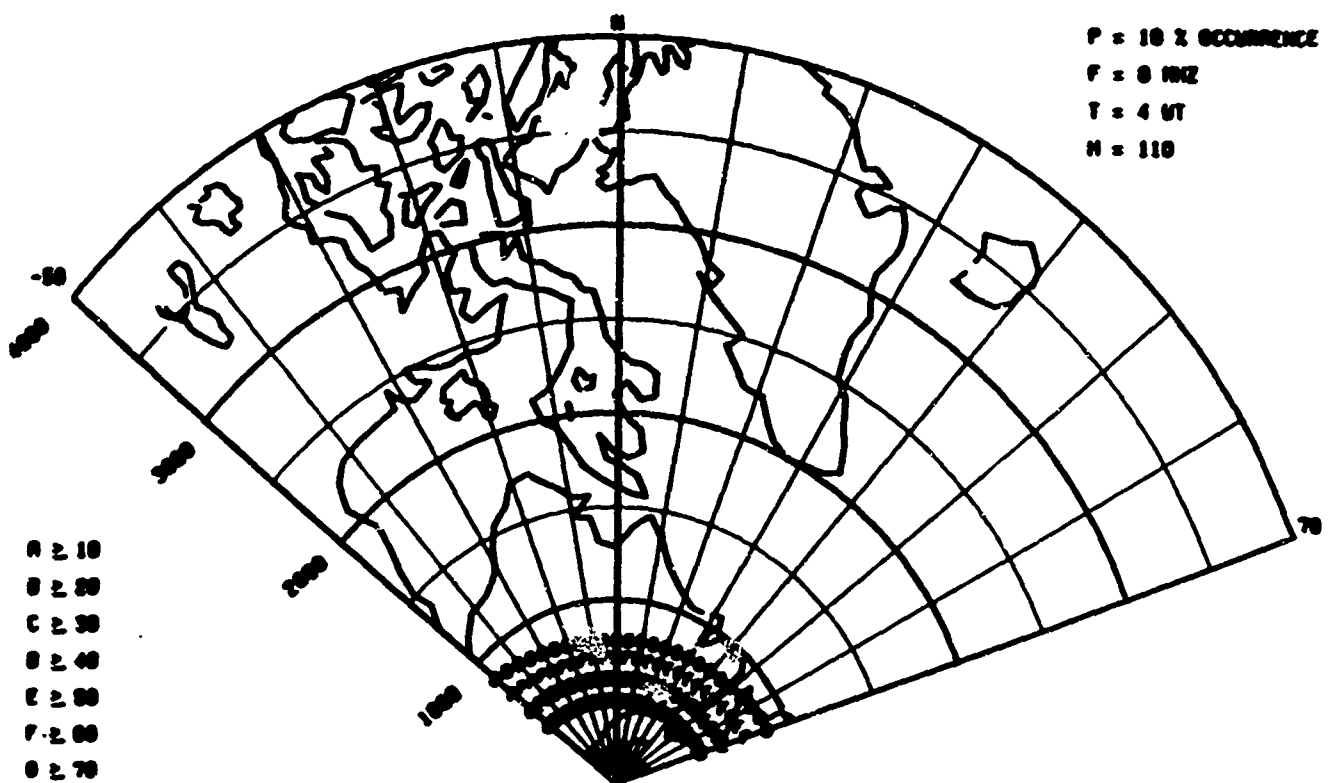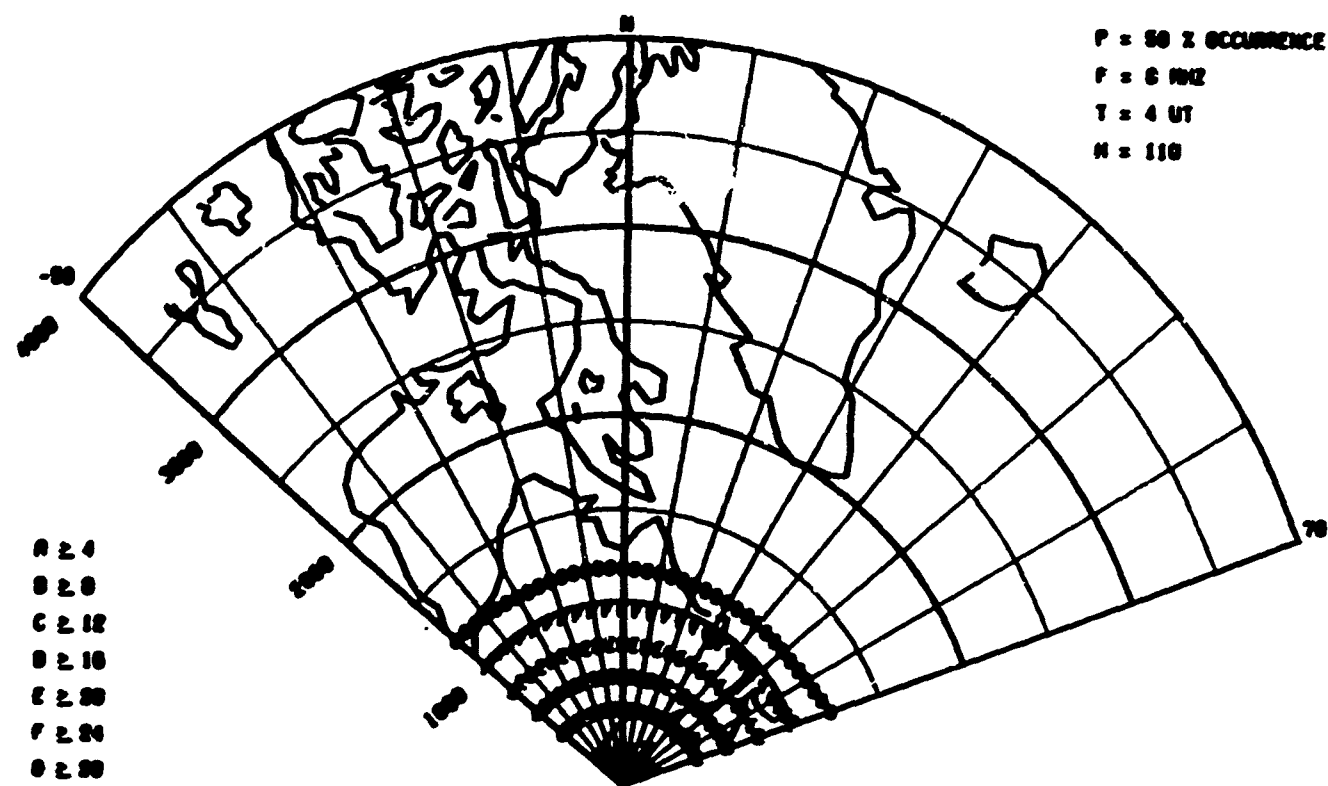
Fig. 24 - Radar Auroral Absorption F=8MHz, T=04UT, H=110km
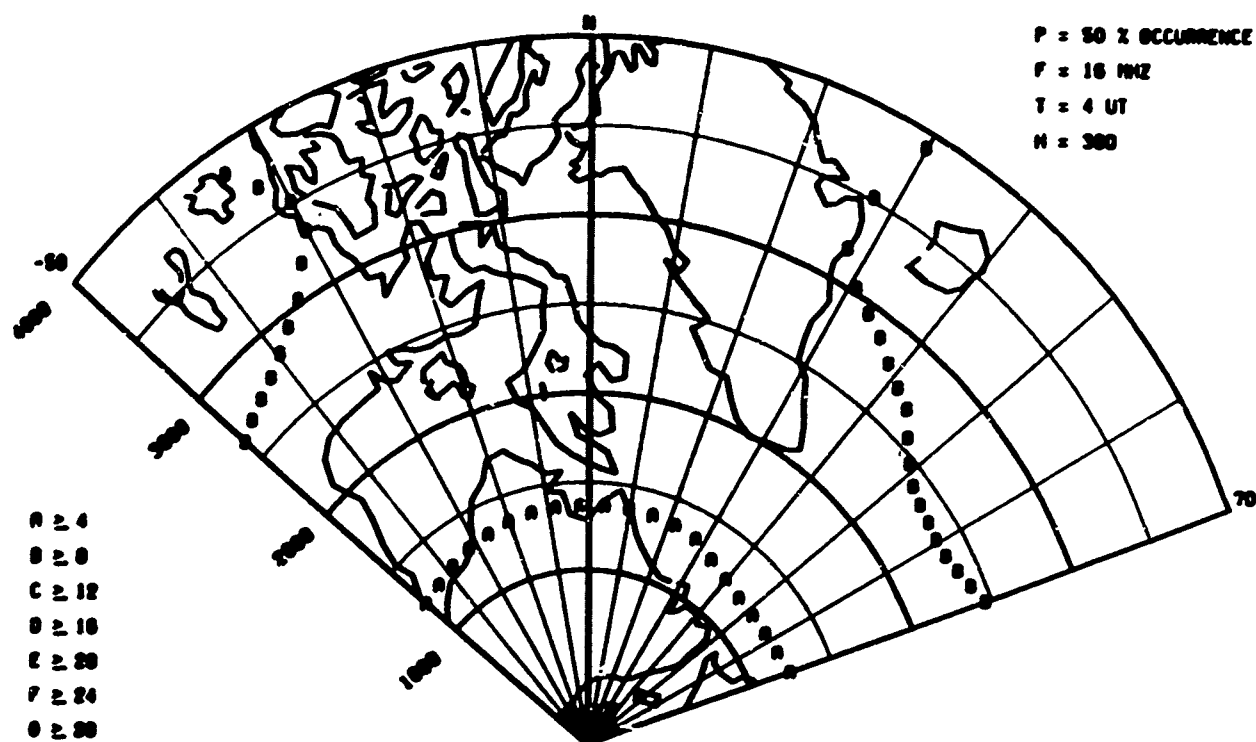
65

RADAR AURORAL ABSORPTION

P = 60 % OCCURRENCE
F = 8 MHZ
T = 12 UT
H = 110

A ≥ 4
B ≥ 8
C ≥ 12
D ≥ 16
E ≥ 20
F ≥ 24
G ≥ 28

P = 10 % OCCURRENCE
F = 8 MHZ
T = 12 UT
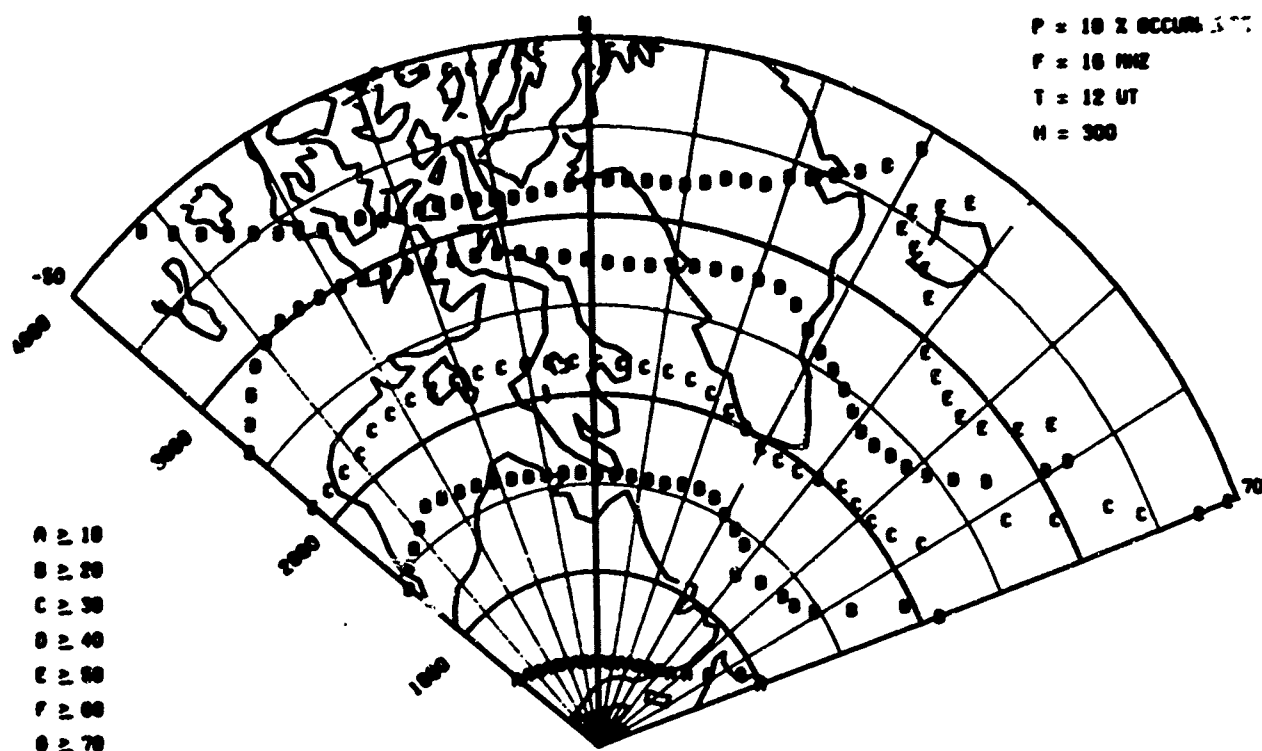H = 110

A ≥ 10
B ≥ 20
C ≥ 30
D ≥ 40
E ≥ 50
F ≥ 60
G ≥ 70
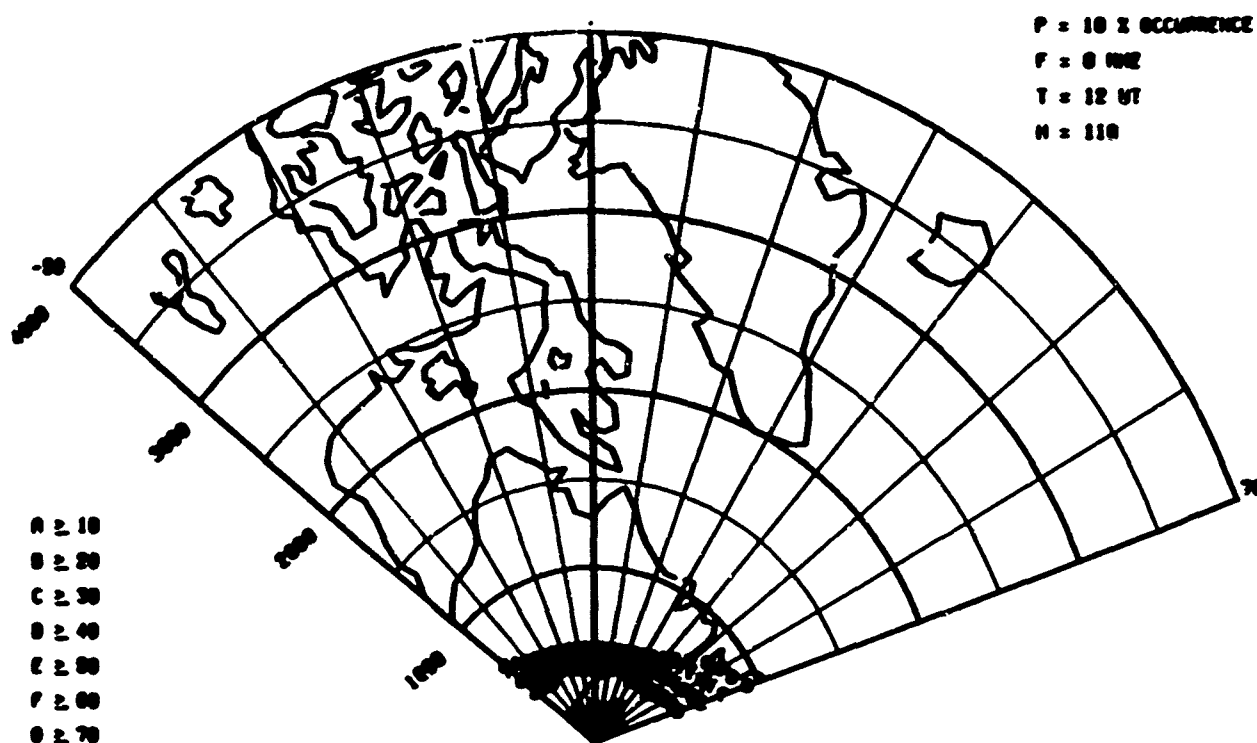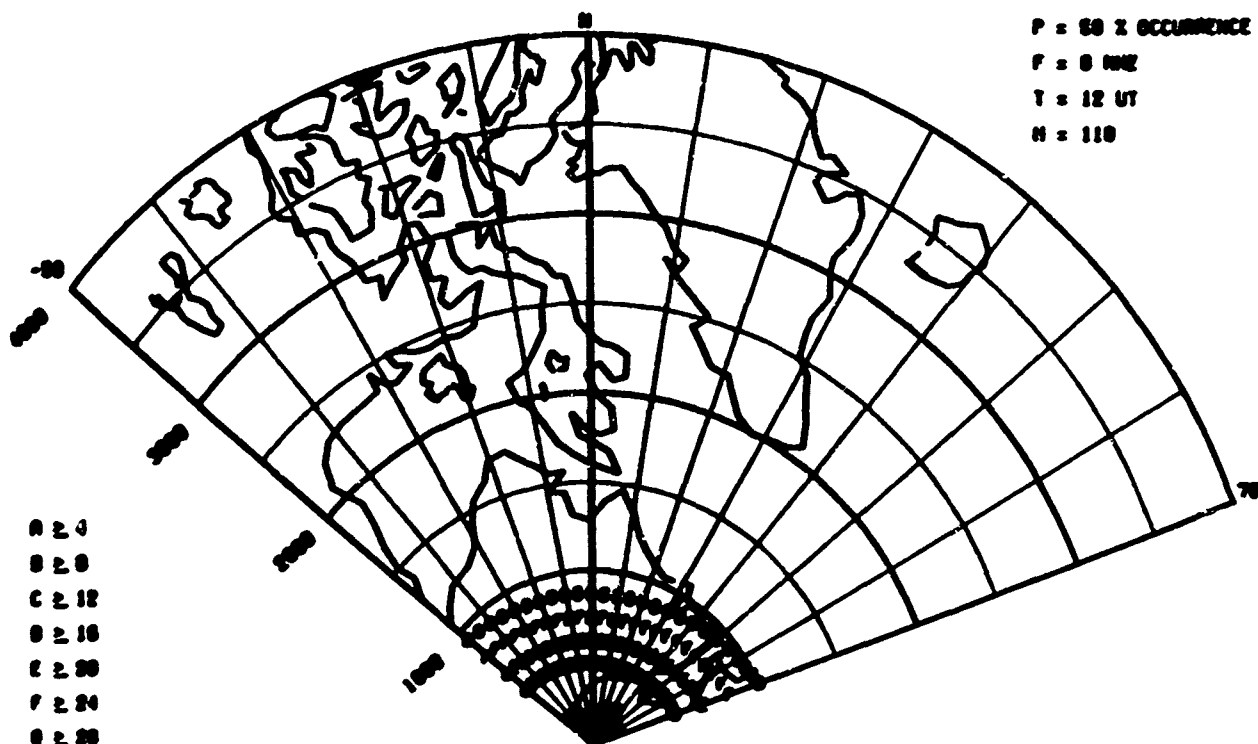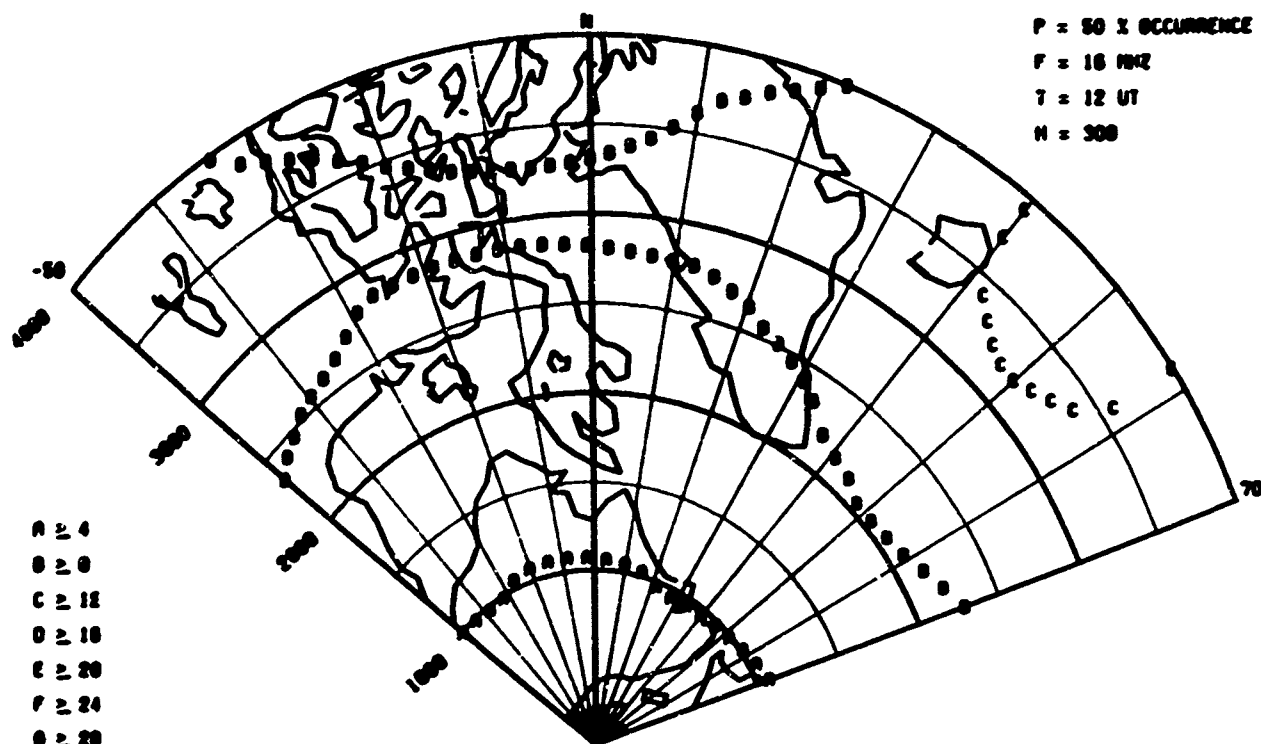
Fig. 25 - Radar Auroral Absorption F=8MHz, T=12UT, H=110km

66

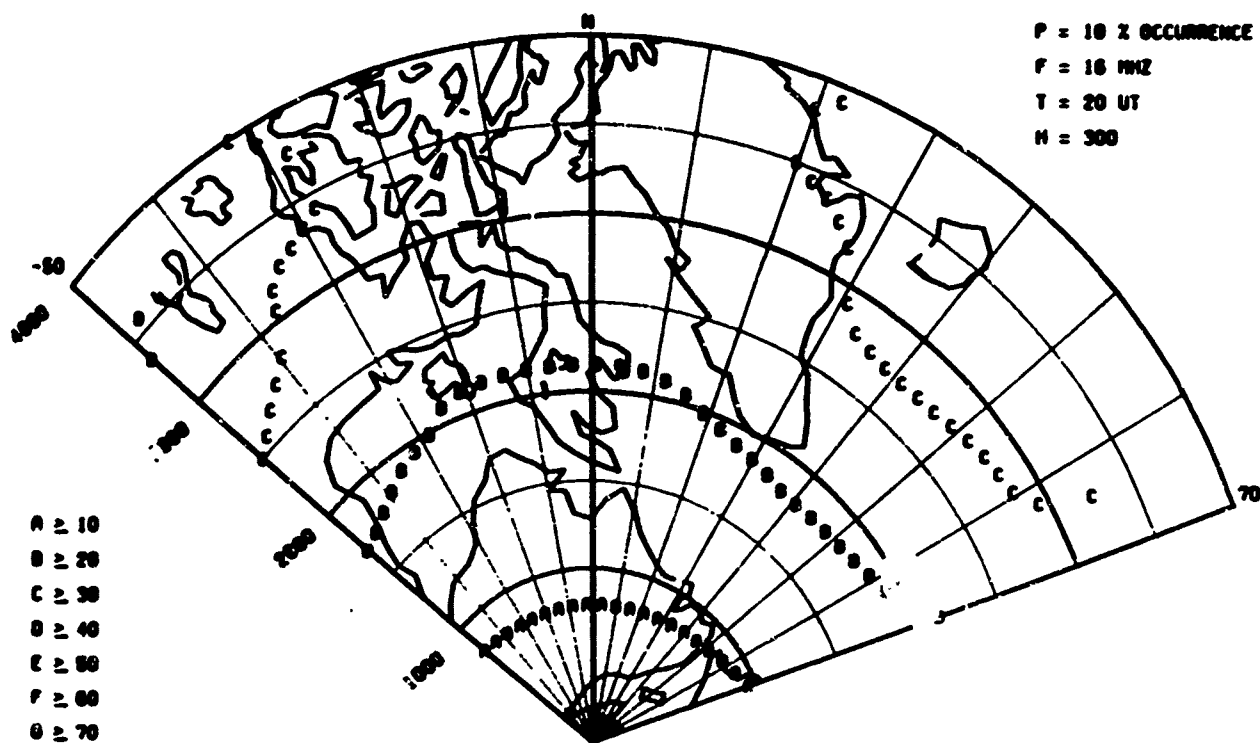# RADAR AURORAL ABSORPTION
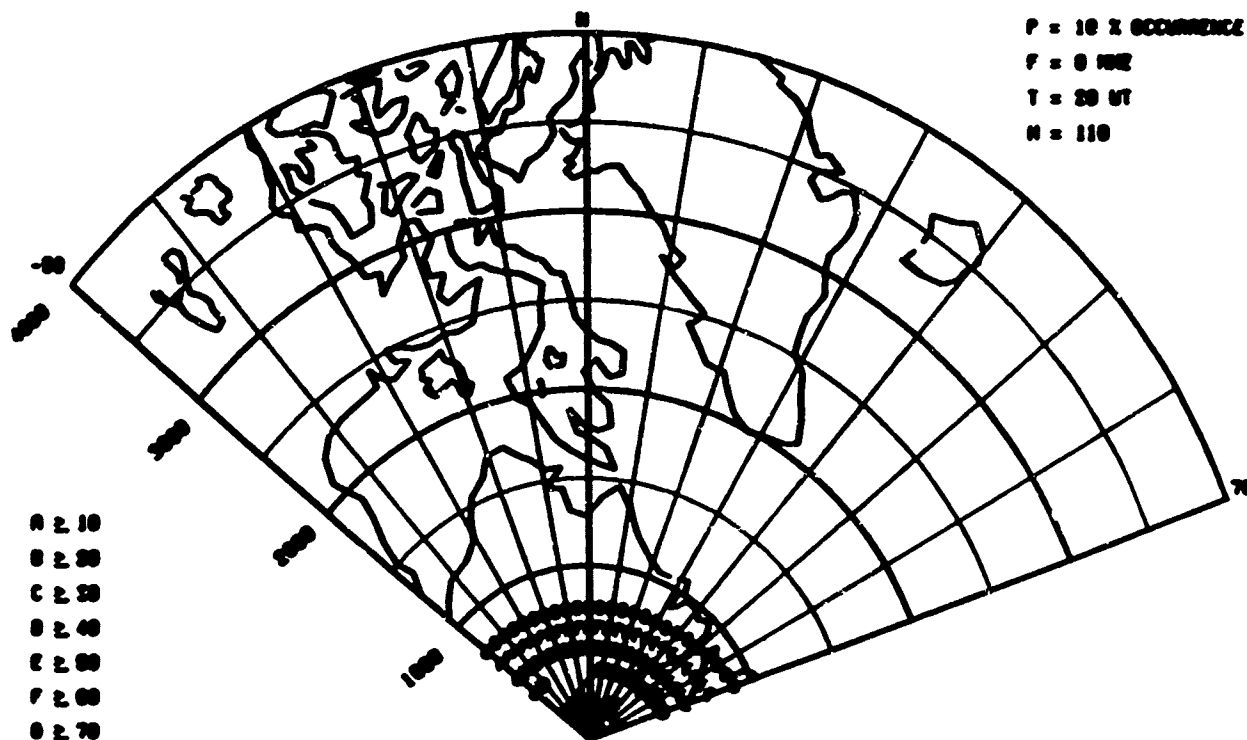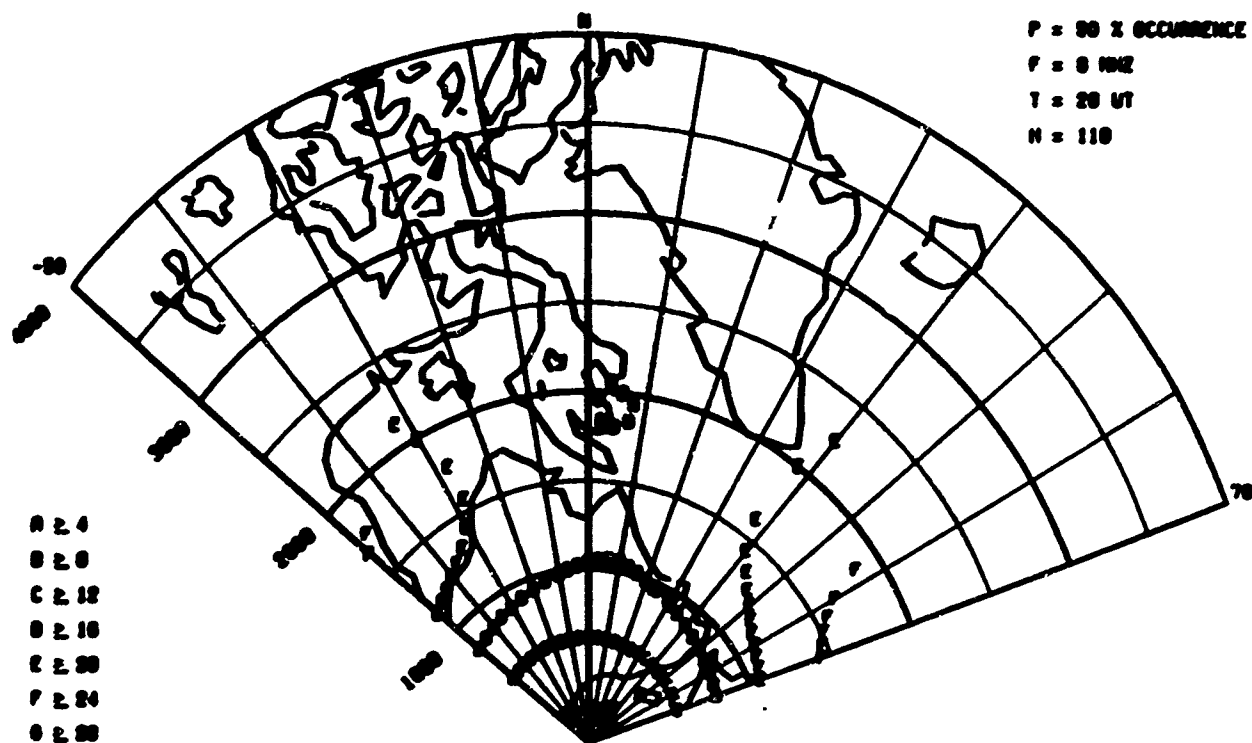
Fig. 26 - Radar Auroral Absorption F=8MHz, T=20UT, H=110km

RADAR AURORAL ABSORPTION
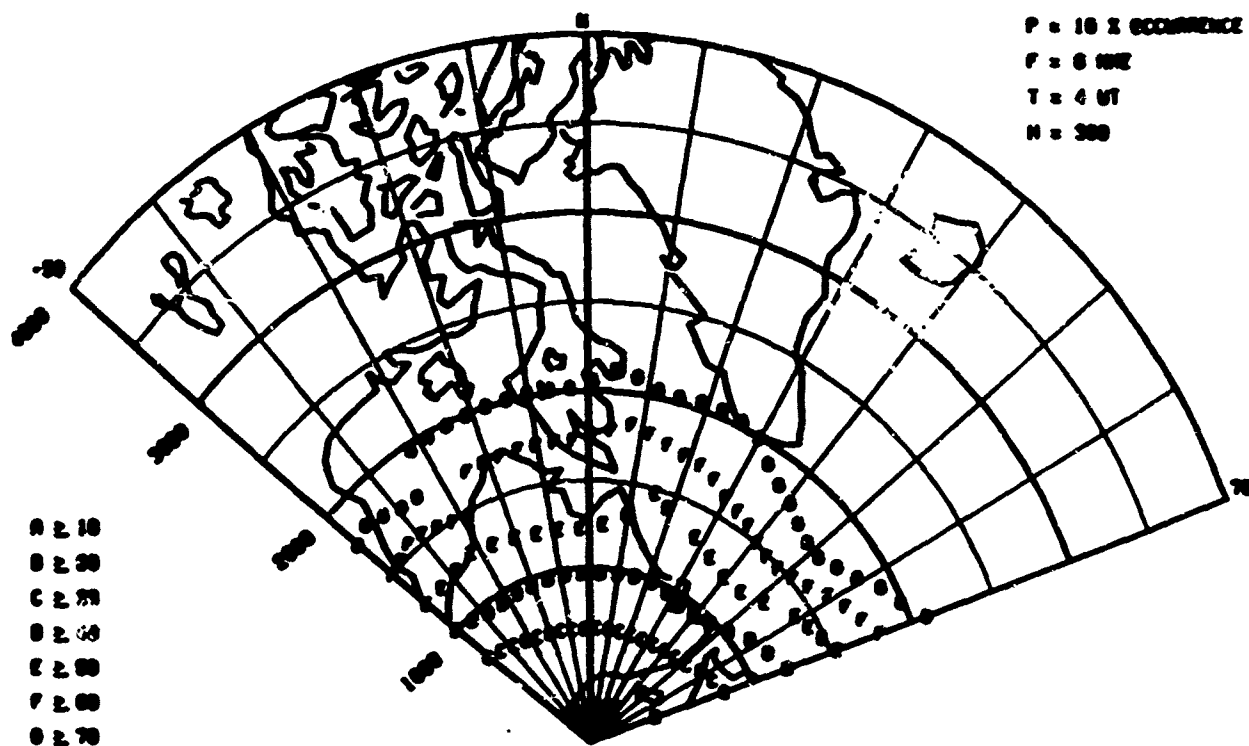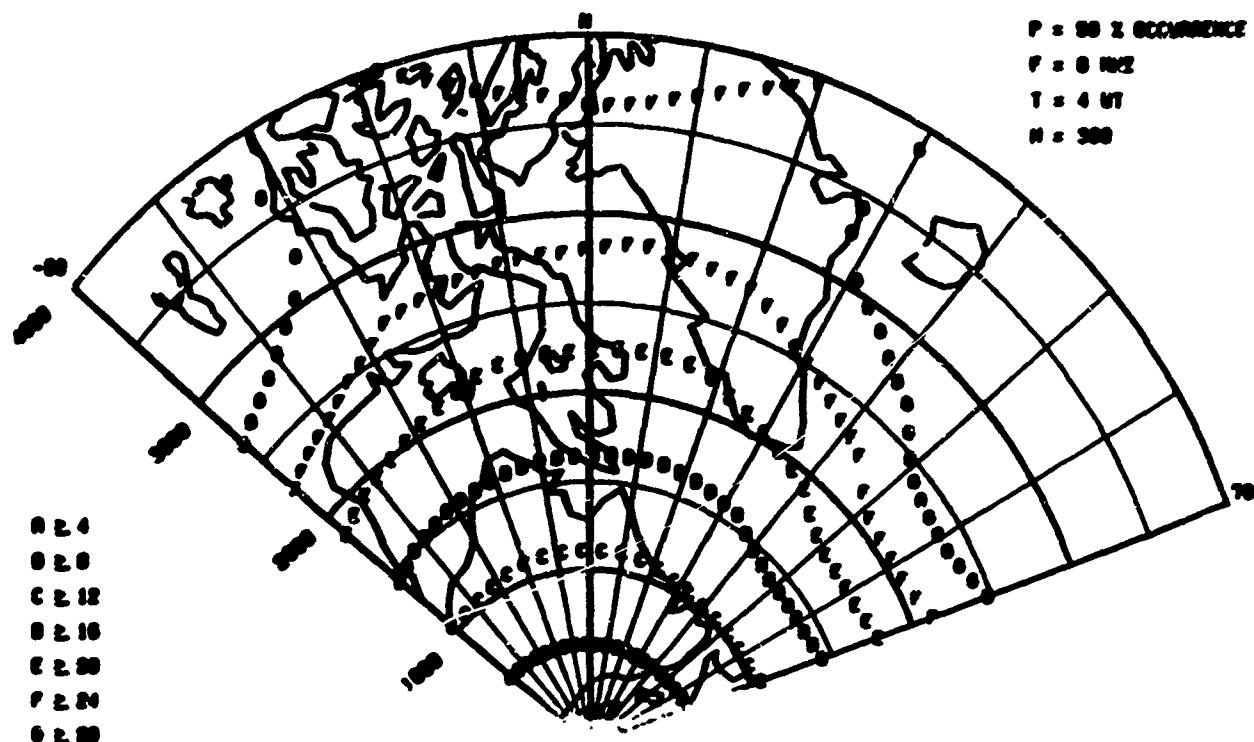
Fig. 27 - Radar Auroral Absorption F-8MHz, T-04UT, H=300km

RADAR AURORAL ABSORPTION
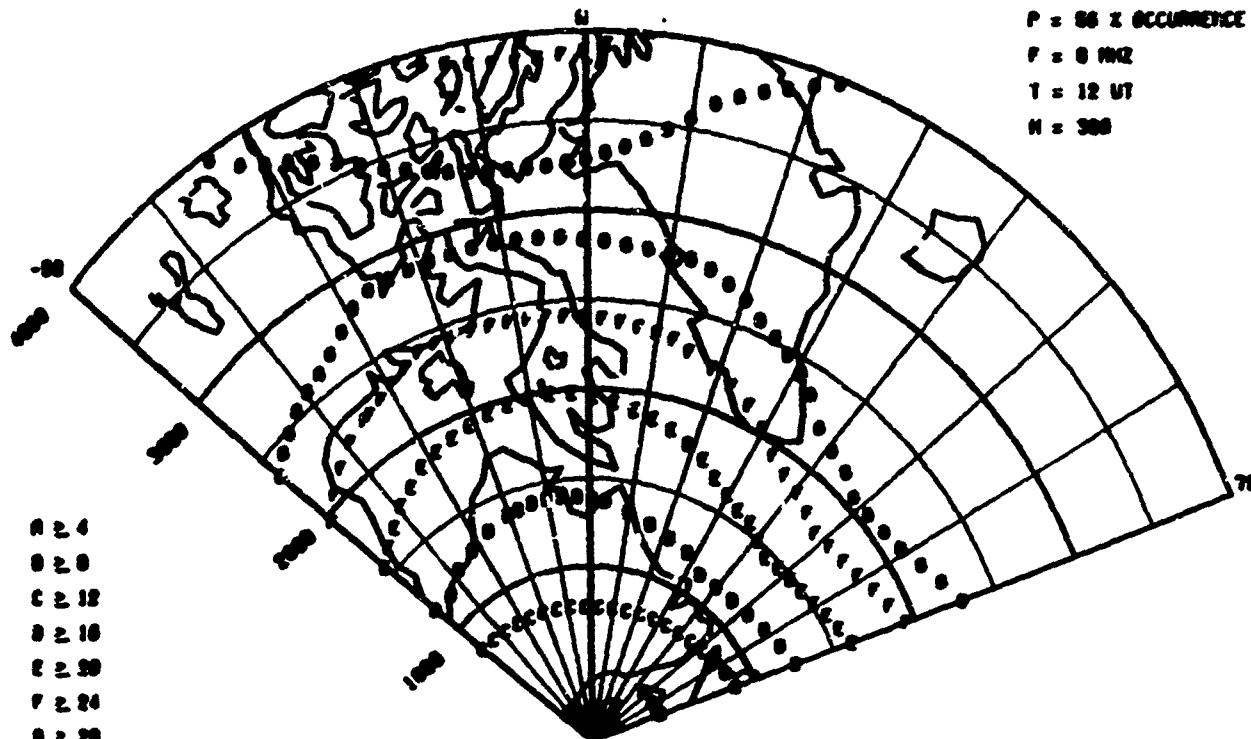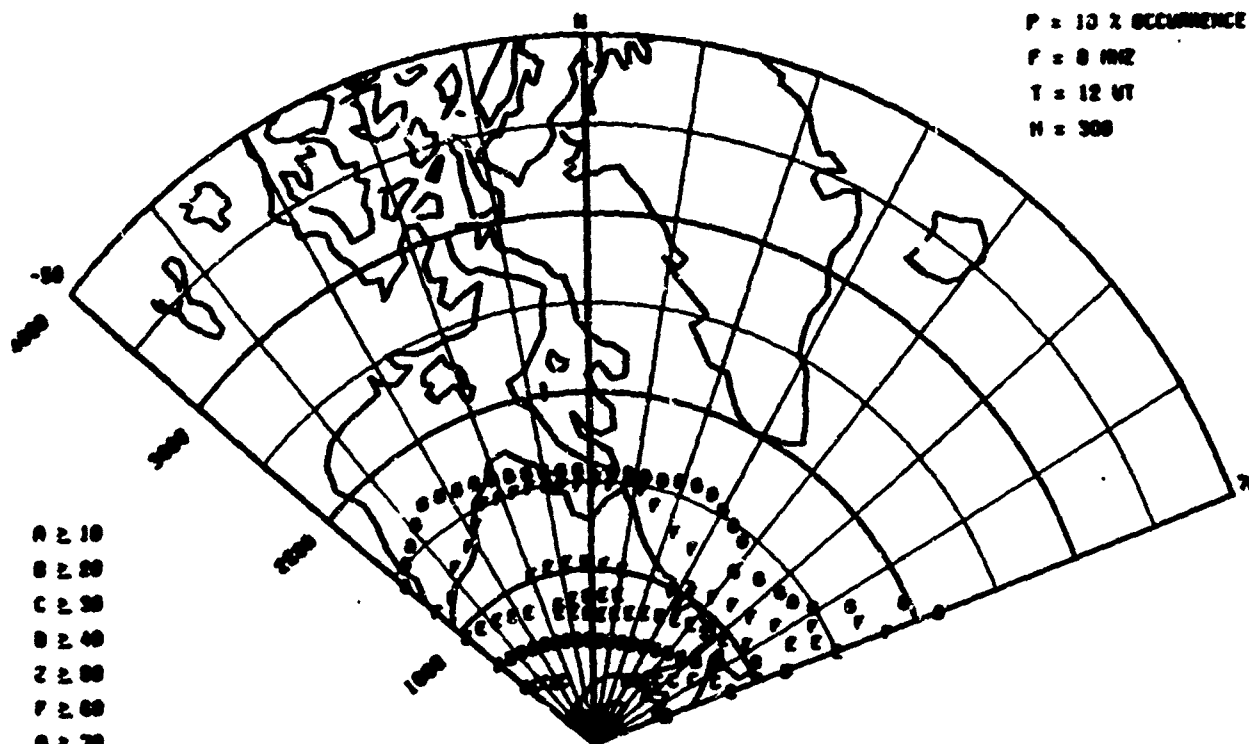
Fig. 28 - Radar Auroral Absorption F-8MHz, T=12UT, H=300km

69

RADAR AURORAL ABSORPTION
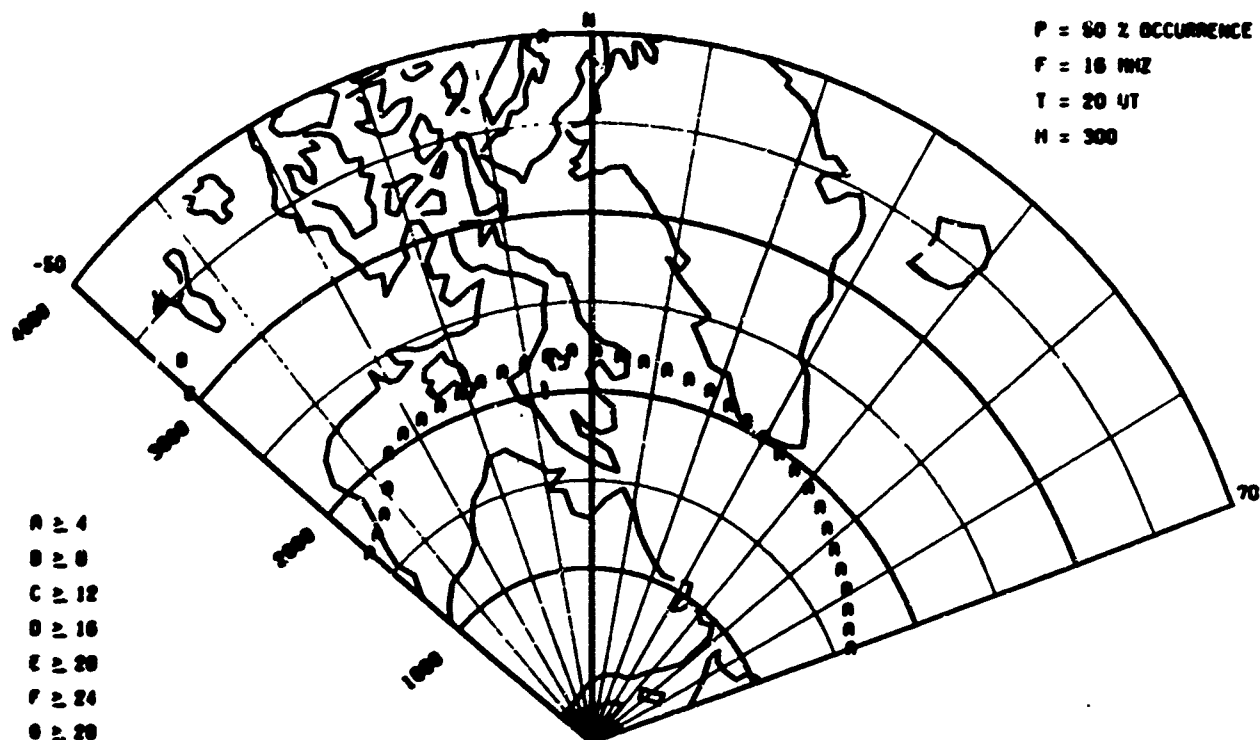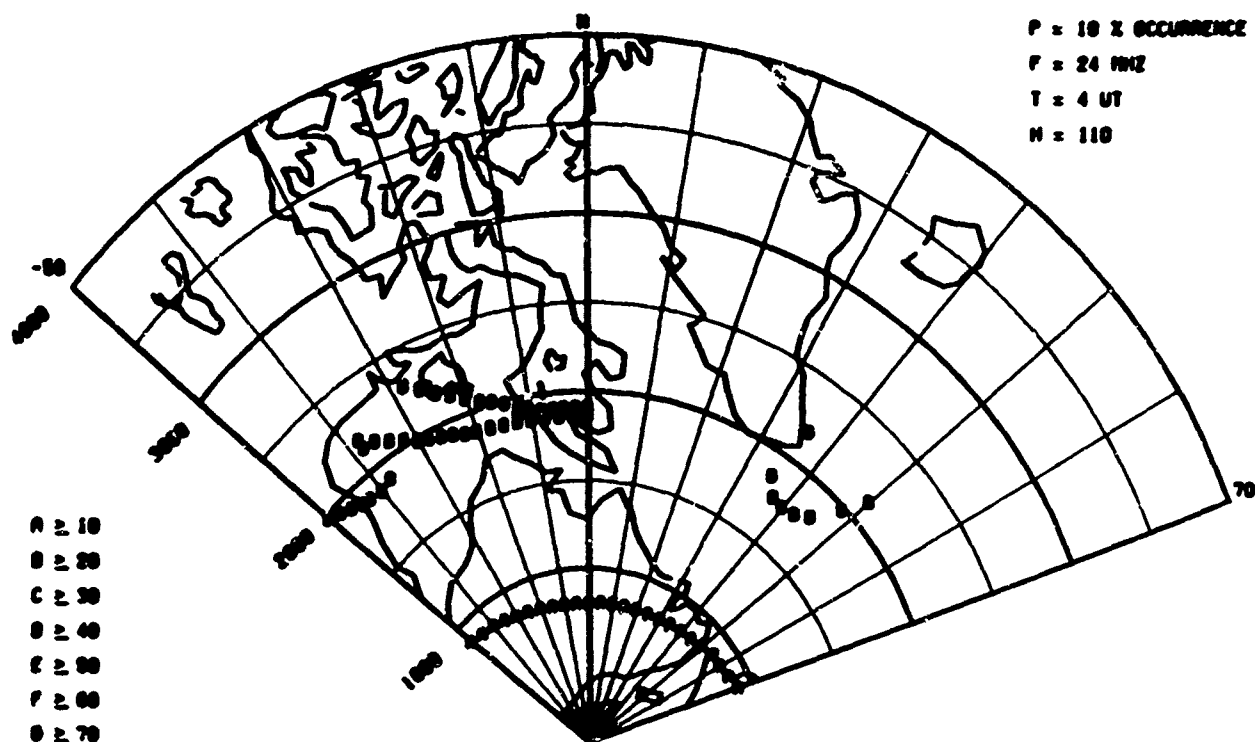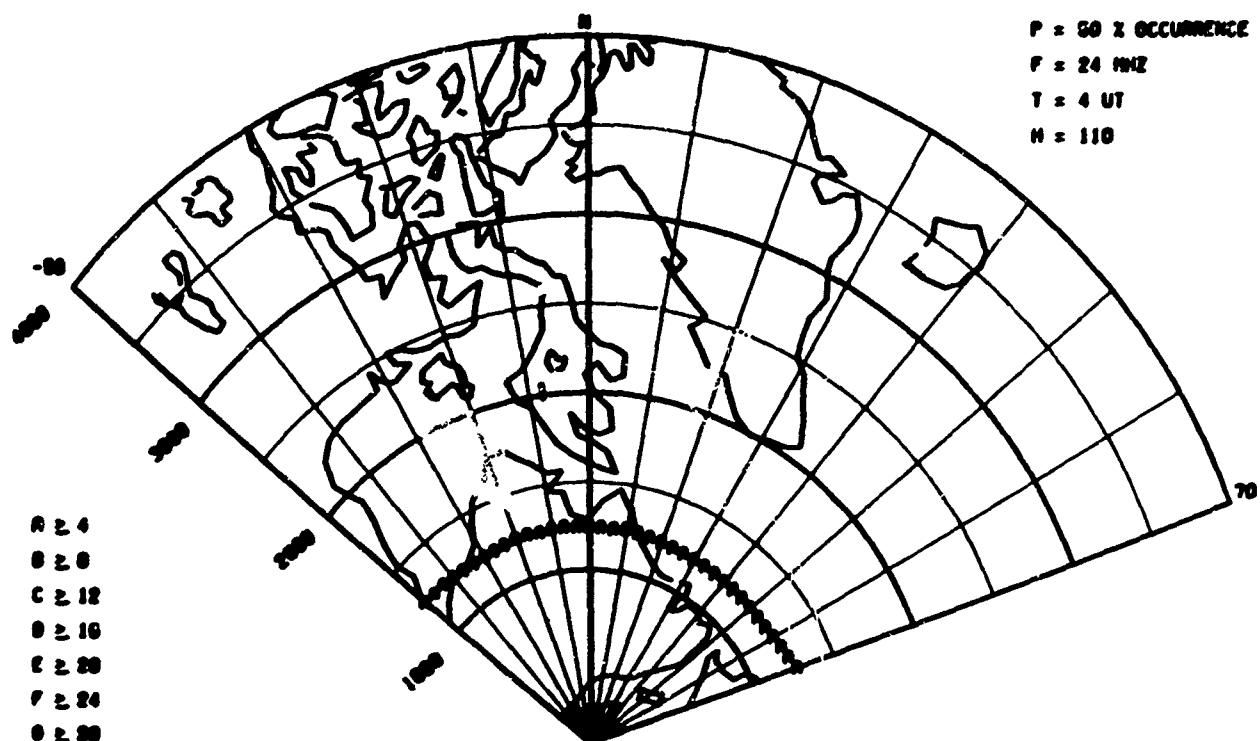
P = 80 % OCCURRENCE
F = 8 MHZ
T = 20 UT
H = 300

A ≥ 4
B ≥ 8
C ≥ 12
D ≥ 16
E ≥ 20
F ≥ 24
G ≥ 28

P = 10 % OCCURRENCE
F = 8 MHZ
T = 20 UT
H = 300

A ≥ 10
B ≥ 20
C ≥ 30
D ≥ 40
E ≥ 50
F ≥ 60
G ≥ 70
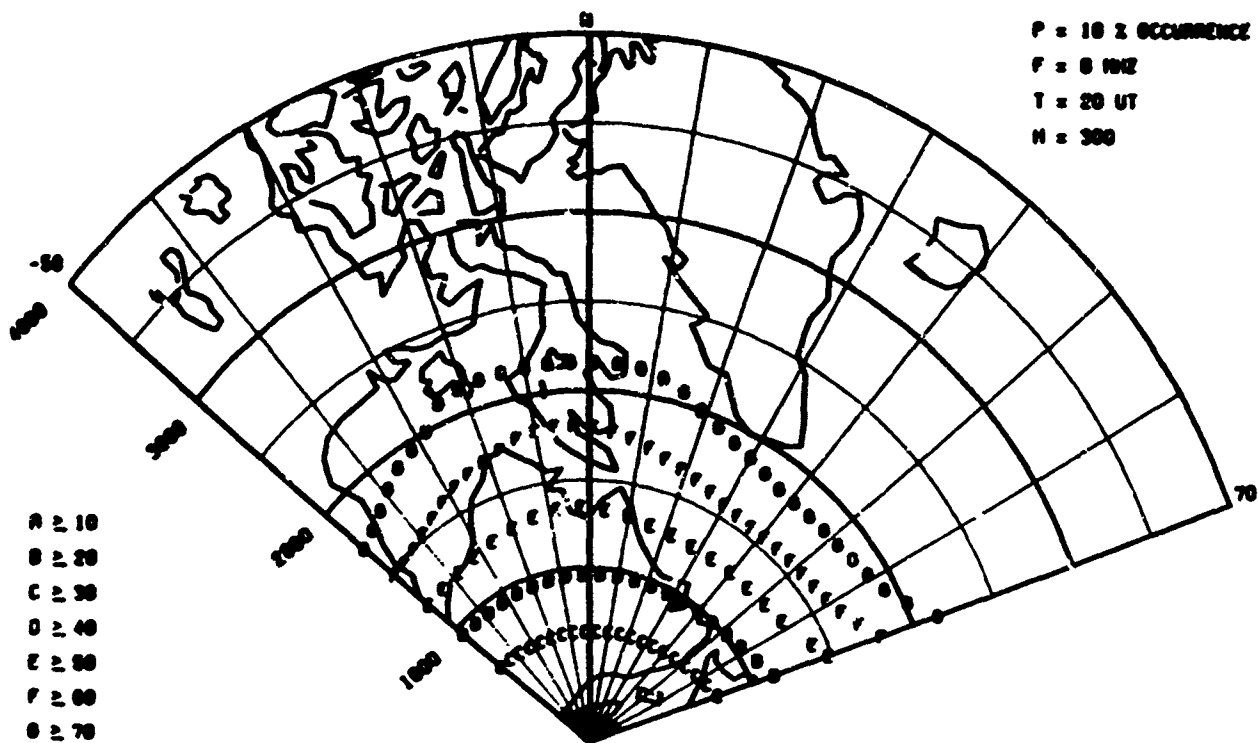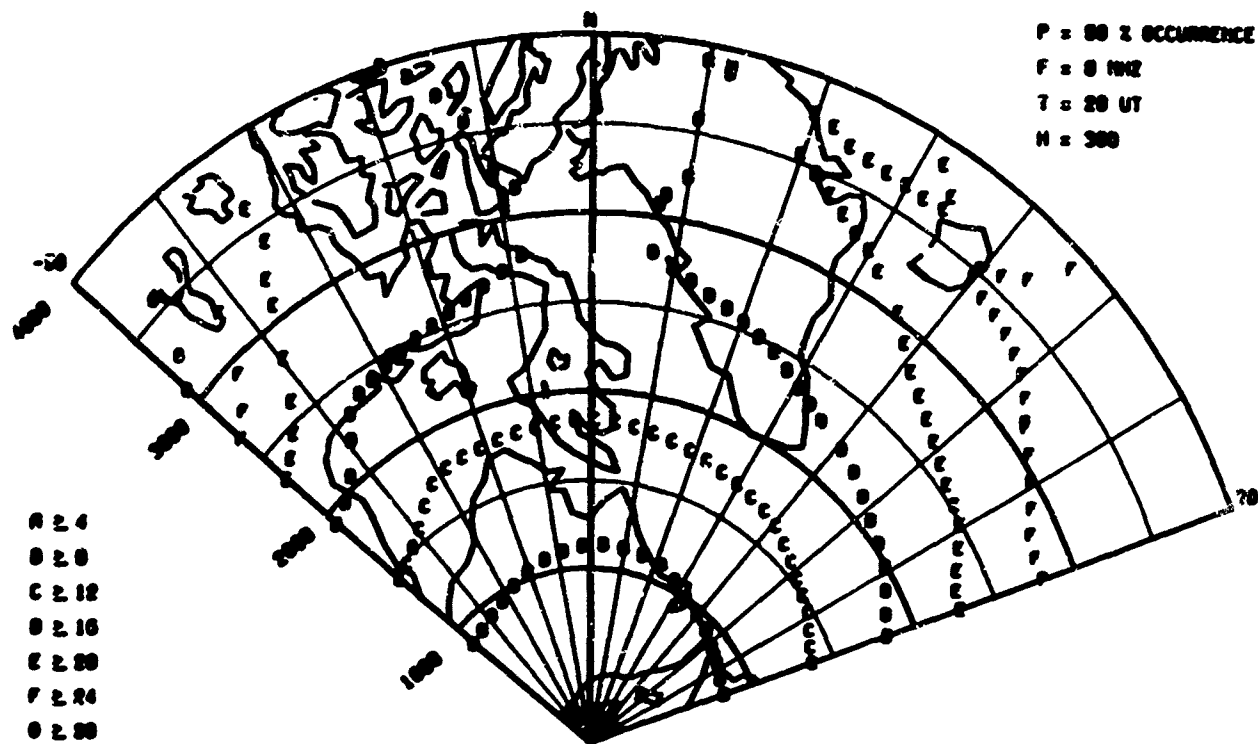
Figl 29 - Radar Auroral Absorption F=8MHz, T=20UT, H=300km

70

RADAR AURORAL ABSORPTION
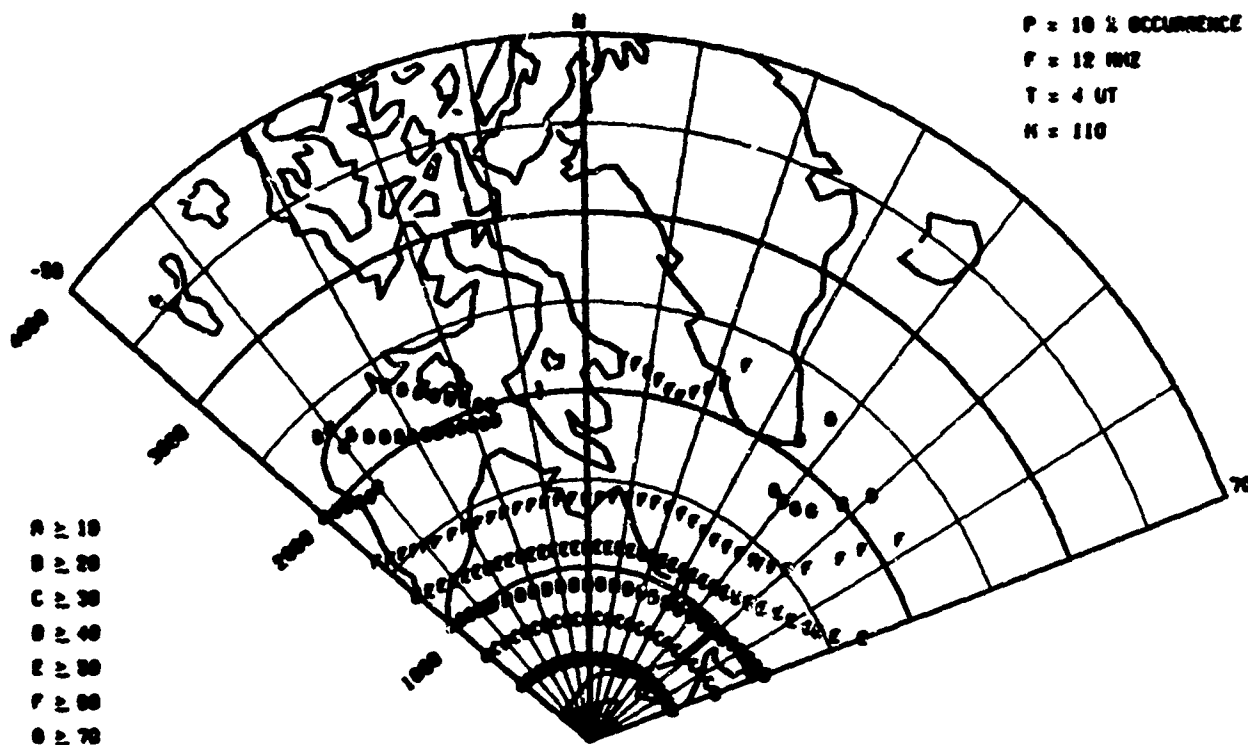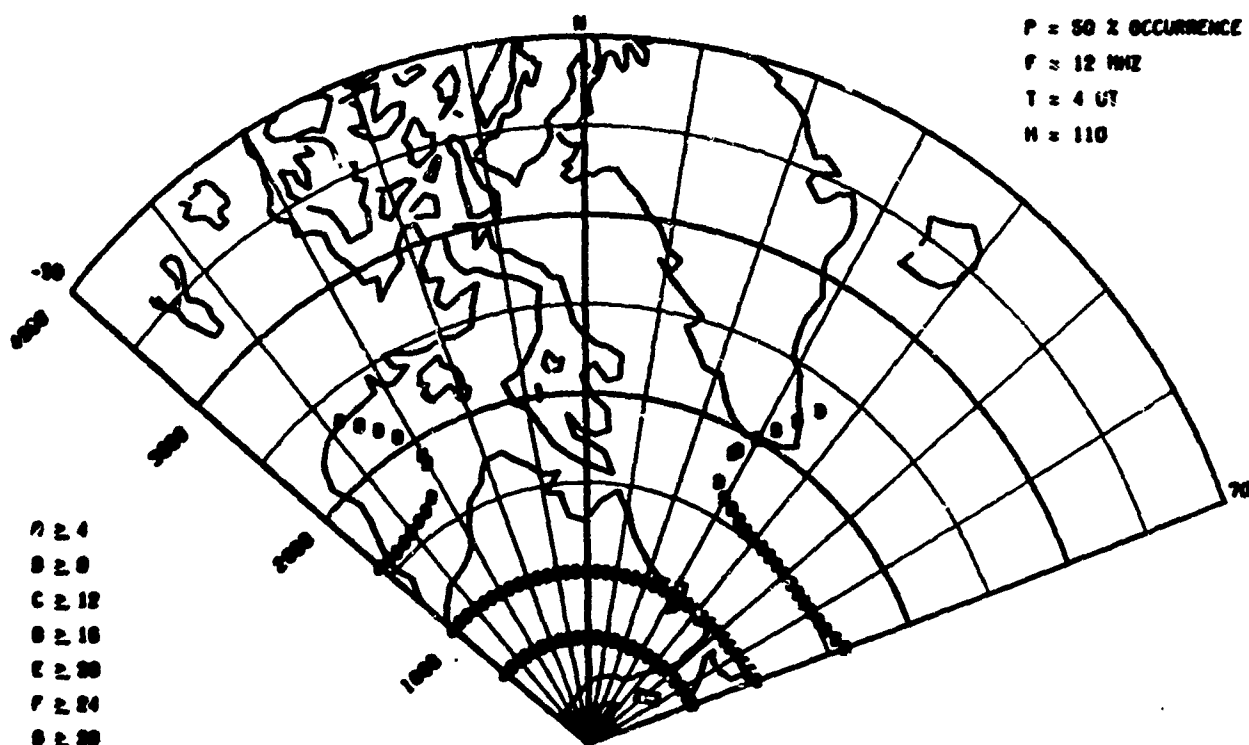
Fig. 30 – Radar Auroral Absorption F=12MHz, T-04UT, H=110km
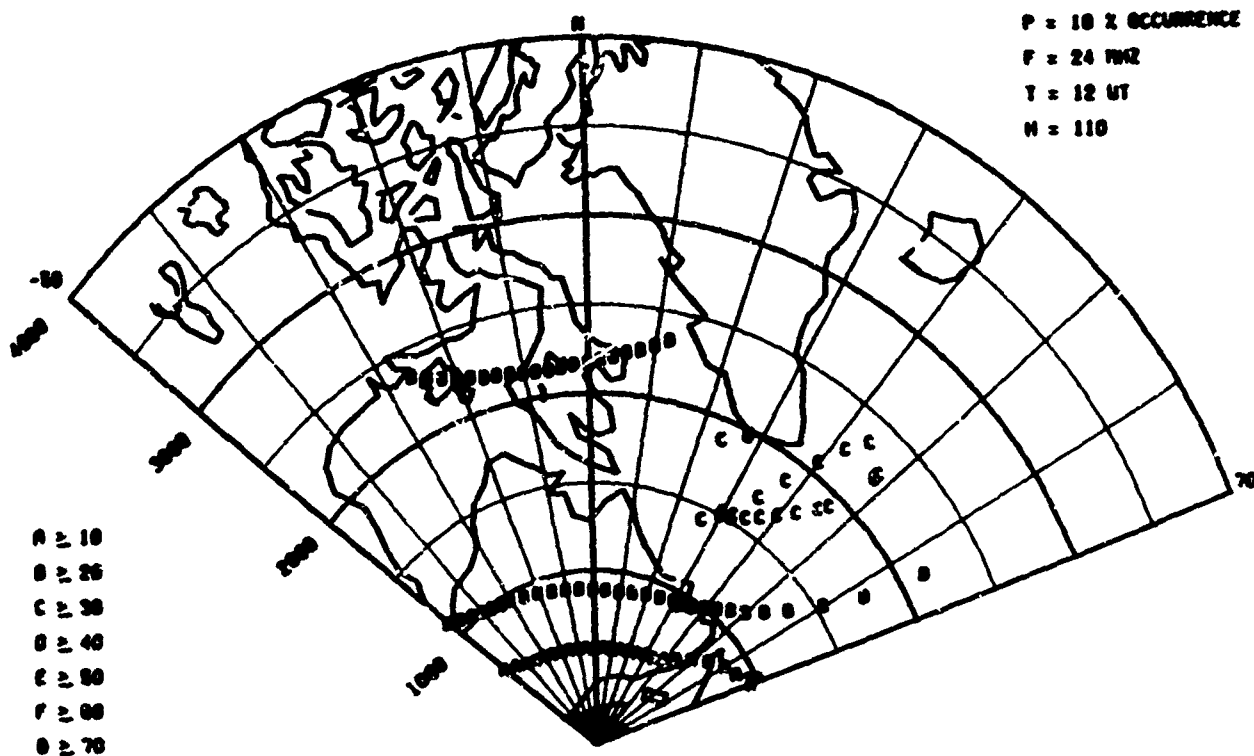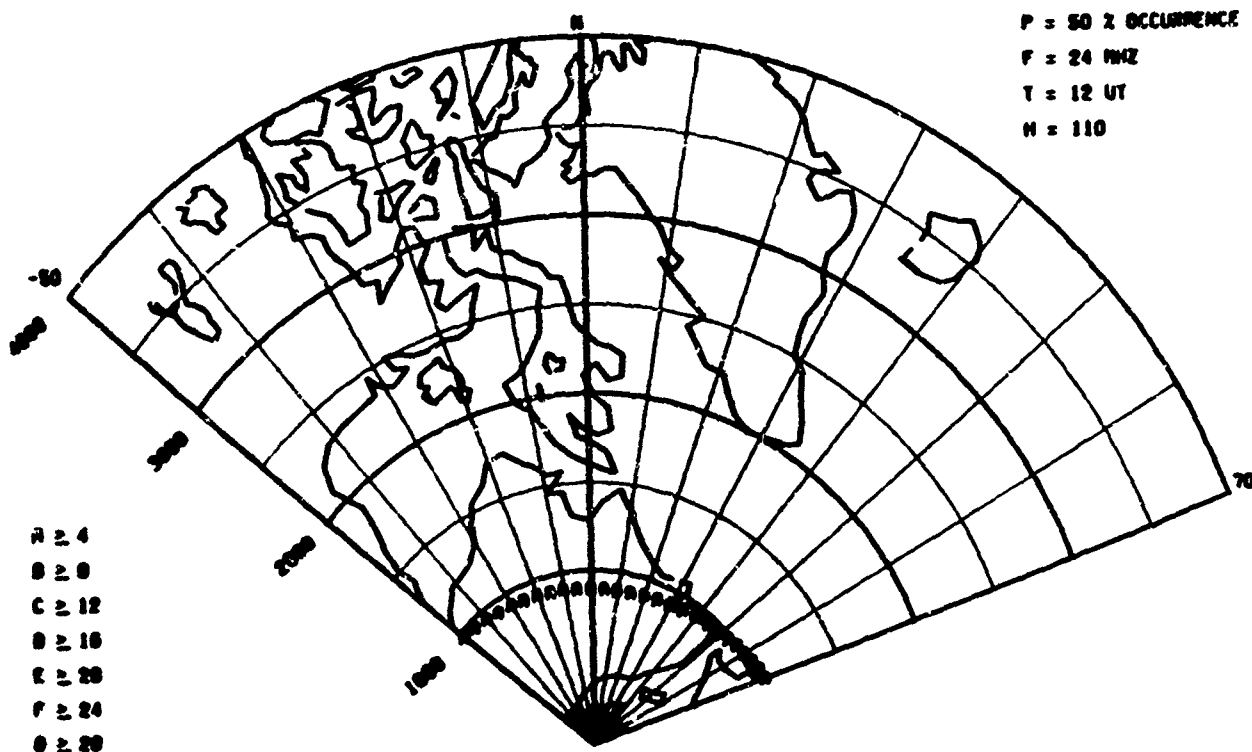
71

RADAR AURORAL ABSORPTION
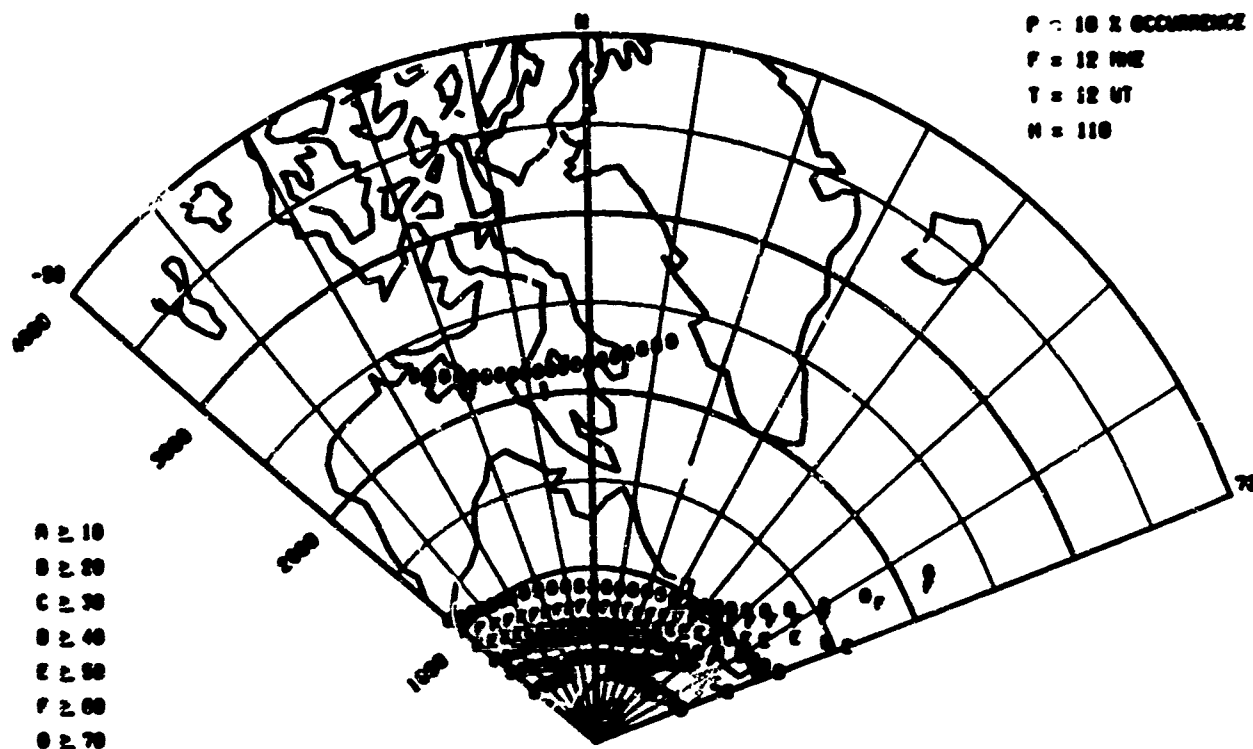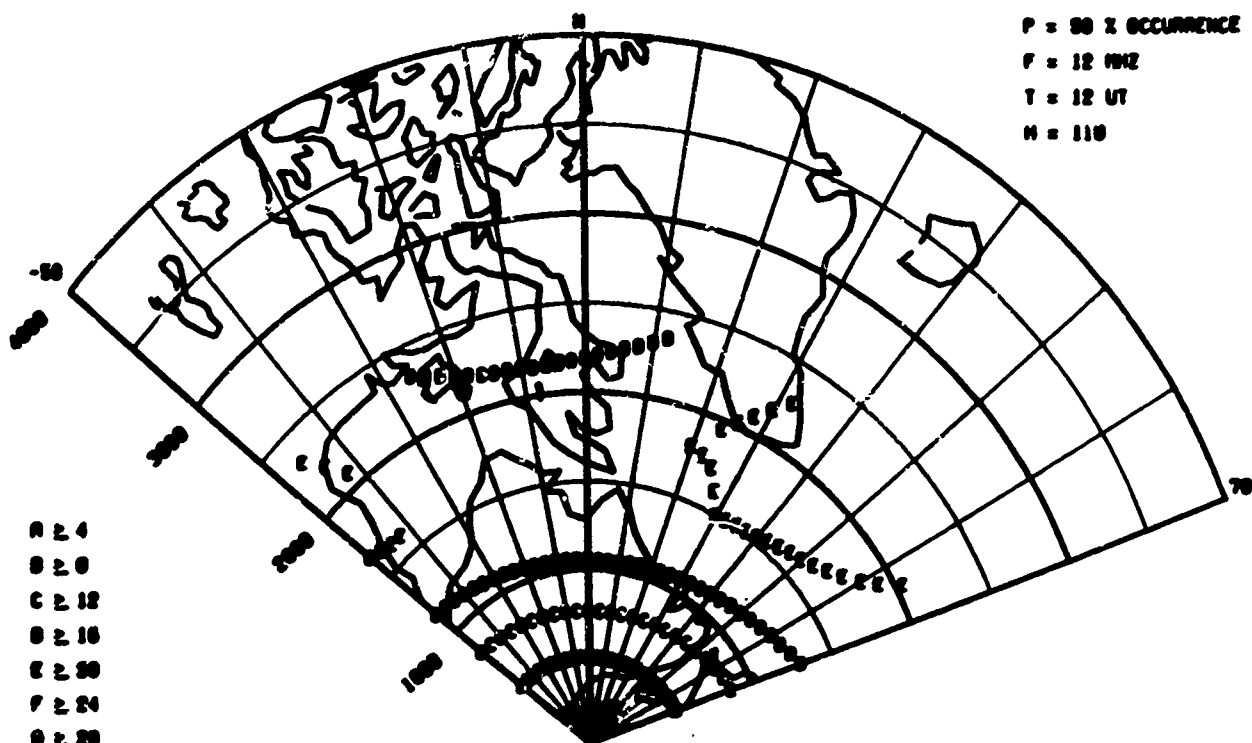
Fig. 31 - Radar Auroral Absorption, F=12MHz, T=12UT, H=110km

72

RADAR AURORAL ABSORPTION

P = 80 % OCCURRENCE
F = 12 MHZ
T = 20 UT
H = 110

A ≥ 4
B ≥ 8
C ≥ 12
D ≥ 16
E ≥ 20
F ≥ 24
G ≥ 28

P = 10 % OCCURRENCE
F = 12 MHZ
T = 20 UT
H = 110

A ≥ 10
B ≥ 20
C ≥ 30
D ≥ 40
E ≥ 50
F ≥ 60
G ≥ 70

Fig. 32 - Radar Auroral Absorption F=12MHz, 20UT, H-110km

73

RADAR AURORAL ABSORPTION
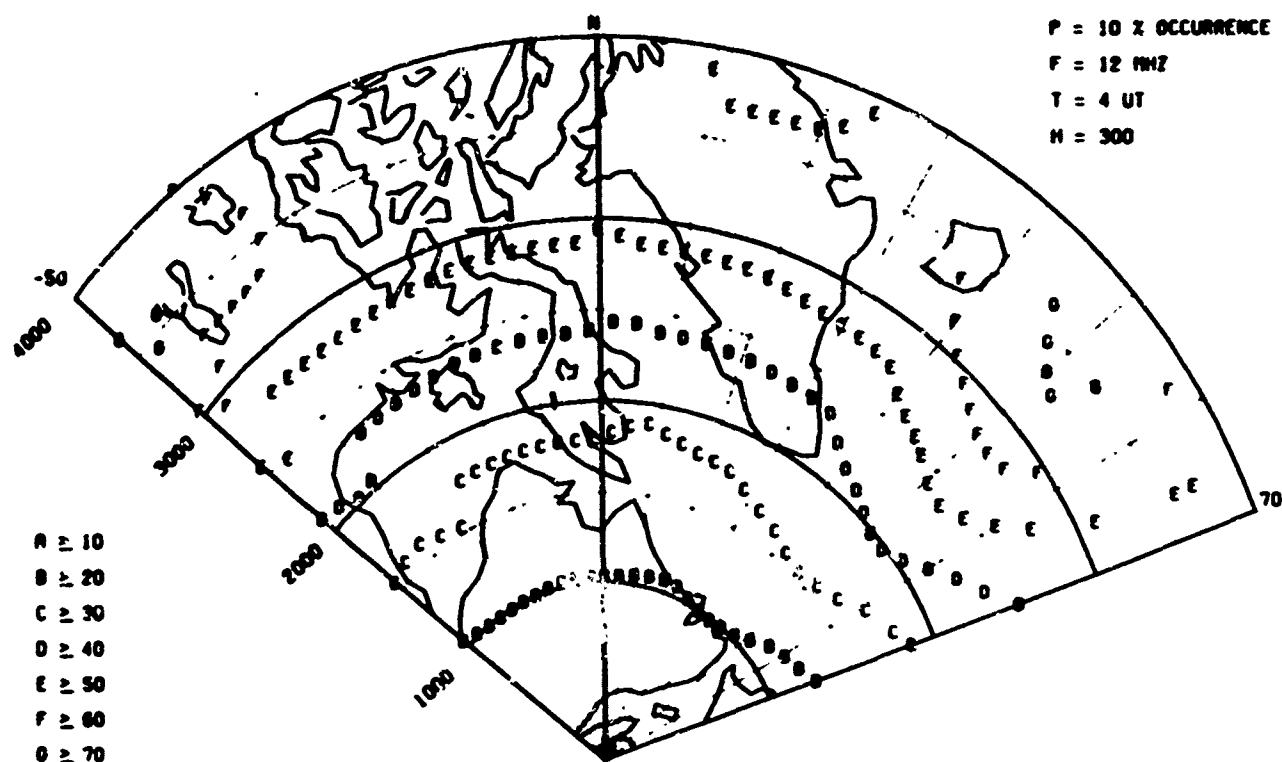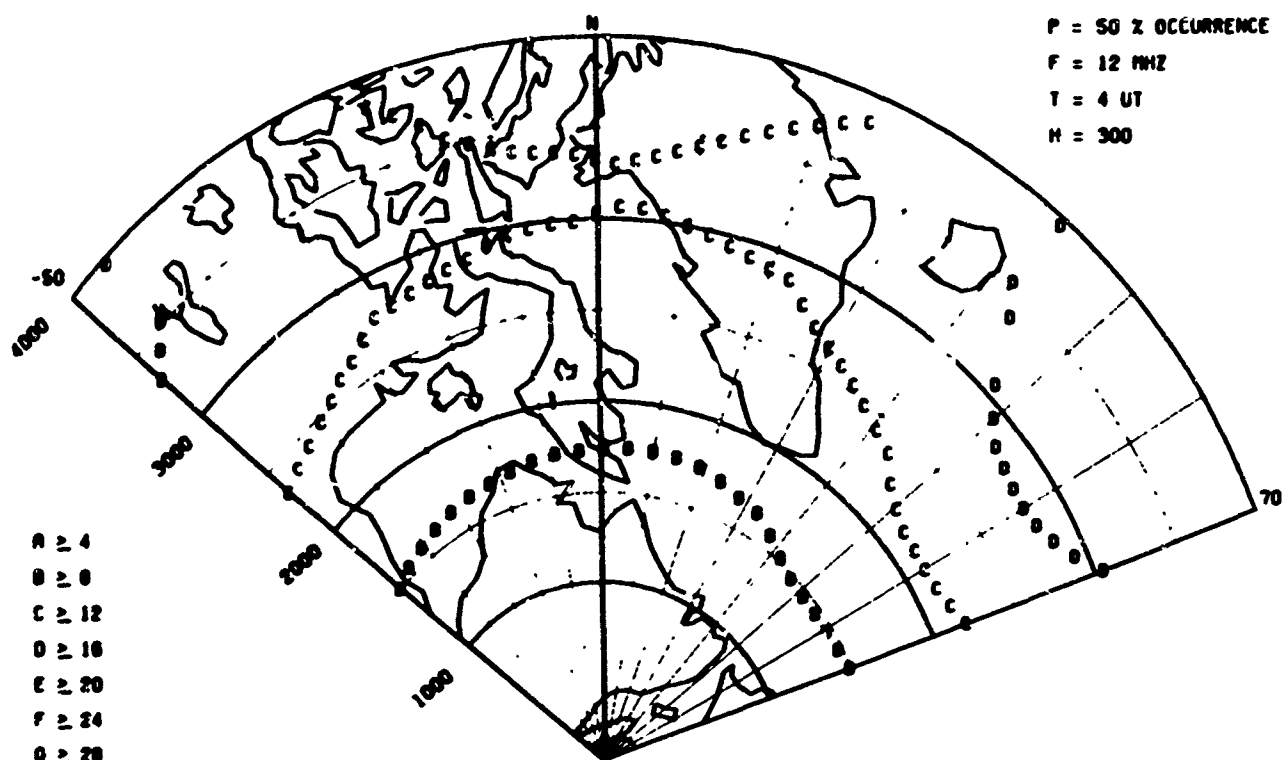
Fig. 33 - Radar Auroral Absorption F=12MHz, T=04UT, H=300km

RADAR AURORAL ABSORPTION
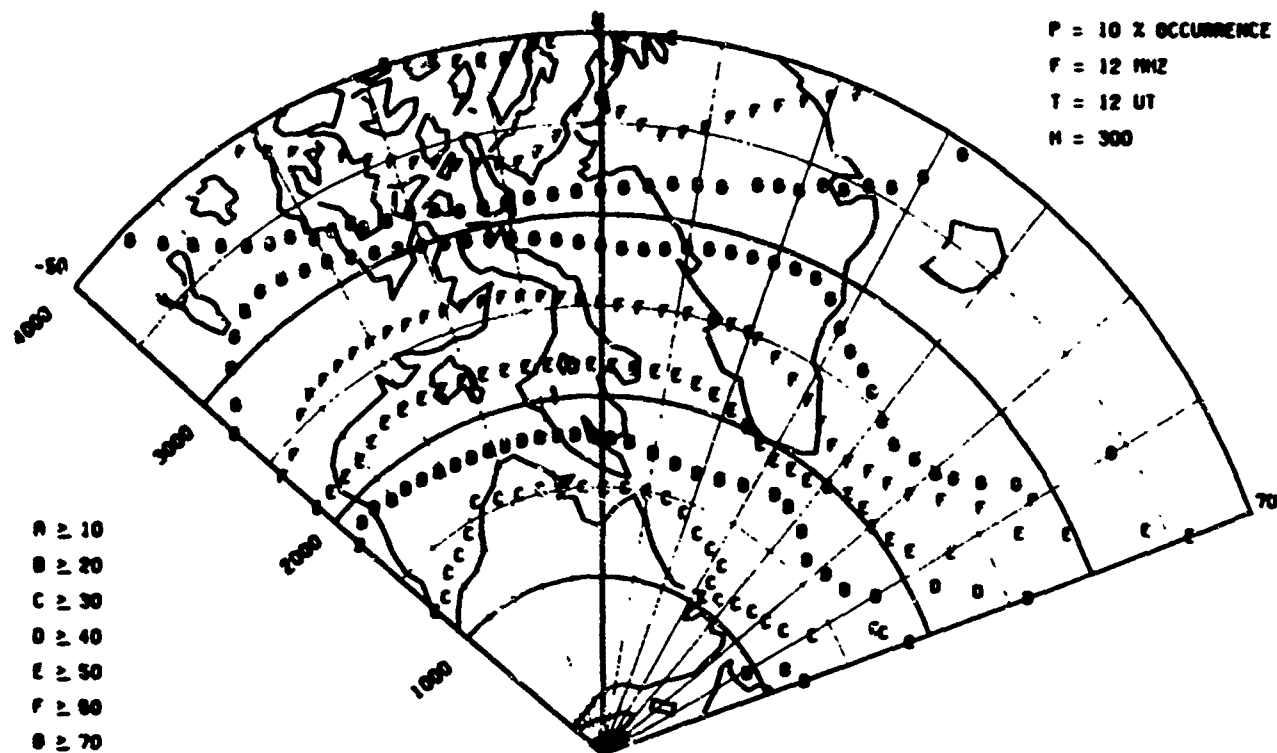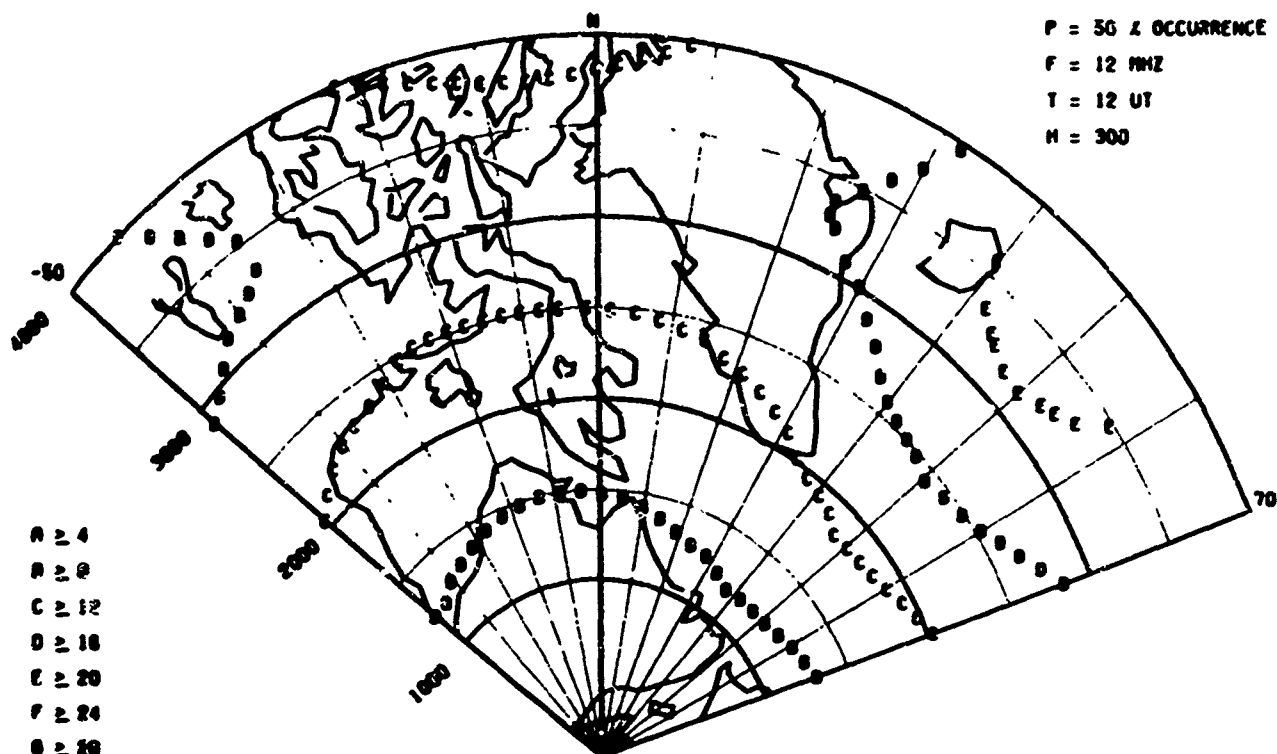
Fig. 34 - Radar Auroral Absorption F=12MHz, T=12UT, H=300km
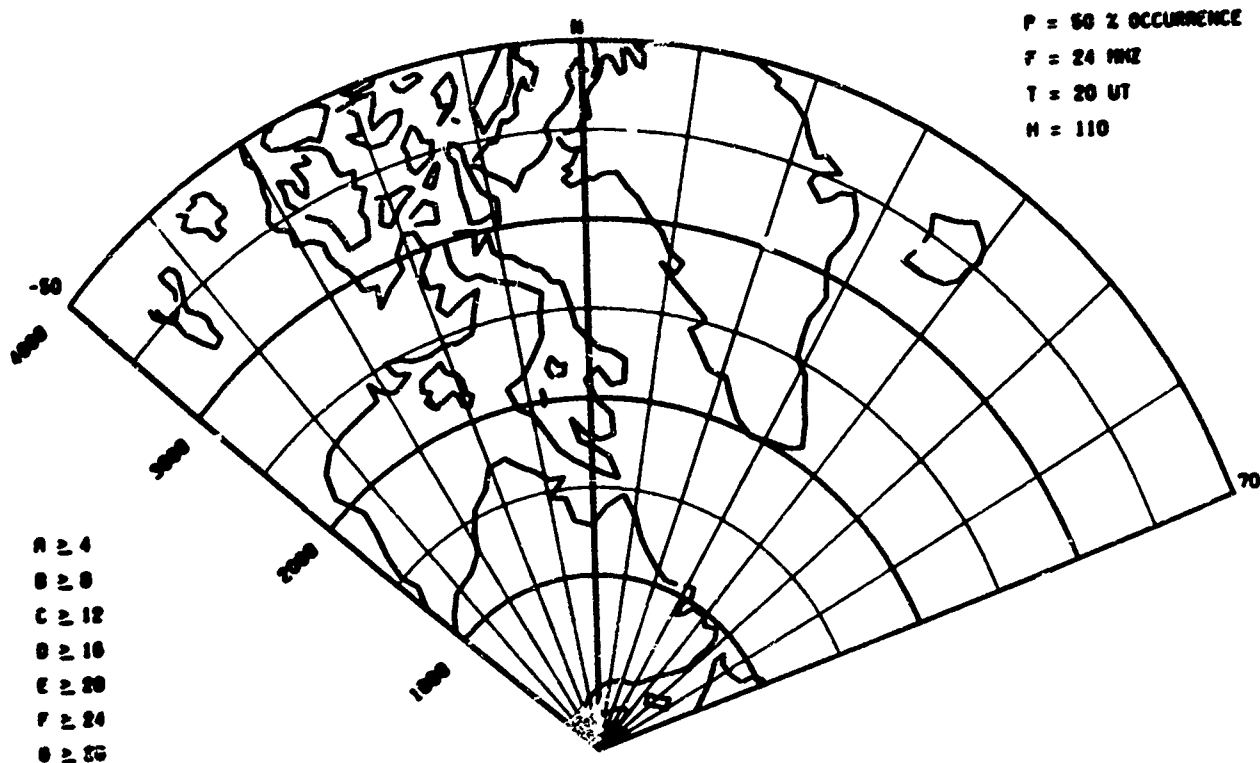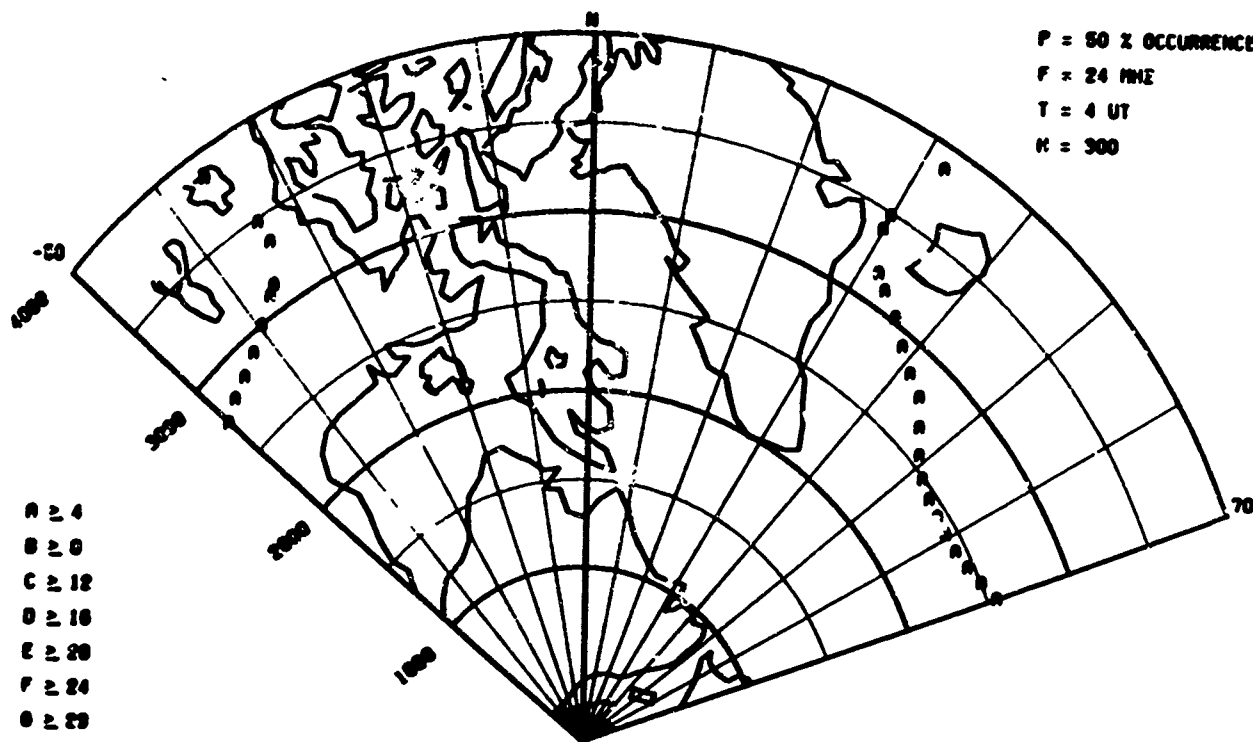
75

RADAR AURORAL ABSORPTION

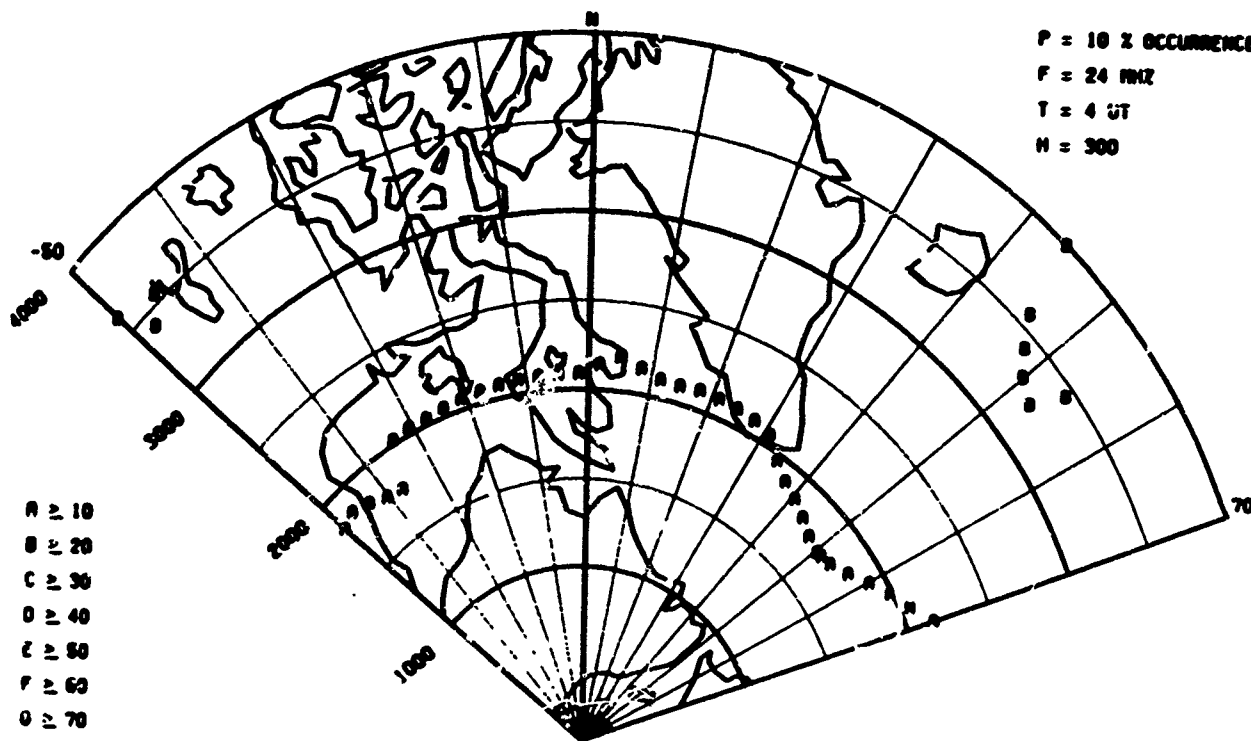Fig. 35 - Radar Auroral Absorption F=12MHz, T=20UT, H=300km

RADAR AURORAL ABSORPTION

P = 50 % OCCURRENCE
F = 16 MHZ
T = 4 UT
H = 110

A ≥ 4
B ≥ 8
C ≥ 12
D ≥ 16
E ≥ 20
F ≥ 24
G ≥ 28

P = 10 % OCCURRENCE
F = 16 MHZ
T = 4 UT
H = 110

A ≥ 10
B ≥ 20
C ≥ 30
D ≥ 40
E ≥ 50
F ≥ 60
G ≥ 70
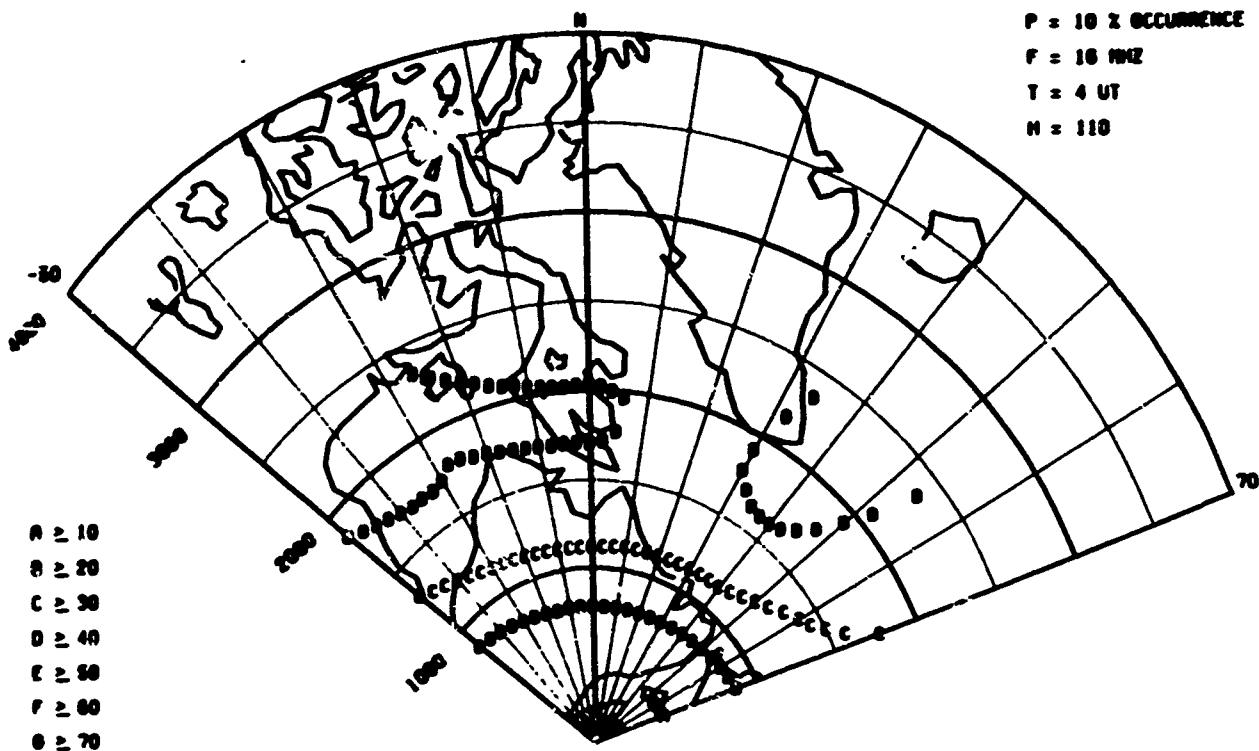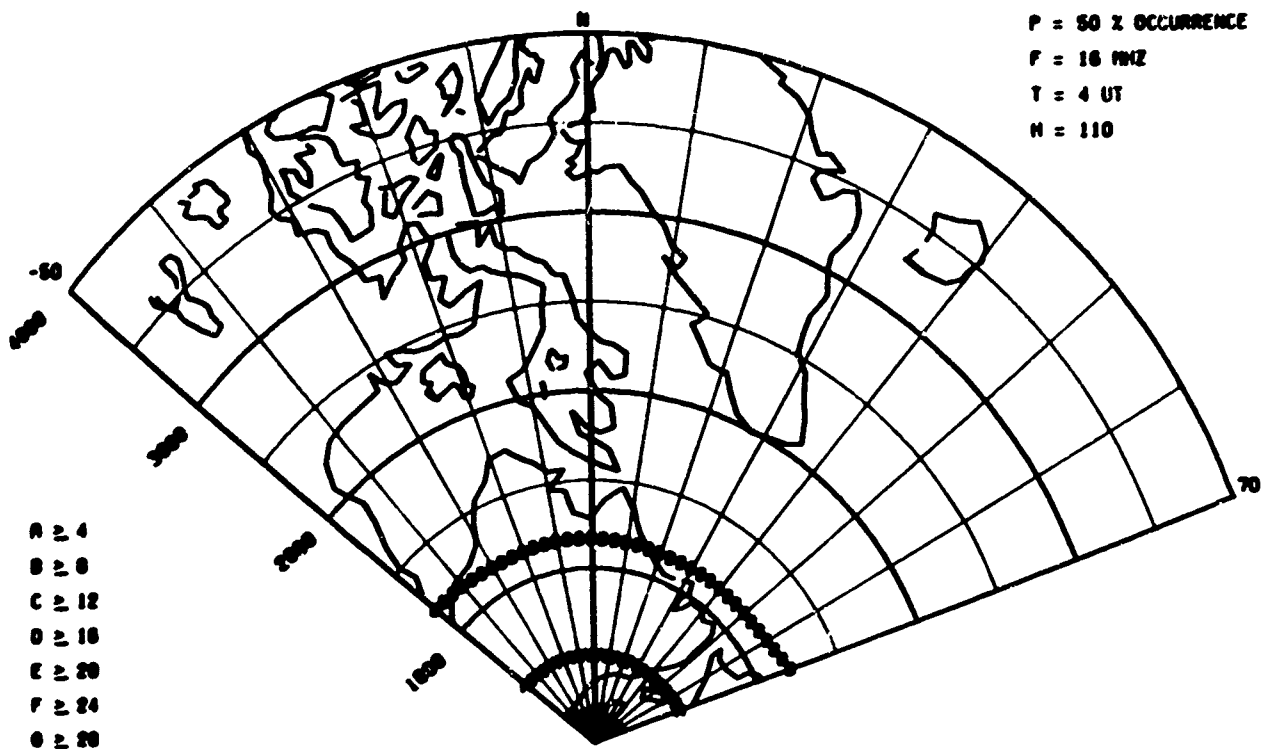
Fig   36 - Radar Auroral Absorption F=16MHz, T=04UT, H=110km

77

RADAR AURORAL ABSORPTION
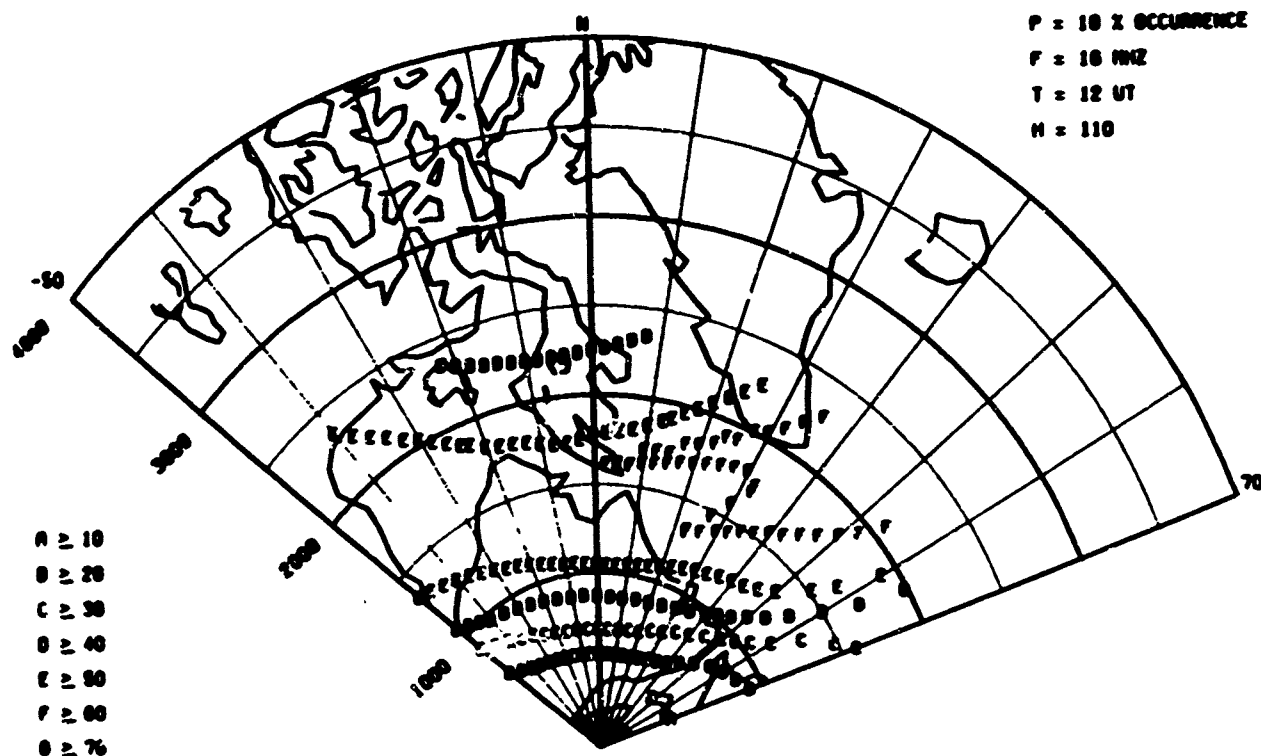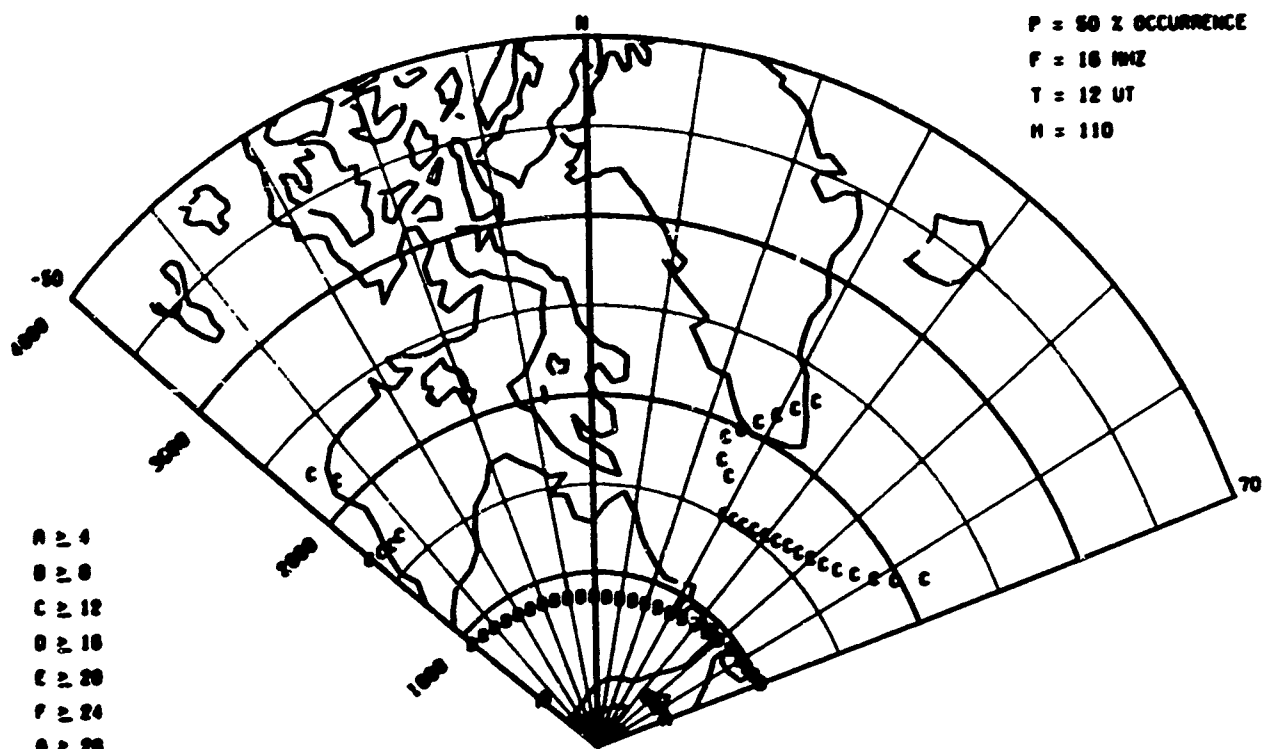
Fig. 37 - Radar Auroral Absorption F=16MHz, T=12UT, H=110km

78

RADAR AURORAL ABSORPTION

Fig. 38 - Radar Auroral Absorption F=16MHz, T=20UT, H=110km

79

RADAR AURORAL ABSORPTION

P = 50 % OCCURRENCE
F = 16 MHz
T = 4 UT
H = 300

A ≥ 4
B ≥ 8
C ≥ 12
D ≥ 16
E ≥ 20
F ≥ 24
G ≥ 28

P = 10 % OCCURRENCE
F = 16 MHz
T = 4 UT
H = 300

A ≥ 10
B ≥ 20
C ≥ 30
D ≥ 40
E ≥ 50
F ≥ 60
G ≥ 70

Fig. 39 - Radar Auroral Absorption F=16MHz, T=04UT, H=300km
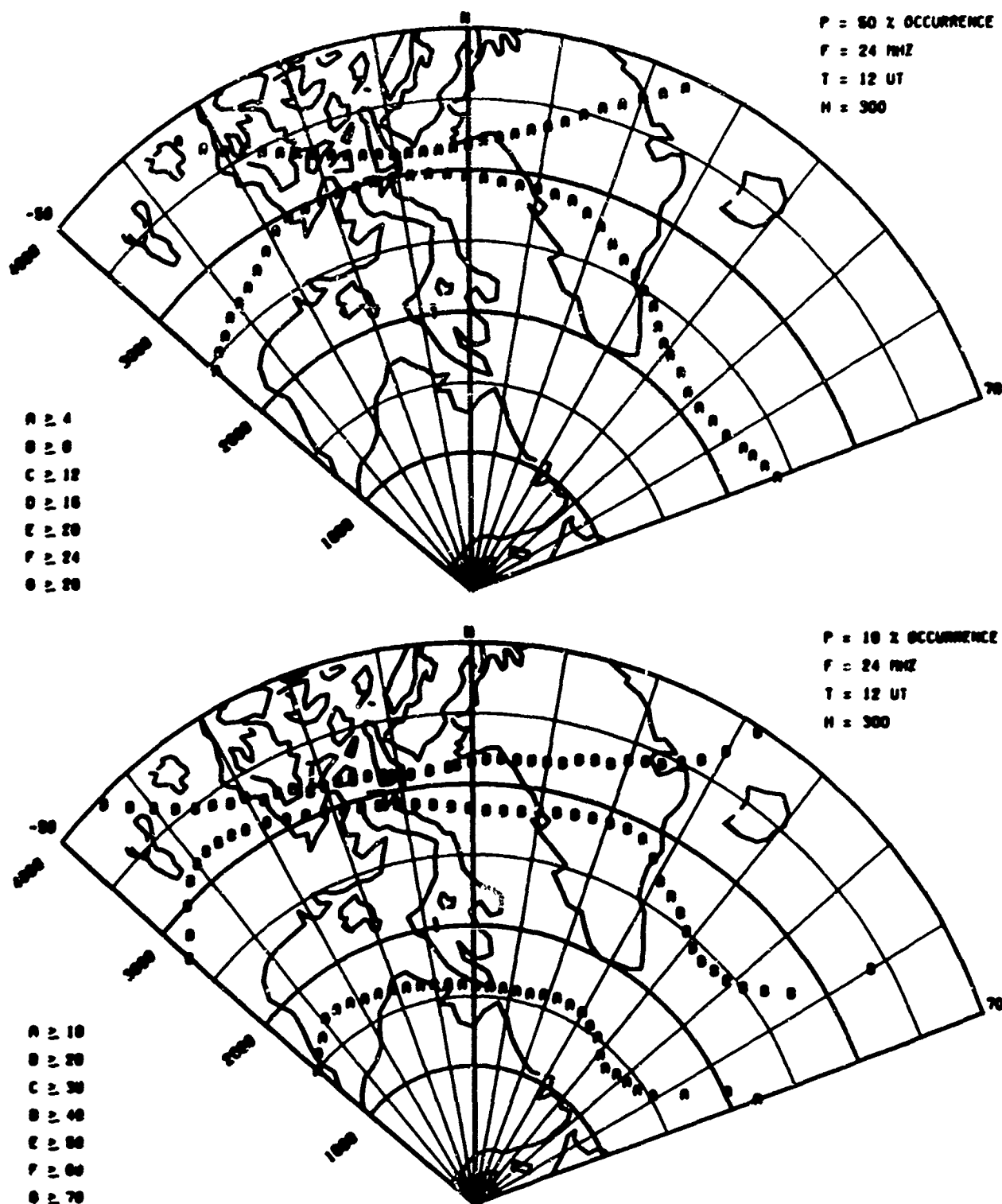
80

RADAR AURORAL ABSORPTION

Fig. 40 - Radar Auroral Absorption F=16MHz, T=12UT, H=300km

81

RADAR AURORAL ABSORPTION

Fig. 41 - Radar Auroral Absorption F=16MHz, T=20UT, H=300km

RADAR AURORAL ABSORPTION

P = 50 % OCCURRENCE

F = 24 MHZ

T = 4 UT

H = 110

A ≥ 4
B ≥ 8
C ≥ 12
D ≥ 16
E ≥ 20
F ≥ 24
G ≥ 30

P = 10 % OCCURRENCE

F = 24 MHZ

T = 4 UT

H = 110

A ≥ 10
B ≥ 20
C ≥ 30
D ≥ 40
E ≥ 50
F ≥ 60
G ≥ 70

Fig. 42 - Radar Auroral Absorption F=24MHz, T=04UT, H=110km

83

RADAR AURORAL ABSORPTION

Fig. 43 - Radar Auroral Absorption F=24MHz, T=12UT, H=110km

RADAR AURORAL ABSORPTION

P = 60 % OCCURRENCE
F = 24 MHZ
T = 20 UT
H = 110

A ≥ 4
B ≥ 8
C ≥ 12
D ≥ 16
E ≥ 20
F ≥ 24
G ≥ 28

P = 10 % OCCURRENCE
F = 24 MHZ
T = 20 UT
H = 110

A ≥ 10
B ≥ 20
C ≥ 30
D ≥ 40
E ≥ 50
F ≥ 60
G ≥ 70
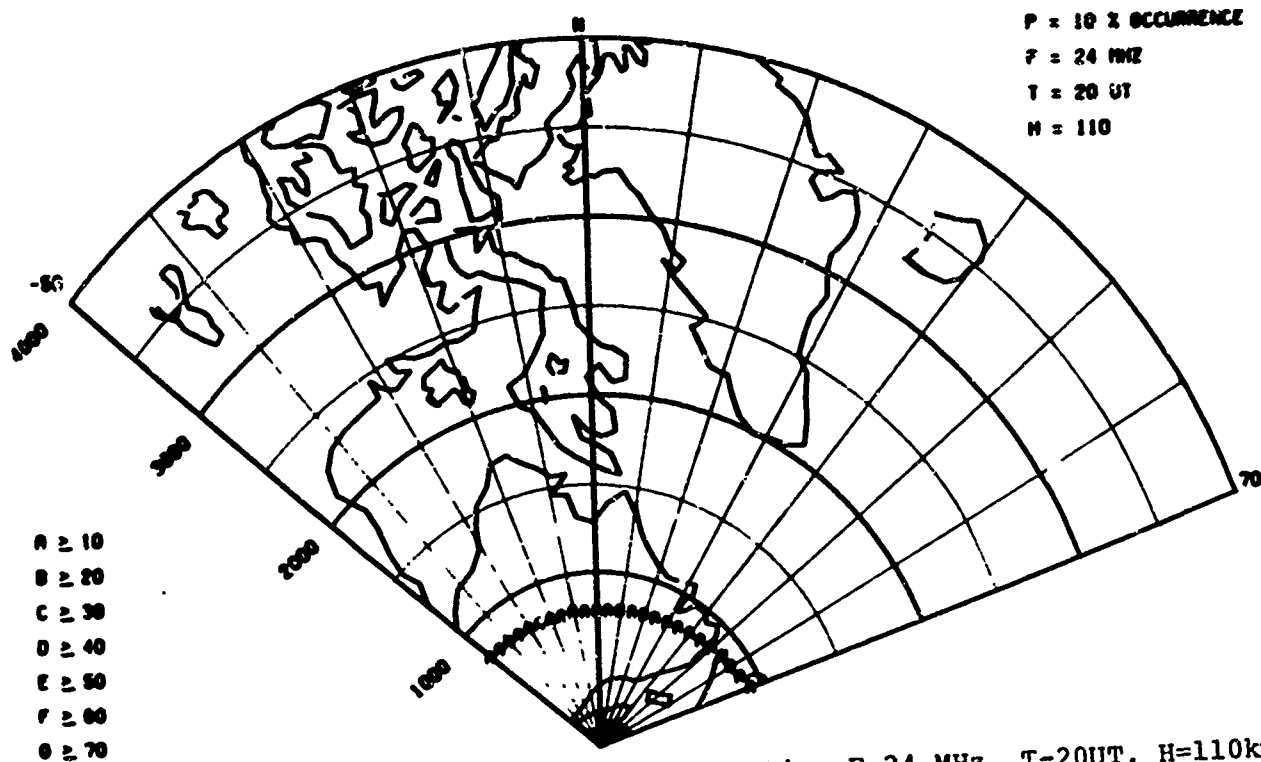
Fig. 44 – Radar Auroral Absorption F=24 MHz, T-20UT, H=110km

85

RADAR AURORAL ABSORPTION

Fig. 45 - Radar Auroral Absorption F=24MHz, T=04UT, H=300km

86

RADAR AURORAL ABSORPTION

Fig. 46 - Radar Auroral Absorption F=24MHz, T=12UT, H=300km

RADAR AURORAL ABSORPTION
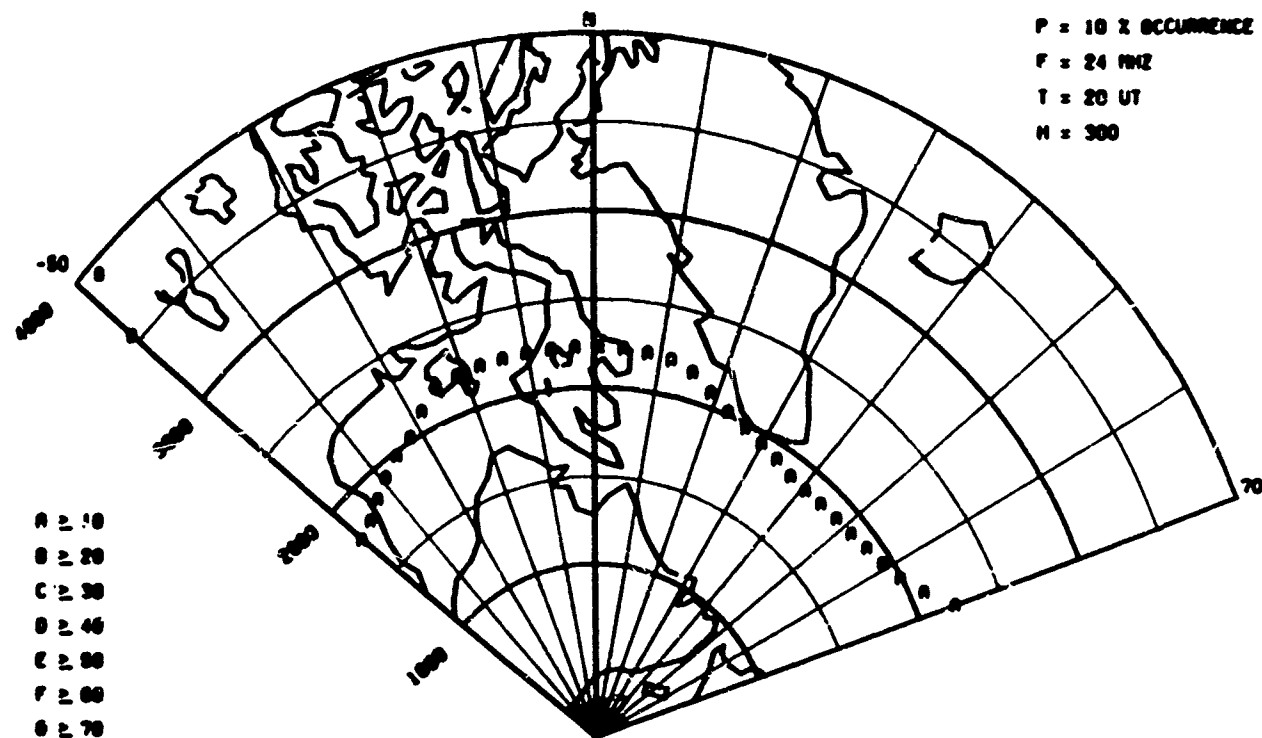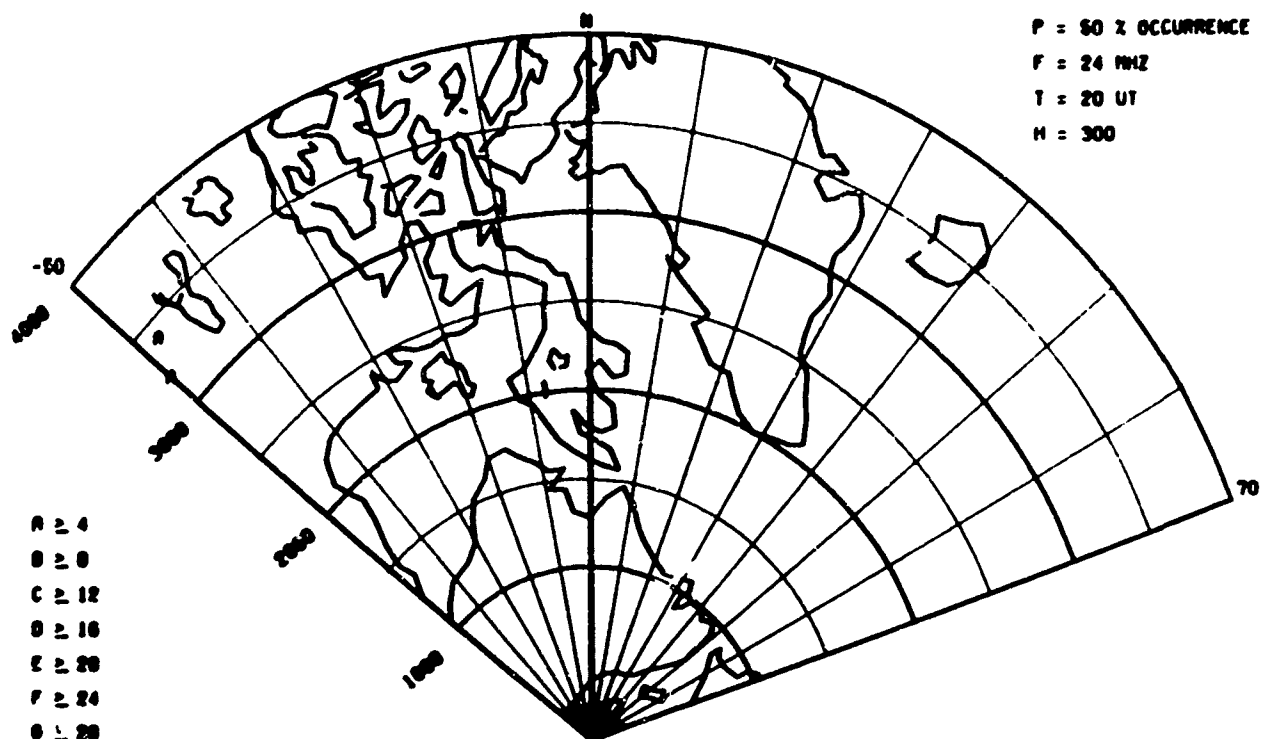
Fig. 47 - Radar Auroral Absorption F=24MHz, T=20UT, H=300km
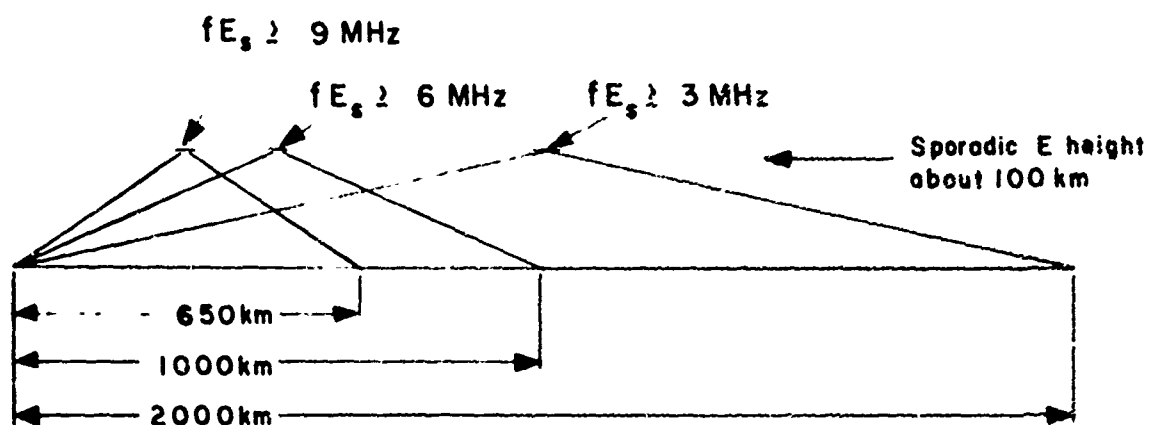
Fig. 48 HF forward scatter propagation model for 30 MHz or less
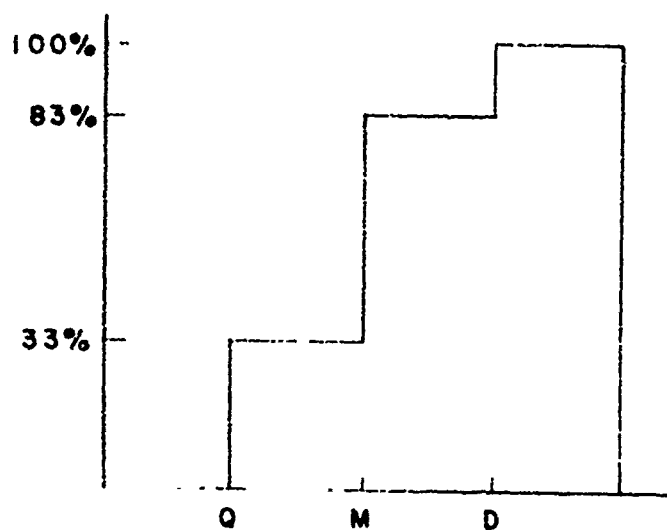
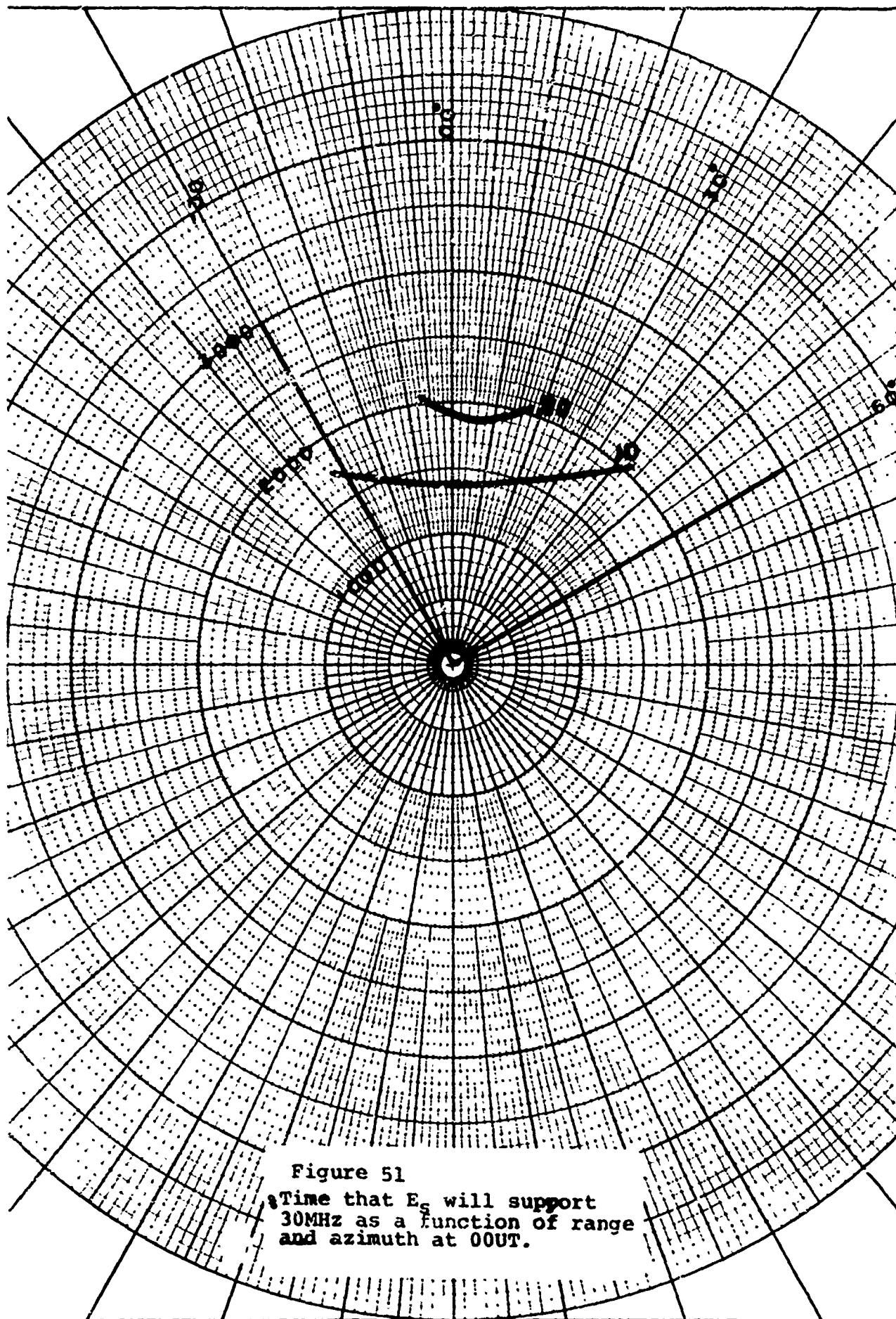Fig. 49 - Assumed Cummulative Probability Distribution
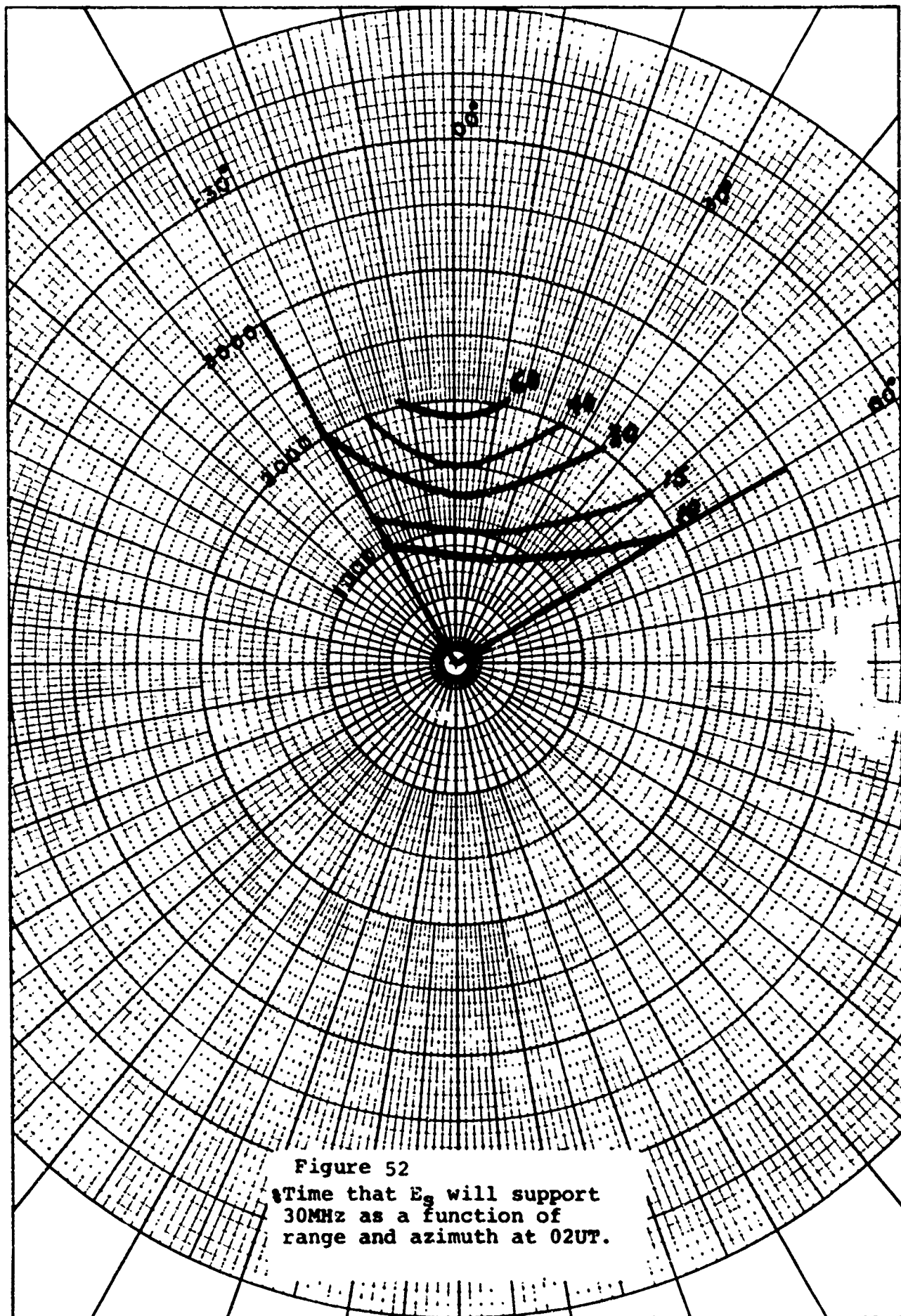
for Magnetic Activity

Fig. 50 – % Time that E_s will support 30MHz as a function of range and azimuth at 22UT.
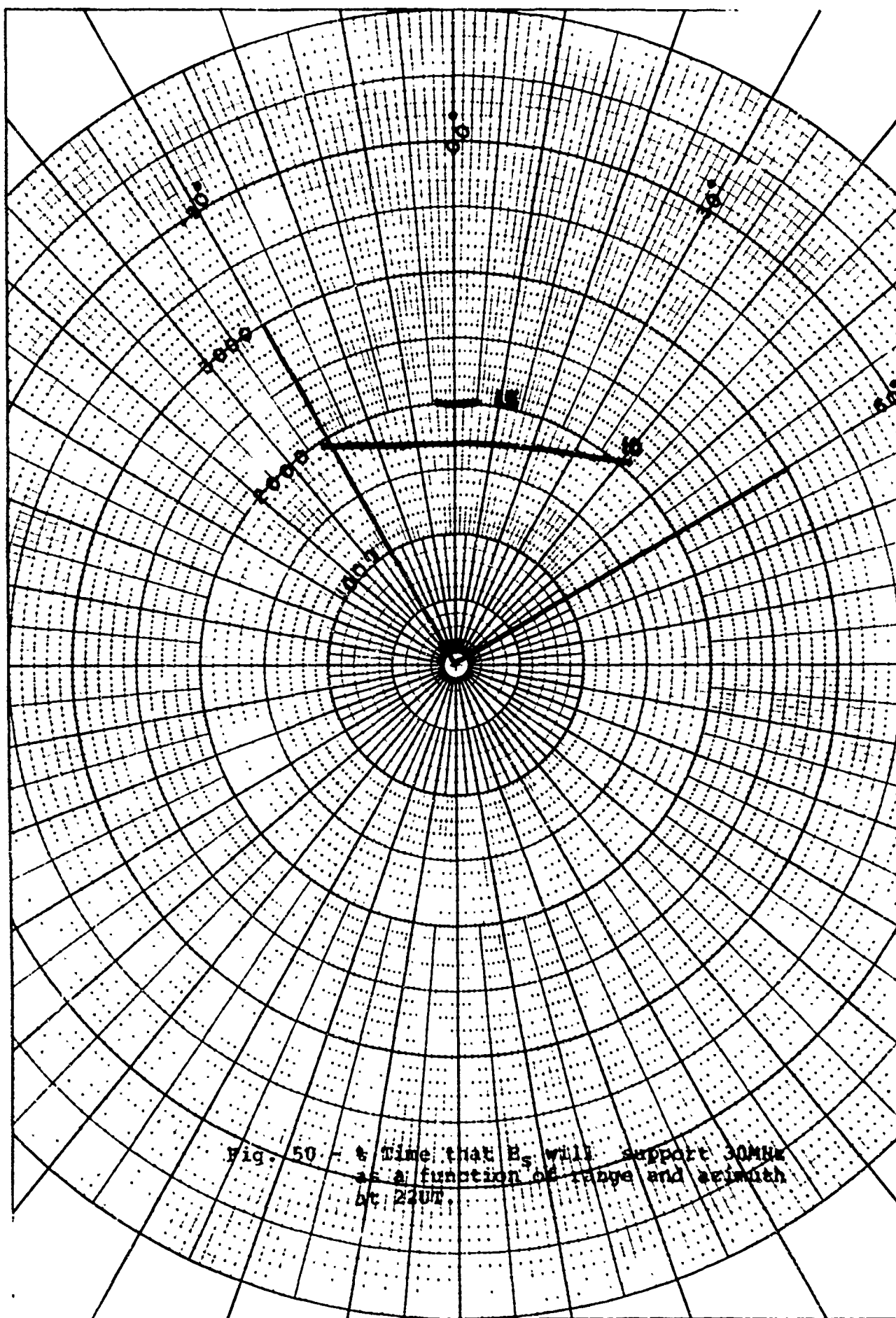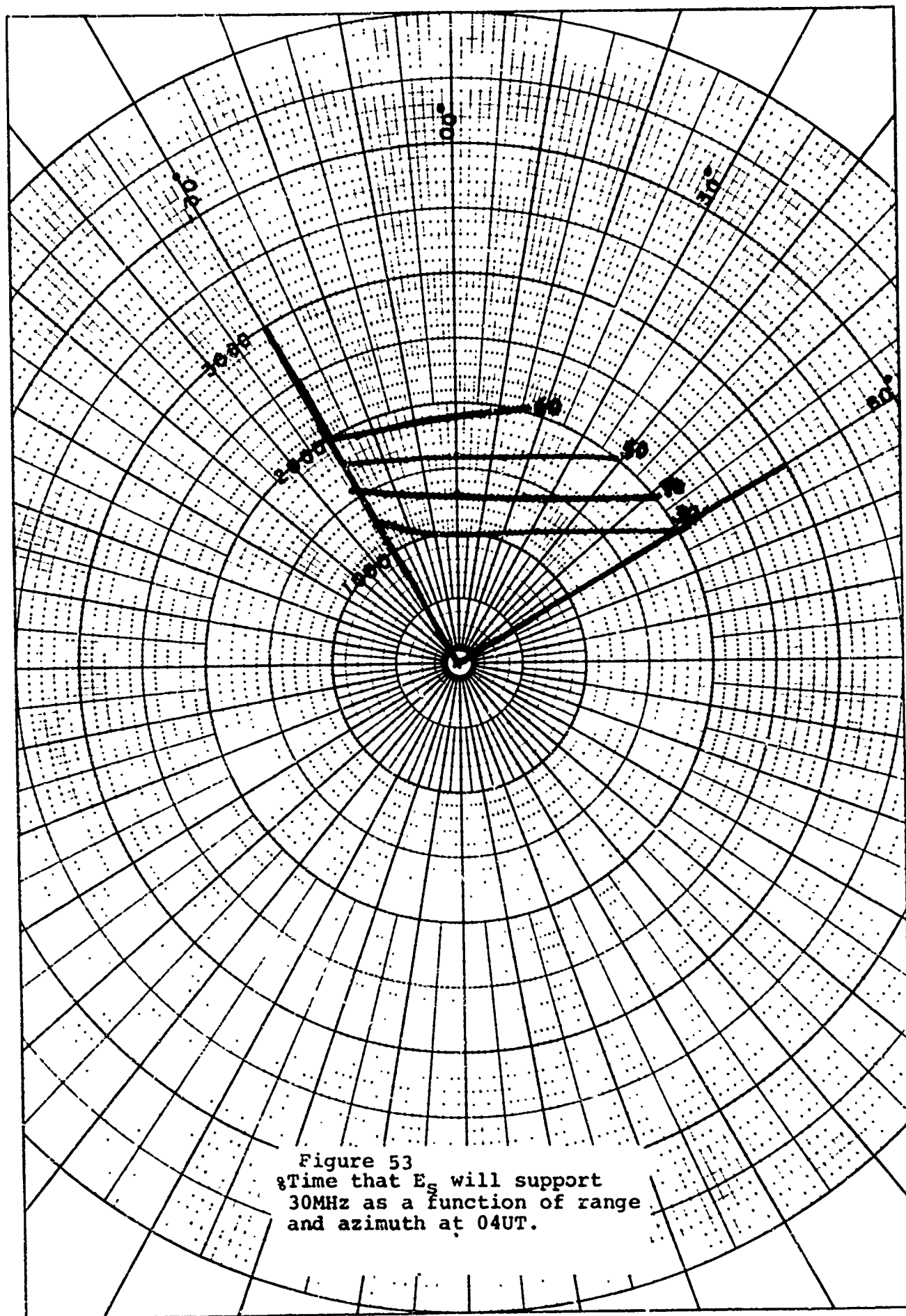
Figure 51

Time that E_s will support 30MHz as a function of range and azimuth at 00UT.

Figure 52
Time that E$_s$ will support
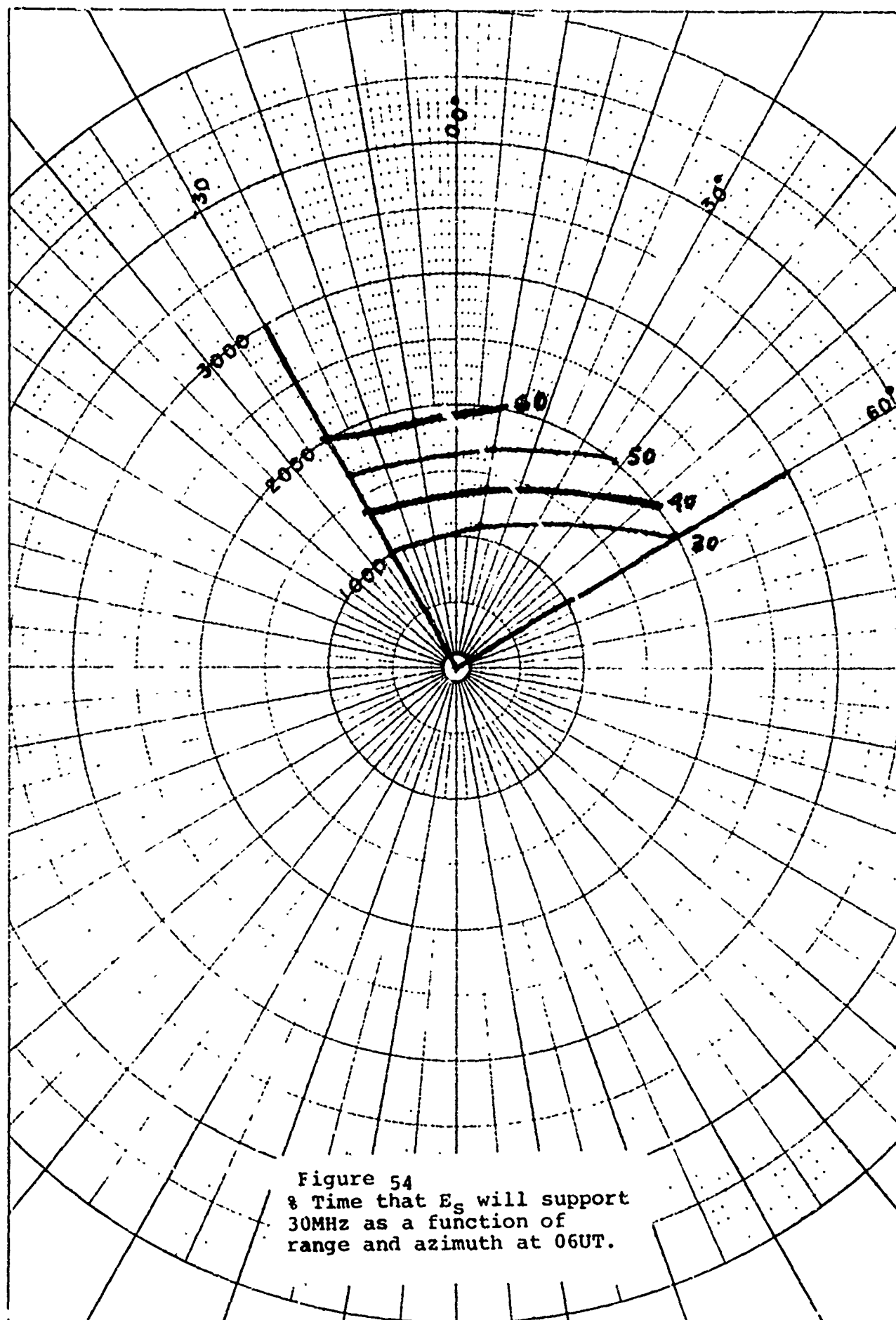30MHz as a function of
range and azimuth at 02UT.

Figure 53
%Time that E$_s$ will support
30MHz as a function of range
and azimuth at 04UT.

Figure 54
% Time that E_s will support
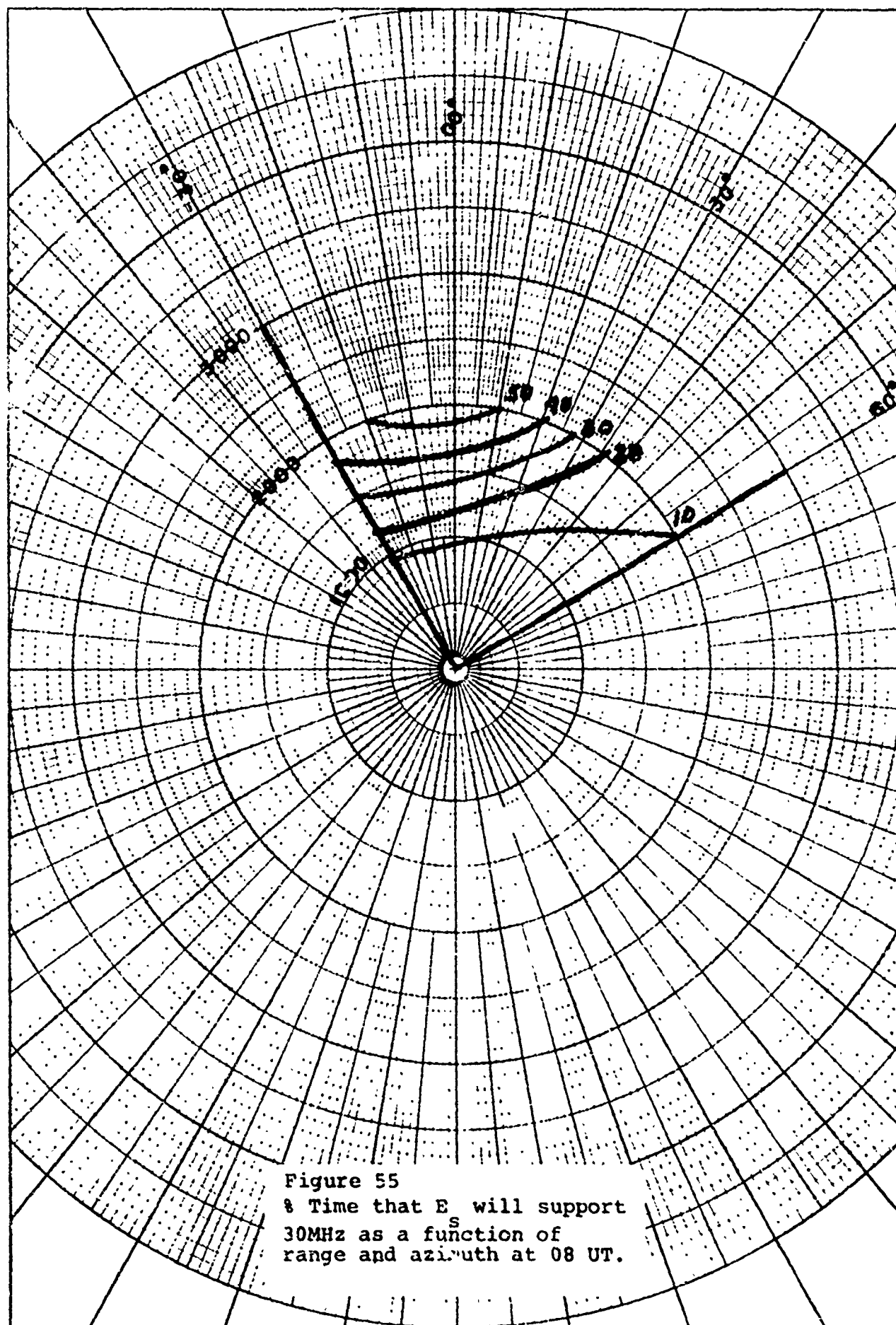30MHz as a function of
range and azimuth at 06UT.

Figure 55
% Time that E_s will support
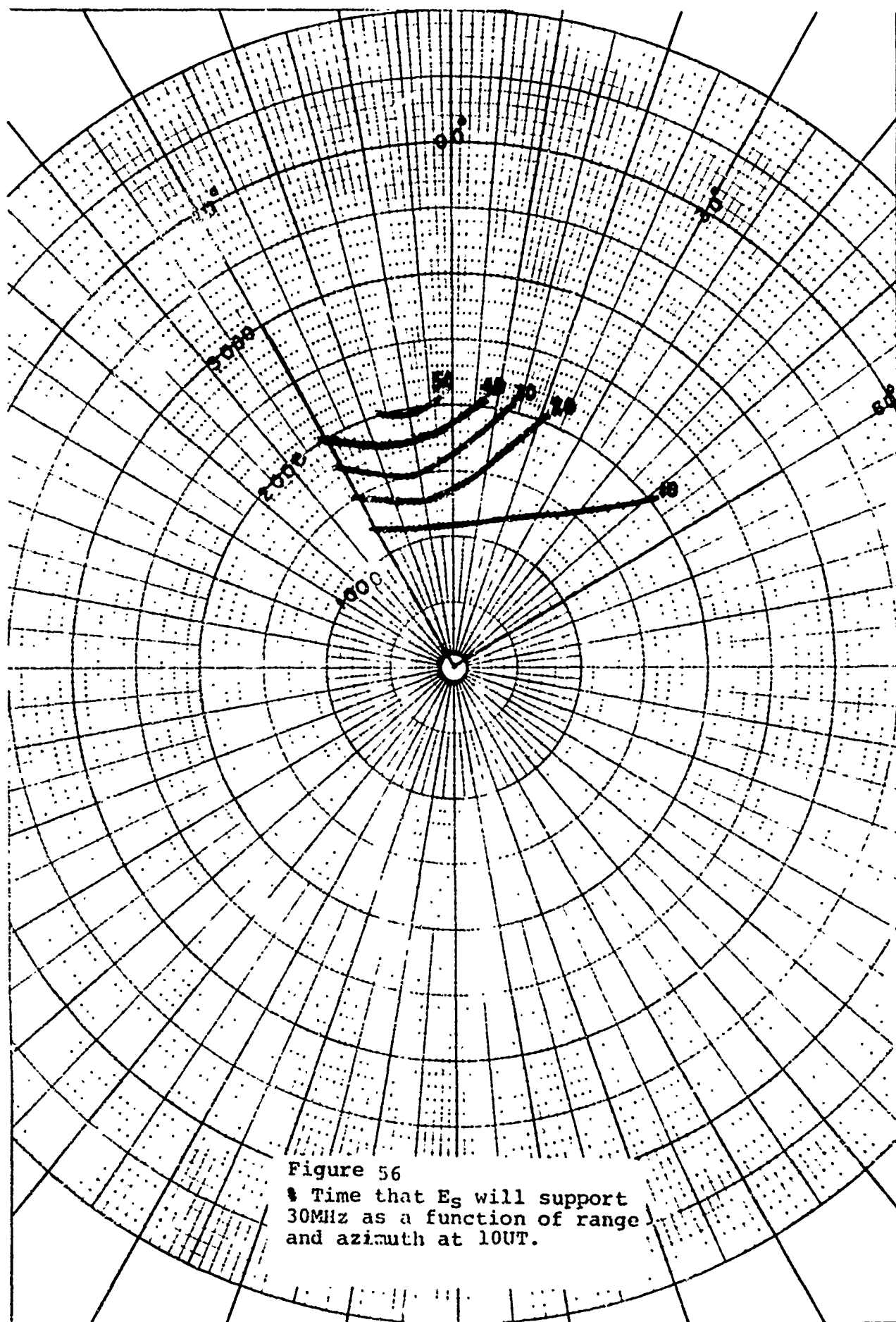30MHz as a function of
range and azimuth at 08 UT.

Figure 56

% Time that E_s will support
30MHz as a function of range
and azimuth at 10UT.

Figure 57
% Time that E_s will support
30MHz as a function of
range and azimuth at 12UT.

Figure 58
% Time that E_s will support
30MHz as a function of range
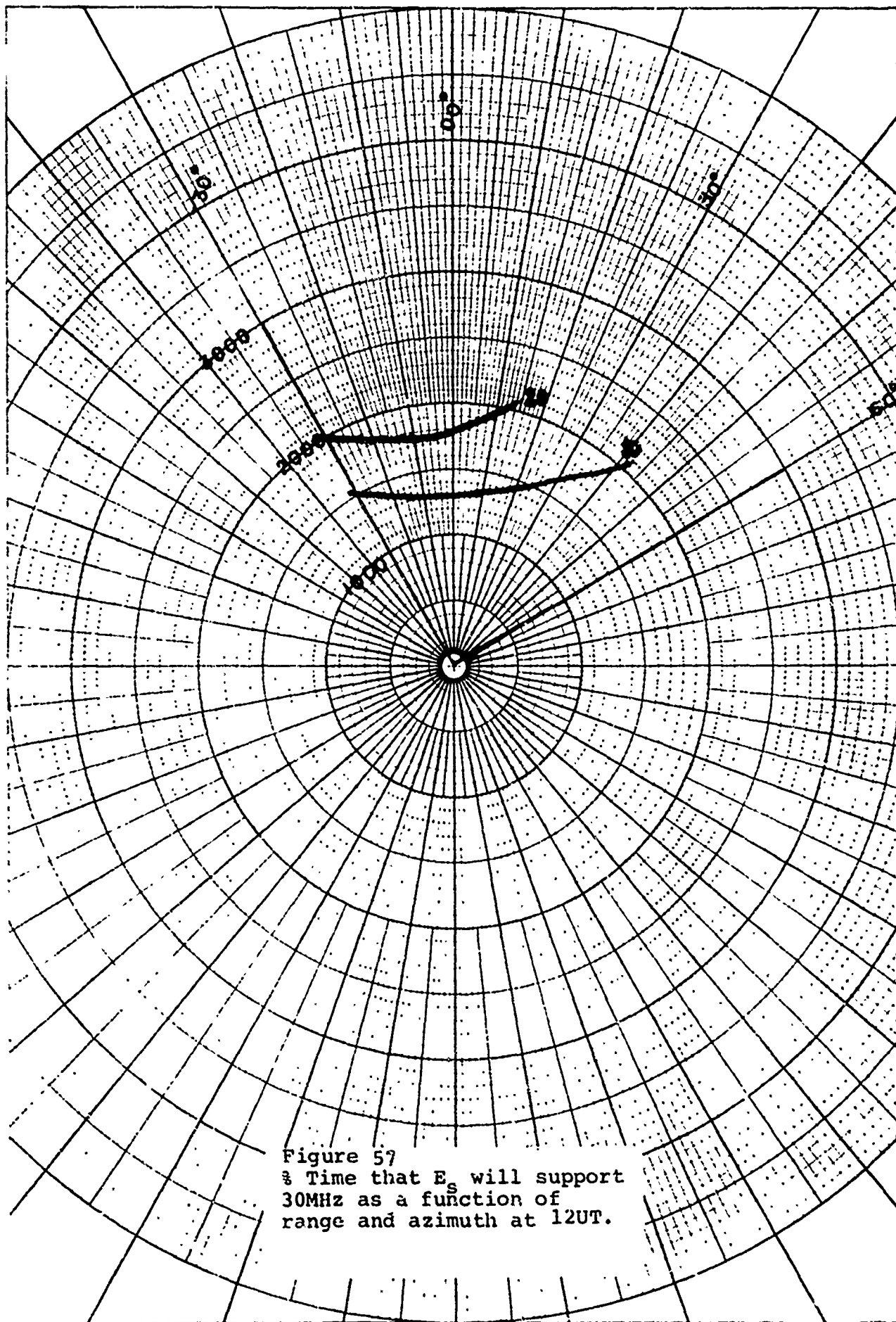and azimuth at 14UT.